DISCONTINUITIES IN RECIPROCAL AND NONRECIPROCAL INHOMOGENEOUS WAVEGUIDES

by

W. KENNETH McRITCHIE

B.Sc., Queen's University, Kingston, 1969
M.Sc., Queen's University, Kingston, 1971

A THESIS SUBMITTED IN PARTIAL FULFILMENT OF
THE REQUIREMENTS FOR THE DEGREE OF

DOCTOR OF PHILOSOPHY

in the Department of Electrical Engineering

We accept this thesis as conforming to the
required standard

Research Supervisor

Members of the Committee

Members of the Department
of Electrical Engineering
THE UNIVERSITY OF BRITISH COLUMBIA

May, 1975

In presenting this thesis in partial fulfilment of the requirements for an advanced degree at the University of British Columbia, I agree that the Library shall make it freely available for reference and study. I further agree that permission for extensive copying of this thesis for scholarly purposes may be granted by the Head of my Department or by his representatives. It is understood that copying or publication of this thesis for financial gain shall not be allowed without my written permission.

Department of Electrical Engineering

The University of British Columbia
2075 Wesbrook Place
Vancouver, Canada
V6T 1W5

Date May 26, 1975

ABSTRACT

Four types of waveguide discontinuity are investigated:

(1) the interface between reciprocal homogeneous and reciprocal inhomogeneous waveguides;

(2) the interface between reciprocal homogeneous and nonreciprocal inhomogeneous waveguides;

(3) a thin metal diaphragm in a reciprocal inhomogeneous waveguide;

(4) a thin metal diaphragm in a nonreciprocal inhomogeneous waveguide.

Mode matching is used to obtain theoretical solutions for discontinuities of types (1)-(3); experimental results are obtained for type (3) and type (4) discontinuities.

Detailed studies are made of the two types of interface discontinuity. Both E-plane and H-plane dielectric loading are investigated for the reciprocal case while the configuration used for the nonreciprocal structure is that of the twin-slab ferrite loaded waveguide. Based on these analyses, the interface and the two waveguides, homogeneous and inhomogeneous, are described by relatively simple equivalent transmission circuits. In these circuits, unique normalized equivalent transmission line characteristic admittances are defined for the inhomogeneous waveguide. These admittances are shown to be not generally proportional to the wave admittances, even when such can be defined. In the nonreciprocal case, the characteristic admittances are nearly the same in the two directions of propagation although the phase coefficients can be very different.

The two types of diaphragm discontinuity are investigated experimentally at a frequency of 8.5 GHz. The experimental procedure is the same for both types and requires the measurement of reflection and transmission coefficients of unmatched sections of the inhomogeneous waveguide. Theoretical results are obtained for the reciprocal case which indicate that the error in the measurements is less than ±6%.

CONTENTS

FIGURES

TABLES

SYMBOLS

a = broad dimension of both waveguides A and B

a_i = complex amplitude coefficient of the TE_{i0} mode in waveguide A

A = reciprocal homogeneous waveguide

A_1, A_3 = interface wave-transmission matrices

A_2 = wave-transmission matrix of a length of inhomogeneous waveguide

A_d = diaphragm wave transmission matrix

A_n, B_n, C_n, D_n = amplitude constants for the n^{th} mode in waveguide B

b = narrow dimension of both waveguides A and B

b_j = complex amplitude coefficient of the LSE_{j0} mode (E-plane loading) or the LSE_{1j} or LSM_{1j} mode (H-plane loading) in waveguide B

$b_j^{\pm}$ = complex amplitude coefficient of the $TE_{j0}^{\pm}$ mode in waveguide B

B = reciprocal or nonreciprocal inhomogeneous waveguide

= normalized shunt susceptance in the two-element equivalent circuit of a reciprocal interface

= normalized shunt susceptance in the equivalent circuit of a diaphragm in reciprocal waveguide

$B^{\pm}$ = normalized shunt susceptances in the equivalent circuit of a diaphragm in nonreciprocal waveguide

B_2 = normalized shunt susceptance in the three-element equivalent circuit of a reciprocal interface

$B_A^{\pm}$, $B_B^{\pm}$ = normalized shunt susceptances in the equivalent circuit of a nonreciprocal interface with a wave incident from waveguide A and waveguide B, respectively

c = distance between the side wall of waveguide B and the inhomogeneous loading material

d = half the spacing between the two ferrite (or dielectric) slabs

= distance between the side wall of the waveguide and the inside edge of the diaphragm

d_{min} = width of one of the metal strips used to form the diaphragm

d_{max} $\equiv$ c

$\bar{e}_{Ai}$ = transverse electric field of the TE_{i0} mode in waveguide A

$\bar{e}_{Bj}$ = transverse electric field of the LSE_{j0} mode (E-plane loading) or the LSE_{1j} or LSM_{1j} mode (H-plane loading) in waveguide B

$\bar{e}^{\pm}_{Bj}$ = transverse electric field of the $TE^{\pm}_{j0}$ mode in waveguide B

$\bar{E}_A$, $\bar{E}_B$ = total transverse electric fields in waveguides A and B, respectively

h_m = transverse propagation coefficient of the m^{th} mode in the empty region of waveguide B

$\bar{h}_{Ai}$ = transverse magnetic field of the TE_{i0} mode in waveguide A

$\bar{h}_{Bj}$ = transverse magnetic field of the LSE_{j0} mode (E-plane loading) or the LSE_{1j} or LSM_{1j} mode (H-plane loading) in waveguide B

$\bar{h}^{\pm}_{Bj}$ = transverse magnetic field of the $TE^{\pm}_{j0}$ mode in waveguide B

$\bar{H}_A$, $\bar{H}_B$ = total transverse magnetic fields in waveguides A and B, respectively

H_c = coercive force of ferrite material

k_0 = $2\pi/\lambda_0$

K = differential phase shift of an unmatched section of nonreciprocal waveguide due to interface effects

ℓ = length of the inhomogeneous section

ℓ_m = transverse propagation coefficient of the m^{th} mode in waveguide B, in the dielectric region for the reciprocal case and in the ferrite region for the nonreciprocal case

M, N = numbers of modes used to approximate the total transverse fields at a discontinuity

M_r = remanent magnetization of the ferrite

M_s = saturation magnetization of the ferrite

q_m = transverse propagation coefficient of the m^{th} mode in waveguide B in the region between the two ferrite (or dielectric) slabs

r_1, r_2 = semi-infinite interface reflection coefficients with a unit amplitude wave incident on the interface

R = reflection coefficient of an unmatched section of inhomogeneous waveguide

R_i = semi-infinite interface reflection coefficient

$\hat{R}_i$ = normalized semi-infinite interface reflection coefficient

t = half the thickness of the inhomogeneous loading material

t_1, t_2 = semi-infinite interface transmission coefficients

T = transmission coefficient of an unmatched section of inhomogeneous waveguide

$T^{\pm}$ = transmission coefficients of an unmatched section of nonreciprocal waveguide

T_i = semi-infinite interface transmission coefficients

$\hat{T}_i$ = normalized semi-infinite interface transmission coefficients

X = normalized series reactance in the two-element equivalent circuit of a reciprocal interface

= $e^{-\alpha \ell}$ for a reciprocal section

= $e^{-\hat{\alpha} \ell}$ for a nonreciprocal section

$X^{\pm}$ = normalized series reactances in the equivalent circuit of a diaphragm in nonreciprocal waveguide

X_1, X_3 = normalized series reactances in the three-element equivalent circuit of a reciprocal interface

$X_A^{\pm}$, $X_B^{\pm}$ = normalized series reactances in the equivalent circuit of a nonreciprocal interface with a wave incident from waveguide A and waveguide B, respectively

Y = normalized equivalent transmission line characteristic admittance in a reciprocal inhomogeneous waveguide

$Y^{\pm}$ = normalized equivalent transmission line characteristic admittances in a nonreciprocal waveguide

Y_{in} = input admittance

α = attenuation coefficient in waveguide B for reciprocal loading

$\alpha^{\pm}$ = attenuation coefficients in waveguide B for nonreciprocal loading

$\hat{\alpha}$ = $(\alpha^{+} + \alpha^{-})/2$

β = phase coefficient in waveguide B for reciprocal loading

$\beta^{\pm}$ = phase coefficients in waveguide B for nonreciprocal loading

$\hat{\beta}$ = $(\beta^{+} + \beta^{-})/2$

β_A = phase coefficient in waveguide A

$\beta_B^{\pm}$ $\equiv \beta^{\pm}$

γ = the gyromagnetic ratio (= 1.76×10^{7} oe^{-1} sec^{-1})

γ_A, γ_B = propagation coefficients of the dominant modes in waveguides A and B, respectively for reciprocal loading

γ_i = propagation coefficient of the i^{th} mode in waveguide B for nonreciprocal loading

ε = permittivity of the loading material

ε_d = relative permittivity of the dielectric material between the two ferrite slabs

ε_f = relative permittivity of the ferrite

ε_0 = permittivity of free space

ε_r = relative permittivity of the loading material

η = $\phi_2 - \beta\ell$ for reciprocal loading

= $\phi_2 - \hat{\beta}\ell$ for nonreciprocal loading

θ = phase angle of the transmission coefficients of a reciprocal interface (semi-infinite case)

= phase angle of the transmission coefficients of a diaphragm in reciprocal waveguide

$\theta^{\pm}$ = phase angles of the transmission coefficients of a diaphragm in nonreciprocal waveguide

θ_1, θ_2 = phase angles of the transmission coefficients of a nonreciprocal interface (semi-infinite case)

κ = off-diagonal element of the relative permeability dyadic of the ferrite

λ_0 = free space wavelength

μ = permeability of the loading dielectric, reciprocal case

= diagonal element of the relative permeability dyadic of the ferrite

μ_e = effective relative permeability of the ferrite

μ_0 = permeability of free space

μ_r = relative permeability of the loading material

$\bar{\Pi}_e$, $\bar{\Pi}_h$ = electric and magnetic Hertzian potentials

ρ = magnitude of the normalized reflection coefficients

τ = magnitude of the normalized transmission coefficients

ϕ = phase angle of the reflection coefficients of a diaphragm in reciprocal or nonreciprocal waveguide

ϕ_1, ϕ_2 = phase angles of the reflection coefficients of a reciprocal or nonreciprocal interface (semi-infinite case)

ψ = differential phase shift per unit length of nonreciprocal waveguide

ψ_e, ψ_h = electric and magnetic scalar potentials

ψ_{Ai} = scalar potential for the i^{th} mode in waveguide A

ψ_{Bj} = scalar potential for the j^{th} mode in waveguide B

ω = angular frequency

ACKNOWLEDGEMENT

It has been a valuable experience to work with Dr. M. Kharadly. His interest and enthusiasm were unflagging throughout the course of this project.

I am grateful for the financial support afforded by two W.C. Sumner Memorial Fellowships for the years 1971-1973 and an H.R. MacMillan Family Fellowship for the year 1973-1974. The project was supported by the National Research Council of Canada under grant A-3344.

I wish to thank Mr. C. Chubb and especially Mr. J. Stuber for their excellent work and advice in making the various waveguide components required for the experimental measurements.

Finally, I wish to thank Miss S. Lund for doing an excellent job of typing the manuscript.

Chapter 1

INTRODUCTION

1.1 Background

Electronic beam steering of antenna arrays is one of the more recent major advances in antenna systems, mainly because of the development of variable phase shifters. The nonreciprocal ferrite type of phase shifter has proven to be practical and is now widely used in these systems. The usefulness of this type of device was realized theoretically in the early 1950's, with much of the work done to analyse a waveguide containing transversely-magnetized ferrite slabs[1-3]. The twin-slab configuration shown in Fig. 1(a) was found to have significantly different propagation coefficients, depending on the sense of the magnetization. To produce the required transverse magnetization, external magnets were originally used - a somewhat impractical proposition. It was not until late in the 1950's that the idea of a ferrite toroid with a magnetizing wire passing through the centre was proposed[4]. This actually marked the beginning of the development of present-day nonreciprocal ferrite phase shifters, as virtually all such devices since then have employed a toroid configuration[5-9]. The most commonly used types are shown diagrammatically in Figs. 1(b) - 1(d).

The toroid design had the further advantage of considerably reduced power requirements for switching the sense of the magnetization. This was achieved through the proper design of the ferrite material so that its remanent magnetization could be 75-80% of its saturation value. Thus, it was only necessary to apply a current pulse to the magnetizing wire and the device operated with the remanent magnetization - hence, the name latching ferrite phase shifter. With the proper choice of the length

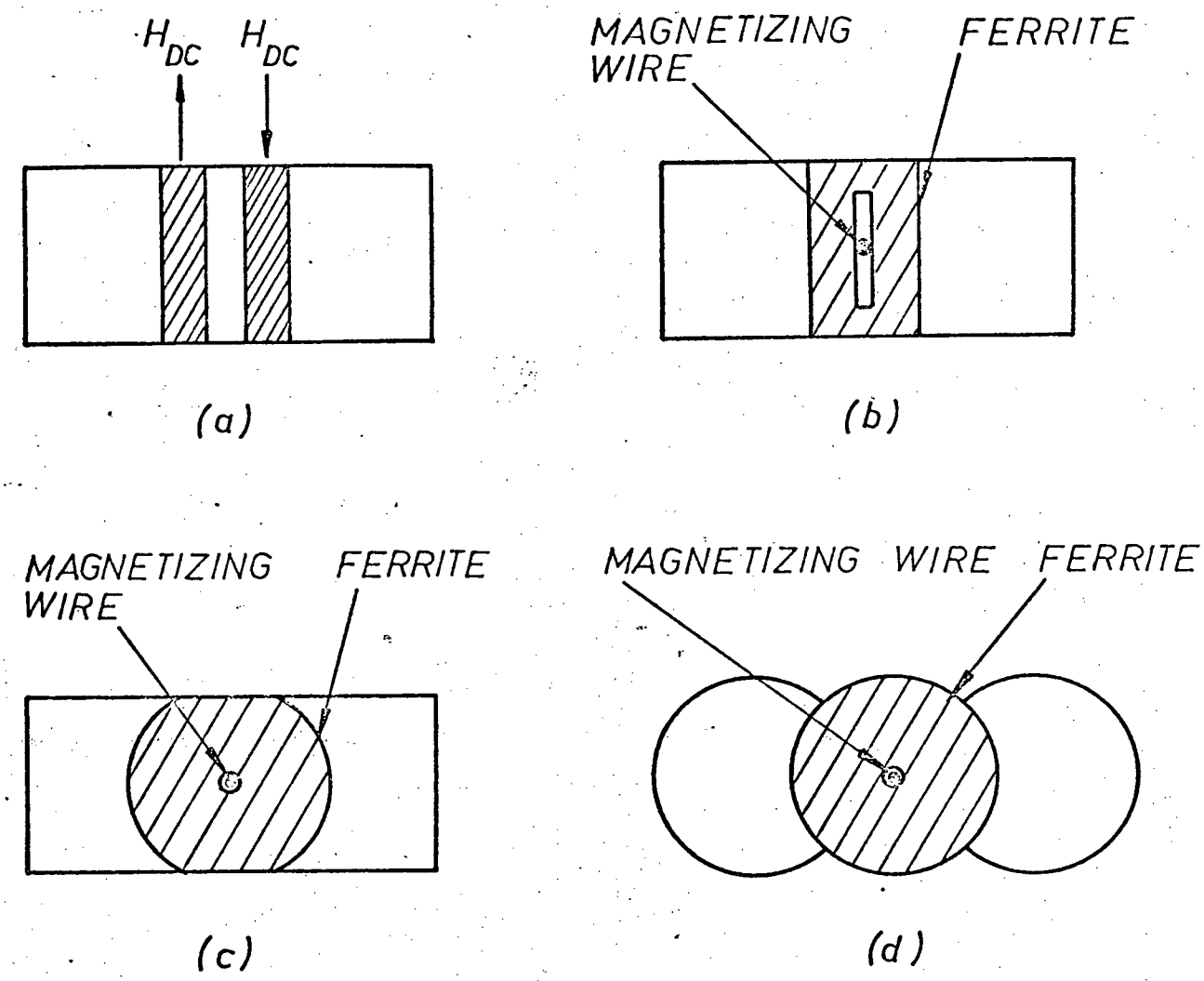

Fig. 1. Nonreciprocal ferrite phase shifter configurations.
(a) theoretical model; (b)-(d) practical toroid designs.

of the ferrite-loaded section, the device could be made to have the desired value of differential phase shift (the differential phase shift per unit length constitutes the figure of merit of the nonreciprocal type of phase shifter). A typical phase shifter design consisted of a series of different lengths of ferrite toroids, each with its own magnetizing wire (see Fig. 2) and providing differential phase shifts of, for example, 180°, 90°, 45° and 22.5°. This allowed the phase difference between the feeds of each element of an array to be varied digitally, in steps of 22.5°, from 0° to 360°. The large size of the array, which could be of the order of 10,000 elements or more, permitted this digital operation to scan the beam over a continuous range.

A large number of phase shifters is used in a single system, since one is required for each element of the array. Thus, any reduction in the size, weight or switching power of the phase shifter would constitute a significant improvement in the design of the system. In an attempt to achieve such an improvement a recent development by Spaulding[8,9] involved loading the ferrite phase shifter periodically with thin metallic diaphragms. His experimental investigation showed that such loading could provide significant enhancement of the differential phase shift over a wide bandwidth. Although the waveguide configuration he used, Fig. 1(d), was quite unconventional, the results of the investigation were noteworthy. A subsequent theoretical analysis of nonreciprocal transmission lines periodically loaded with diaphragms showed similar trends[10]. This indicated that Spaulding's results were not peculiar to the type of waveguide he used but were typical of what could be expected by loading any form of nonreciprocal waveguide.

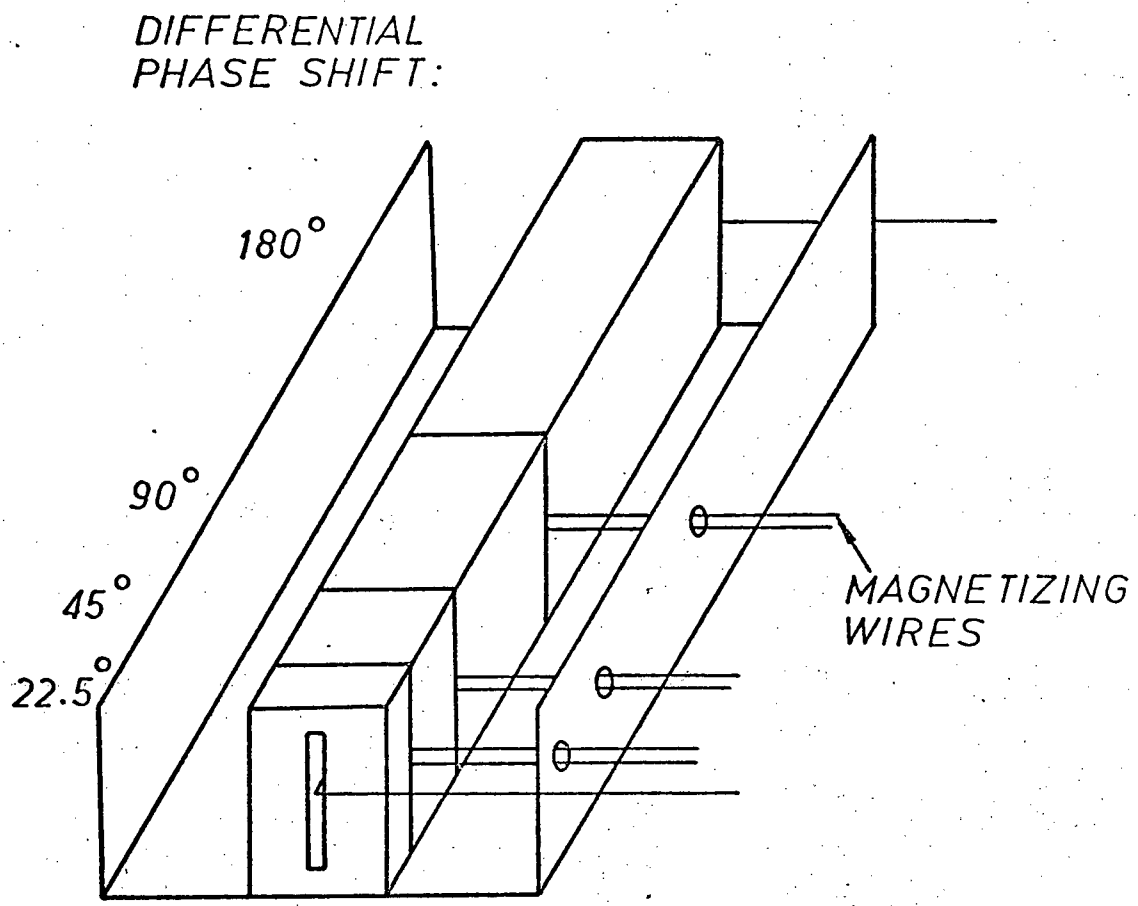

Fig. 2. Cutaway diagram of a four-bit ferrite phase shifter.

1.2 Objectives

The application of periodic loading to simple waveguide structures appeared to be an attractive proposition and provided the incentive to start the work in this thesis. To implement the theory in reference (10), it was necessary to determine the equivalent circuit of a single metallic diaphragm in a nonreciprocal waveguide. In attempting to achieve this objective, however, there were some fundamental problems which had to be solved in order to answer certain questions. These questions are:

(1) What is the equivalent characteristic admittance of an inhomogeneous nonreciprocal waveguide? This must be determined before the theory can be applied.

(2) In fact, how does one define an equivalent characteristic admittance even in a reciprocal inhomogeneous waveguide where a wave admittance cannot be defined? (There seemed to be little unanimity amongst workers on the subject.)

(3) Can the effect of an interface between reciprocal homogeneous waveguide and nonreciprocal inhomogeneous waveguide be evaluated? This is also necessary in order to measure the effect of a diaphragm.

Because of the lack of fundamental work on discontinuities in inhomogeneous waveguides, the problem is tackled in three stages:

(1) The reciprocal inhomogeneous waveguide interface is analysed in an attempt to define the equivalent characteristic admittance of an inhomogeneous waveguide. This work is presented in Chapter 2.

(2) The properties of a nonreciprocal inhomogeneous waveguide interface are determined and appropriate characteristic admittances for the two directions of propagation are defined. This work is presented in Chapter 3.

(3) With the insight provided by the work in Chapter 3, the properties of a thin diaphragm in a nonreciprocal inhomogeneous waveguide are determined. This is done experimentally since the nonreciprocal waveguide configurations used in practice make an analytical solution very difficult, if not impossible. To assess the accuracy of the results, at least indirectly, a basis for comparison is needed. This is provided by comparing the experimental results for a metal diaphragm in reciprocal inhomogeneous waveguide with numerically obtained results for the same configuration. The experimental work is presented in Chapter 4.

Chapter 2

RECIPROCAL INHOMOGENEOUS INTERFACE

2.1 Introduction

As discussed in Section 1.2, it is necessary to consider this problem and determine a unique method of defining the equivalent characteristic admittance of an inhomogeneous waveguide before tackling the nonreciprocal case. The problem of the junction between homogeneous and inhomogeneous waveguides is important in its own right and is encountered in many practical devices. The most thoroughly examined inhomogeneity has been that of E-plane dielectric-slab loading, Fig. 3(a). Such a junction has been described in terms of a lumped-element circuit joining two equivalent transmission lines of different characteristic admittances, when only the dominant mode propagates in each waveguide[11,12]. The parameters of this circuit depend on the value of the equivalent transmission-line characteristic admittance for the dominant mode in the inhomogeneously filled waveguide relative to that of the empty waveguide. The definition of this quantity, the characteristic admittance, has itself been subject to various interpretations[11-15]. To date, neither the interface problem nor the definition of characteristic admittance has been resolved in a manner that is both physically meaningful and sufficiently general.

The situation under consideration is depicted in Fig. 4, where waveguides A and B are reciprocal and are assumed to have characteristic admittances 1 and Y, respectively. The wave matrix analysis of this junction is straightforward[16]. Let the wave amplitudes, c and d, be normalized so that they represent average power flows. We may then

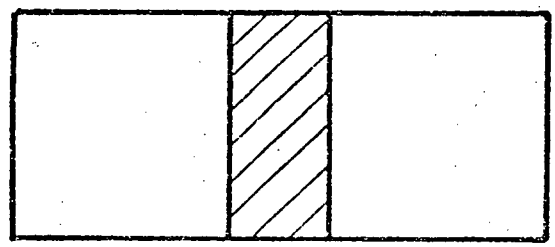

(a)

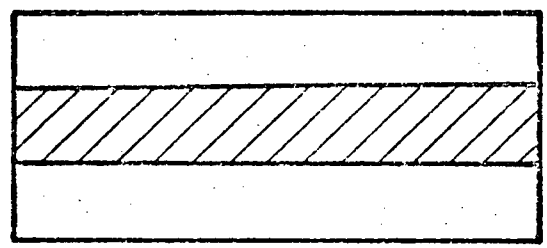

(b)

Fig. 3. Inhomogeneously filled waveguides. (a) E-plane dielectric loading; (b) H-plane dielectric loading.

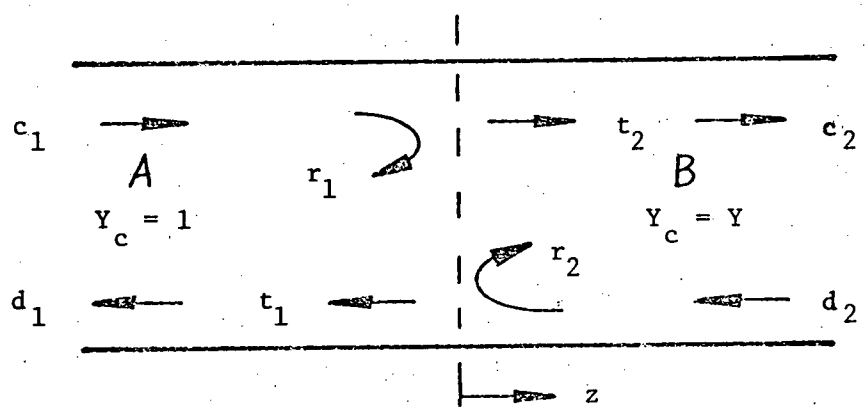

Fig. 4. Junction of two reciprocal waveguides, A and B.

write:

$$
\begin{aligned}
r_1 &= \rho\, e^{-j\phi_1} \\
r_2 &= \rho\, e^{-j\phi_2} \\
t_1 = t_2 &= \tau e^{-j\theta} \\
\rho^2 + \tau^2 &= 1 \\
\phi_1 + \phi_2 - 2\theta &= \pm \pi
\end{aligned}
\qquad (1)
$$

where r_1 and r_2 are the complex reflection coefficients of the dominant mode in waveguides A and B, respectively, and t_1 and t_2 are the corresponding normalized complex transmission coefficients. In the above relations, there are only three independent (measurable) parameters which must be determined to describe the junction completely. For example, these may be ρ, ϕ_1 and θ. Thus an equivalent circuit for the junction can have only three independent parameters. In this respect, there have been two alternatives: (i) Y is considered an unknown quantity and the effect of the junction is represented by a two-element circuit, as in Fig. 5(a); and (ii) Y is assigned a value, Y', according to some criterion and the effect of the junction is represented by a three-element circuit, as in Fig. 5(b). The criterion by which Y has been assumed is essentially that it should be proportional to the wave admittance in the inhomogeneous section (in an effort to give it some physical significance). This will be shown to be approximately true in some cases where a wave admittance can be defined, such as the E-plane loaded waveguide of Fig. 3(a). However, in other cases such as the H-plane loaded waveguide shown in Fig. 3(b), or where both the permittivity and permeability vary over the cross-section of the waveguide, it is not possible to define a unique wave

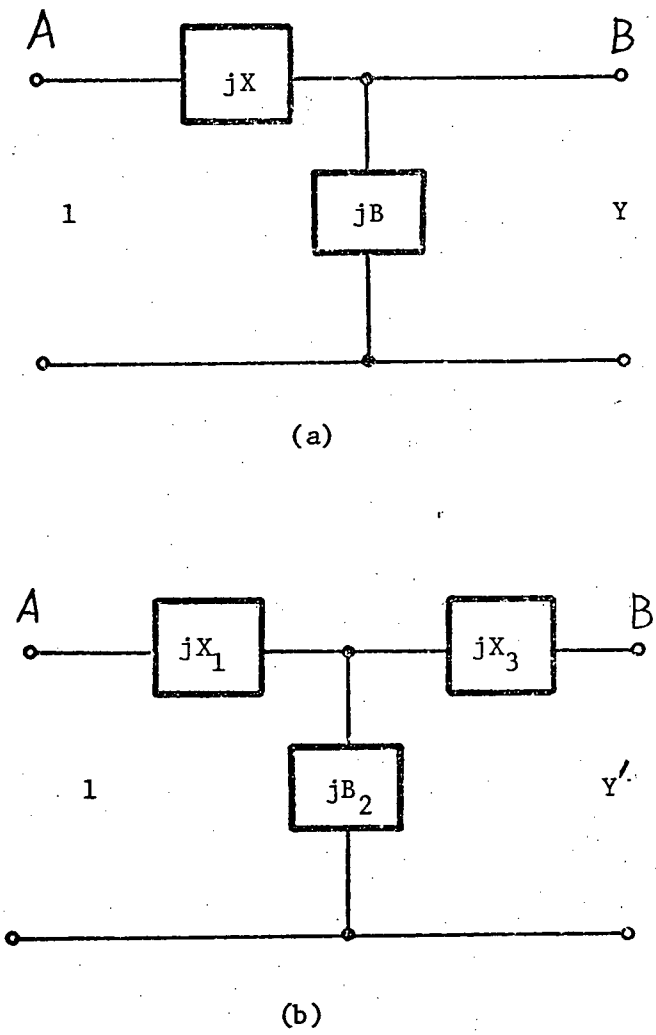

Fig. 5. Equivalent lumped-element circuits used to represent the junction between empty and inhomogeneous waveguides.
(a) two-element representation; (b) three-element representation.

admittance. Either of these representations is mathematically correct since the reflection and normalized transmission coefficients, from which the circuit elements are derived, are the same in both cases. However, while the first representation yields an equivalent circuit that is physically meaningful in all cases, the second does not because it is based on an arbitrarily assumed value for Y.

In this chapter a study is made of the properties of the junction between homogeneous and inhomogeneous waveguides with emphasis on the following points:

(a) The two-element and three-element equivalent circuits for the interface are compared. It is shown that while the former yields results which can be interpreted physically, the use of the latter cannot be justified. In addition, by using the two-element equivalent circuit, a general and meaningful definition of the normalized characteristic admittance of inhomogeneous waveguides is provided.

(b) The junction between empty and H-plane dielectric-loaded waveguide is analysed for the first time.

(c) Computed values are presented for the normalized junction parameters and characteristic admittance to illustrate the properties of inhomogeneous waveguides with various types of dielectric loading.

2.2 E-plane dielectric loading ($\mu=\mu_o$)

E-plane loading is considered first since this type of loading has already been discussed by previous authors, thus providing a basis for comparisons. In addition, a wave admittance can be defined in this case. Collin[11] used the Rayleigh-Ritz method to solve the interface problem and gave a circuit representation which is essentially the same as that shown in Fig. 5(a). The numerical example he used was for a

relatively low value of permittivity of the loading dielectric. From his results it appeared that the normalized characteristic admittance, Y, was equal to the normalized wave admittance (which, in turn, is equal to the ratio of the propagation coefficients, γ_B/γ_A). Chang[12] used mode matching to solve the same problem. Assuming that Y was in fact equal to the normalized wave admittance, he gave the three-element circuit representation shown in Fig. 5(b).

In this work, the amplitudes of the reflected and transmitted waves in waveguides A and B are determined by means of the mode matching technique described in refs.(17)and(18). Values of the equivalent circuit parameters are then obtained from expressions relating them to the reflection and transmission coefficients (Appendix A). These parameters are plotted in Figs. 7 and 8 for the two types of E-plane loading shown in Fig. 6. In Fig. 8, Y is plotted as a function of γ_B/γ_A and is very nearly, but not exactly, equal to the normalized wave admittance. It is also noted that the deviation of the value of Y from γ_B/γ_A is somewhat larger for side loading, Fig. 6(b), than for centre loading, Fig. 6(a). The corresponding two-element parameters, X and B, are plotted as a function of 2t/a in Fig. 7. Note that both X and B are inductive. This is consistent with what one should expect in this case, since the only evanescent modes excited are TE modes for which the energy stored is predominantly magnetic. With the three-element equivalent circuit representation of the interface, where Y' is assumed equal to γ_B/γ_A, different results are obtained. The values of these equivalent circuit parameters, X_1, B_2 and X_3, are also shown in Fig. 7 for centre and side loading. Note that X_1 and B_2 are inductive while X_3 is capacitive.

Examination of the results in Fig. 7 shows that X tends to zero when 2t/a approaches 0 or 1 for both centre and side loading, as it should

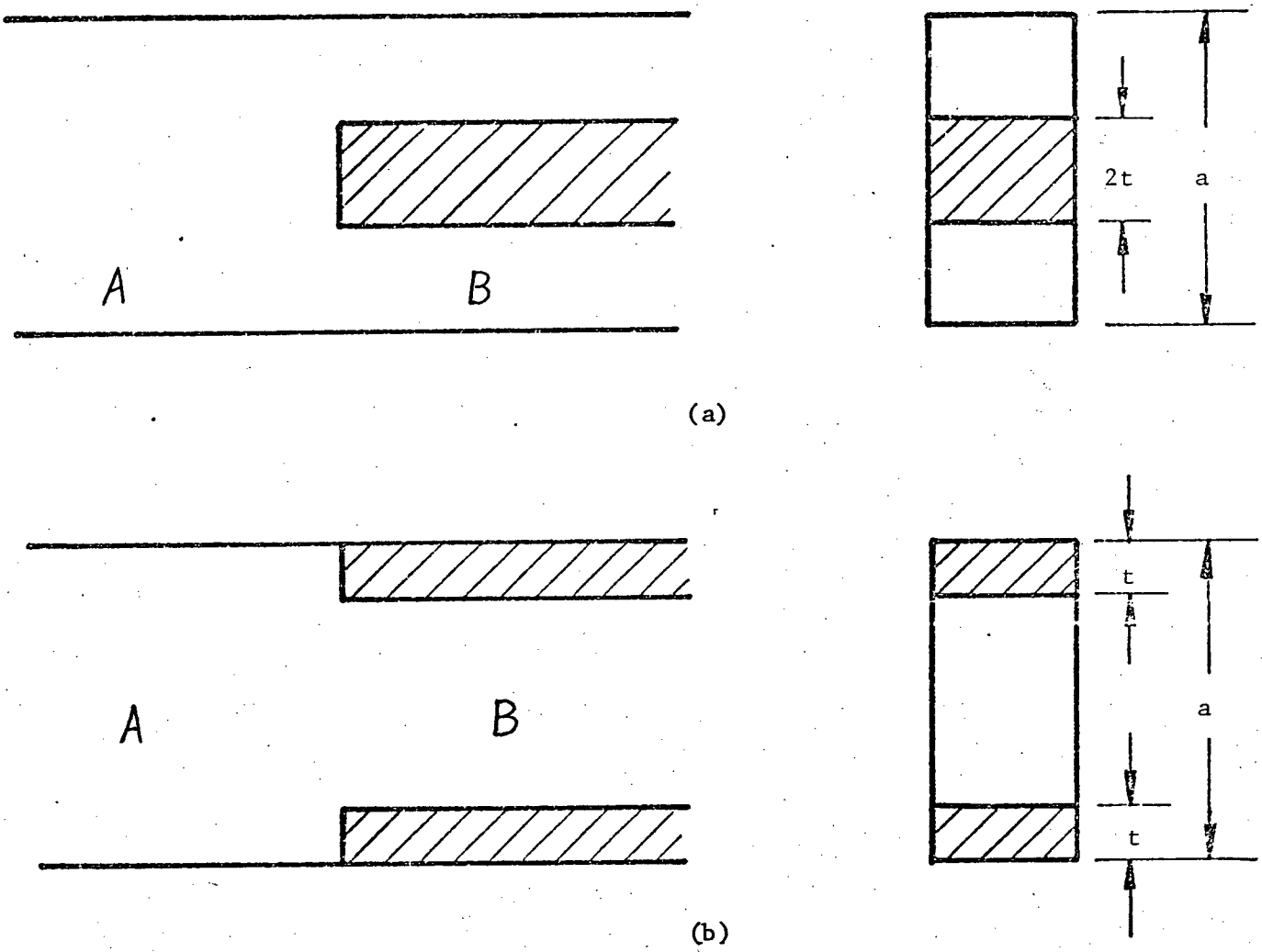

Fig. 6. Junction of empty and E-plane loaded waveguides.
(a) center loading; (b) side loading.

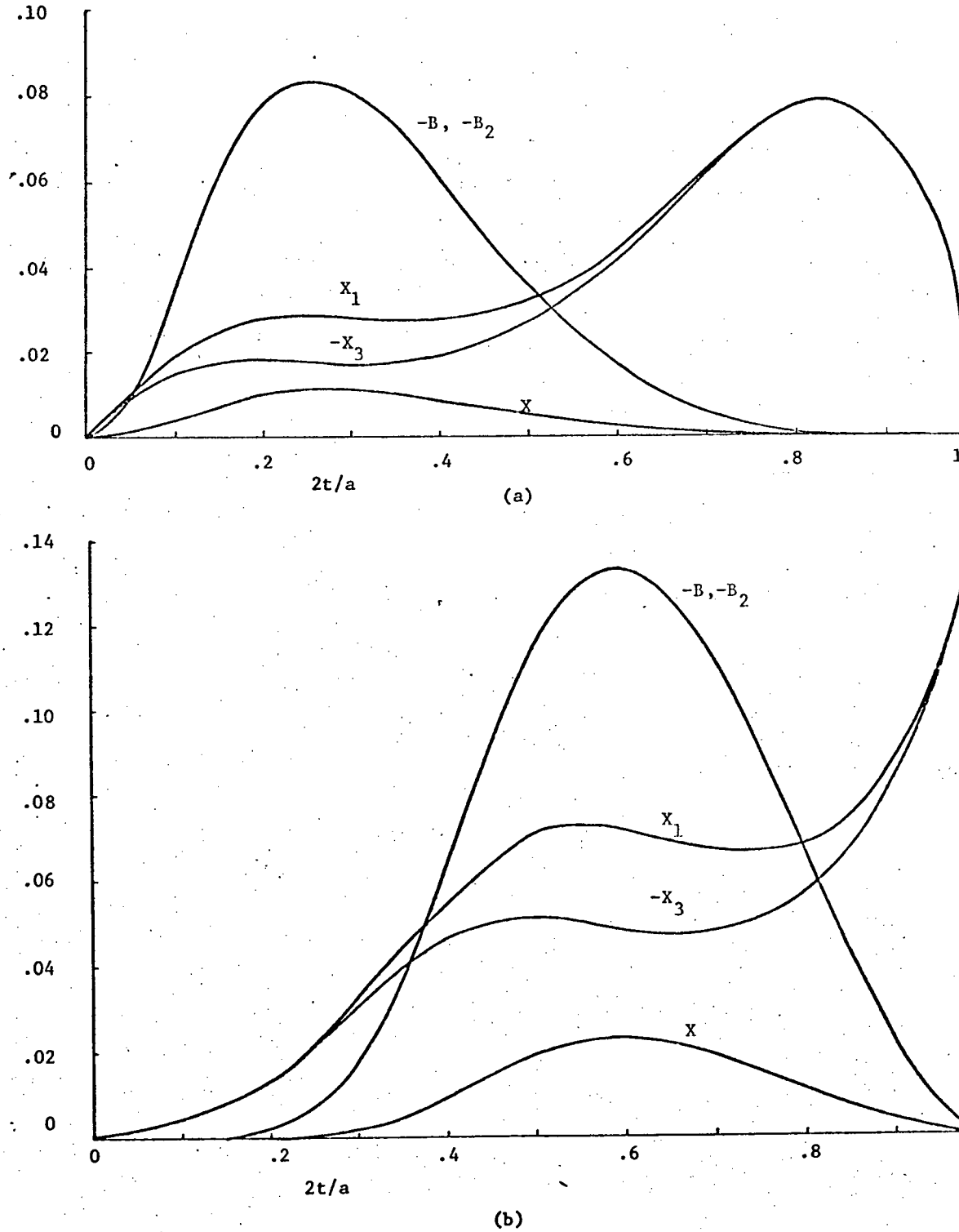

Fig. 7. Equivalent circuit parameters for E-plane loading; $a/\lambda_0 = 0.691$. (a) center loading; (b) side loading.

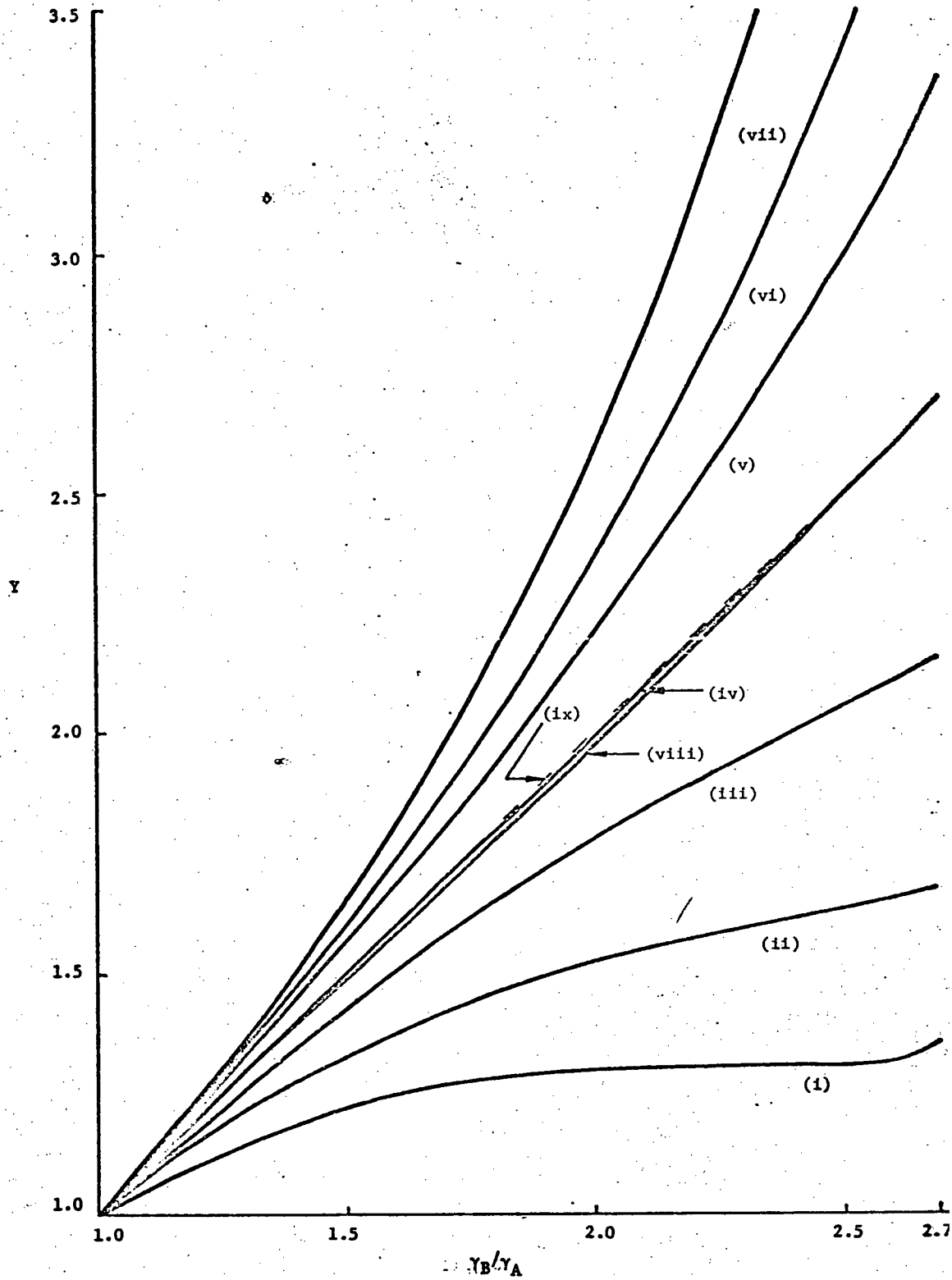

Fig. 8. Normalized characteristic admittance for E-plane center loading; $\varepsilon_r \cdot \mu_r = 4.0$, $a/\lambda_0 = 0.691$.

(i) $\varepsilon_r = 2.0$, $\mu_r = 2.0$

(ii) $\varepsilon_r = 2.5$, $\mu_r = 1.6$

(iii) $\varepsilon_r = 3.2$, $\mu_r = 1.25$

(iv) $\varepsilon_r = 4.0$, $\mu_r = 1.0$

(v) $\varepsilon_r = 5.0$, $\mu_r = 0.8$

(vi) $\varepsilon_r = 6.0$, $\mu_r = 0.66667$

(vii) $\varepsilon_r = 8.0$, $\mu_r = 0.5$

(viii) side loading, $\varepsilon_r = 4.0$, $\mu_r = 1.0$

(ix) reference: $Y = \gamma_B/\gamma_A$

when waveguide B is empty or completely filled with dielectric. The behaviour of X_1 and X_3 is not so predictable, however. With centre loading, Fig. 7(a), X_1 and X_3 approach zero when $2t/a = 1$ but their excessively large values when waveguide B is nearly full can be misleading: it appears that the junction effect is quite large here, but in fact B_2 is small and the 'effective series reactance', $X_1 + X_3$, is also very small. The behaviour of X_1 and X_3 is even more disconcerting for the side loading case, Fig. 7(b). As $2t/a$ approaches unity their magnitudes do not converge to zero but increase rapidly to large values*. While it is not unreasonable to assume that the values of X_1, B_2 and X_3 at $2t/a = 1$ should be approached differently for these two types of E-plane loading (since the field distributions are different in each case), one would expect that, at that point, the values should be the same in the two cases; i.e., $X_1 = B_2 = X_3 = 0$. From the above observations, it appears that an analysis which assumes a value for Y, or indeed for any of the equivalent circuit parameters, can lead to a physically unjustifiable behaviour of the junction parameters.

2.3 E-plane dielectric loading ($\mu \neq \mu_o$)

In many applications, the permeability, μ, of the loading material may be different from μ_o; e.g. for ferrites. In such situations a unique wave admittance is not definable. The computed results shown in Figs. 8 and 9 are for centre loading and are given for values of μ_r between 0.5 and 2. Except in the case of loading with a dielectric whose $\mu = \mu_o$, Y is markedly different from γ_B/γ_A, Fig. 8. In all cases, Y

---

* The results for X_1, B_2 and X_3 plotted in Fig. 7 agree with those given by Chang [12].

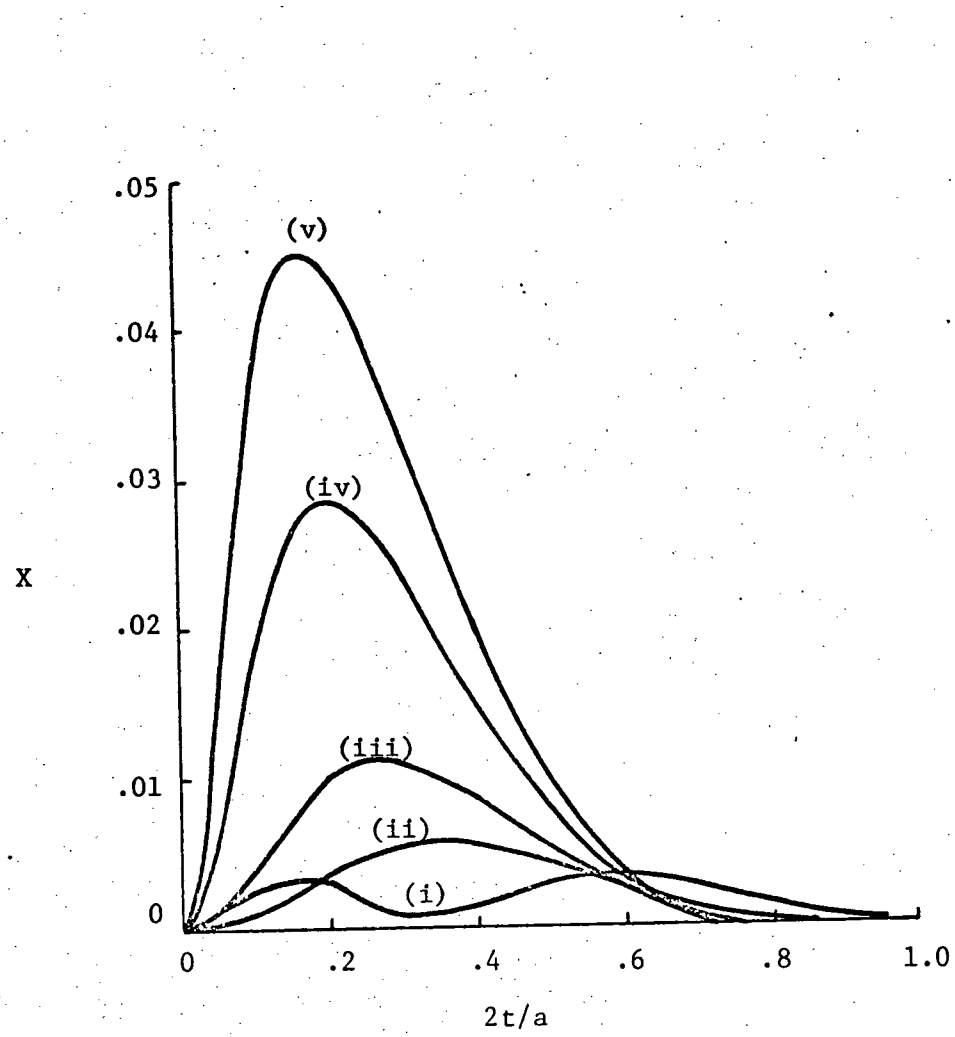

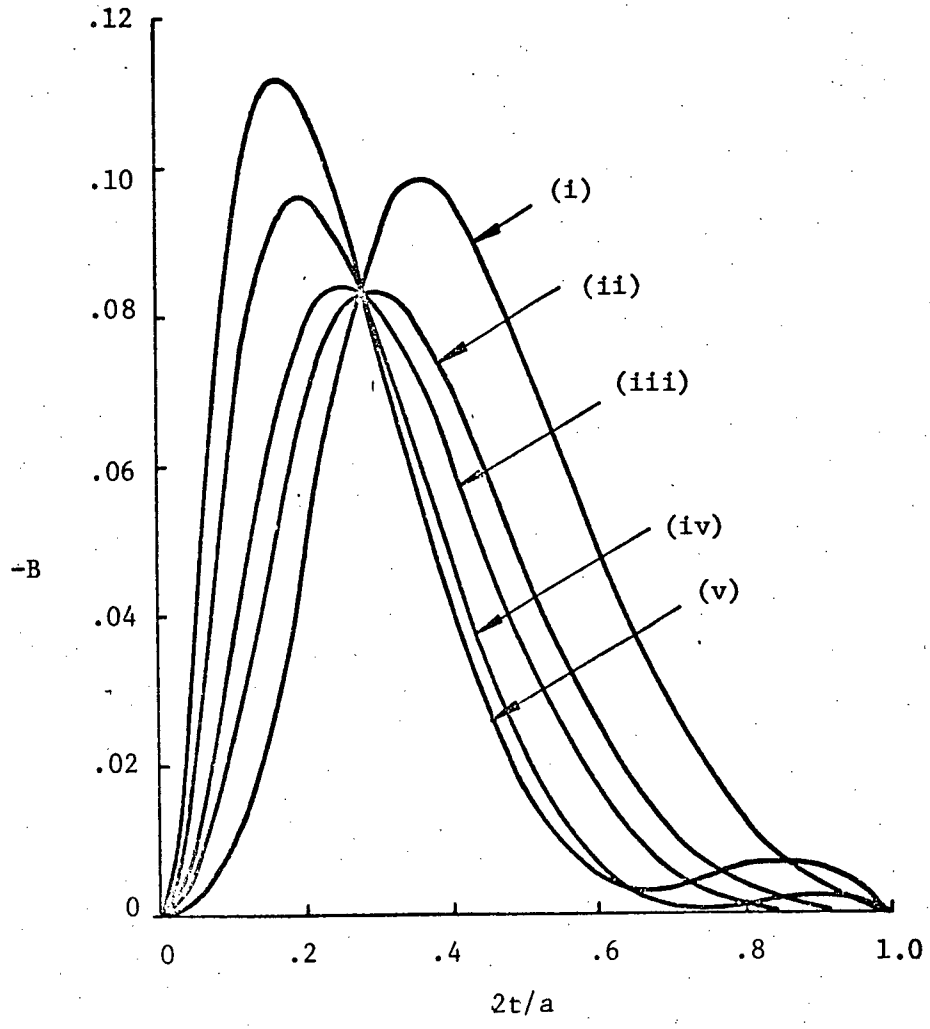

Fig. 9. X and B for E-plane center loading; $a/\lambda_0 = 0.691$.

(i) $\varepsilon_r = 2.0$, $\mu_r = 2.0$
(ii) $\varepsilon_r = 3.2$, $\mu_r = 1.25$
(iii) $\varepsilon_r = 4.0$, $\mu_r = 1.0$
(iv) $\varepsilon_r = 6.0$, $\mu_r = 0.66667$
(v) $\varepsilon_r = 8.0$, $\mu_r = 0.5$

varies rapidly with 2t/a for thin dielectrics and soon reaches a plateau as the dielectric thickness becomes large, Fig. 10. With side loading on the other hand, Y changes very slowly when 2t/a is small and varies almost linearly when 2t/a is large. The junction parameters, X and B, are again inductive and are plotted in Fig. 9. The maximum value of X is approximately proportional to the ratio of permittivity to permeability, ε/μ, of the loading dielectric. The maximum value of B appears to be a more complicated function of ε and μ, but for both X and B, the peak values occur at smaller dielectric thicknesses as ε/μ is increased.

The effect of the junction may be estimated by comparing Y, as determined by using the two-element circuit, with the input admittance at port A (Fig. 5(a)):

$$Y_{in} = \frac{1 - r_1}{1 + r_1} = \frac{Y + jB}{(1 - XB) + jXY} \qquad (2)$$

The maximum difference between Y_{in} and Y occurs where X and Y are largest. For example, with $\varepsilon_r = 8$ and $\mu_r = 0.5$, these occur at $2t/a \doteqdot 0.2$ and the difference between Y and Y_{in} is 1.6%. With smaller ratios of ε/μ the junction effect is smaller: the difference is less than 0.5% with $\varepsilon_r = 6$, $\mu_r = 2/3$, and less than 0.06% with $\varepsilon_r = 4$, $\mu_r = 1$. For impedance matching purposes, then, the lumped-element circuit parameters of the interface can often be neglected and the junction treated as one between two transmission lines with normalized characteristic admittances 1 and Y. Thus it is important to be able to determine a value for Y that is physically meaningful.

2.4 H-plane dielectric loading

The junction between empty and H-plane dielectric-loaded waveguides has not been analysed before. This case is somewhat more

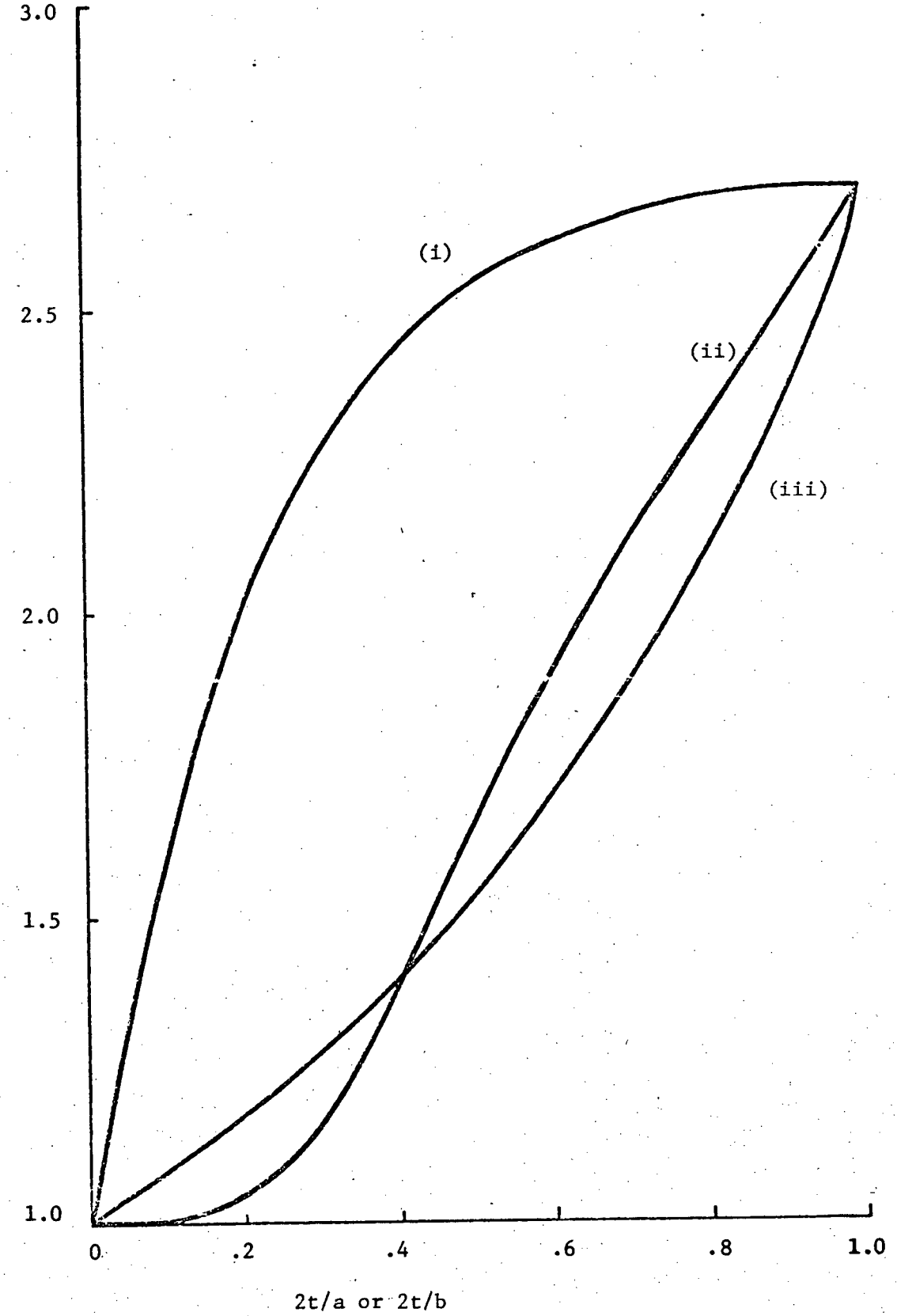

Fig. 10. Variation of Y with dielectric thickness; $\varepsilon_r = 4.0$, $\mu_r = 1.0$, $a/\lambda_0 = 0.691$, $b/\lambda_0 = 0.3$.

(i) E-plane center loading
(ii) E-plane side loading
(iii) H-plane center loading or side loading

complicated than the E-plane case, although the procedure for mode matching is similar. The difficulty here is in deciding which modes must be used to satisfy the boundary conditions at the interface. The analysis is given in Appendix B from which it is seen that the modes excited are:

$$\begin{aligned} &TE_{10} + TE_{1m} + TM_{1m} \quad \text{in waveguide A} \\ &LSE_{1m} + LSM_{1m-1} \quad \text{in waveguide B} \end{aligned} \qquad m = 2,4,6,....$$

The amplitudes of the TE and LSE modes were found to decay much more rapidly with increasing m than the TM or LSM modes (Table 1 is a typical example). Based on this observation, the ratios of TE to TM and LSE to LSM modes were chosen to be about 1:2. The total number of modes in each waveguide was varied and the convergence found to be adequate with 9 each of the TE and LSE modes and 19 each of the TM and LSM modes. The exact ratios of TE to TM and LSE to LSM modes did not seem to be critical but after the results had been obtained, a systematic study was made to determine the importance of these ratios and their effect on the convergence of the results. Figure 11 illustrates the effect on B (in the interface equivalent circuit) of varying the two ratios independently and together. The effect on Y and X is similar though not as pronounced. This indicates that the ratios should be the same, assuming that the correct answer is somewhere near 0.12260. Convergence was then checked using several different ratios from 1:6 to 1:1. The calculated values of B are plotted in Fig. 12 as a function of the total number of modes in either waveguide. For all ratios, the value of B converges to 0.12272, in this case, as the total number of modes is increased. The most rapid convergence occurs with a ratio of 1:3 or less. However, with a ratio of 1:2, approximately that used for all the interface results presented

Table 1. Example of mode amplitude decay for H-plane loading.

$\varepsilon_r = 8$; $\mu_r = 0.75$; $2t/b = 0.105$; $b/\lambda_o = 0.3$

	WAVEGUIDE A				WAVEGUIDE B			
m	TE_{1m}		TM_{1m+2}		LSE_{1m+2}		LSM_{1m+1}	
0	-.42187	-.06642	6.44151	8.71578	-.01110	-.00703	112.90114	-.32990
2	-.00456	.00591	.53971	1.38273	.00002	.00024	9.60478	43.67913
4	.00026	-.00006	-.03760	.01110	.00002	.00007	.31850	.09105
6	.00008	-.00005	-.08434	-.19051	.00001	-.00001	.38655	-.15653
8	-.00000	-.00002	-.04184	-.11722	.00000	-.00001	-.00038	-.06325
10	-.00002	-.00000	-.00245	-.01924	-.00000	-.00001	-.02038	.00110
12	-.00001	.00000	.01415	.03123	.00000	-.00000	-.03948	.01310
14			.01238	.03340			-.03141	.02156
16			.00341	.01236			.00486	-.00043
18			-.00365	-.00723			.00705	-.00213
20			-.00523	-.01352			.01890	-.00948
22			-.00261	-.00800			-.00156	-.00008
24			.00084	.00104			-.00212	.00061
26			.00251	.00621			-.00936	.00409
28			.00187	.00530			-.00063	.00081
30			.00010	.00088			.00090	-.00024
32			-.00123	-.00288			.00309	-.00120
34			-.00131	-.00352			.00308	-.00164
36			-.00042	-.00143			-.00047	.00011
38			.00055	.00119			-.00096	.00034
40			.00089	.00231			-.00309	.00143
42			.00050	.00147			.00022	-.00002

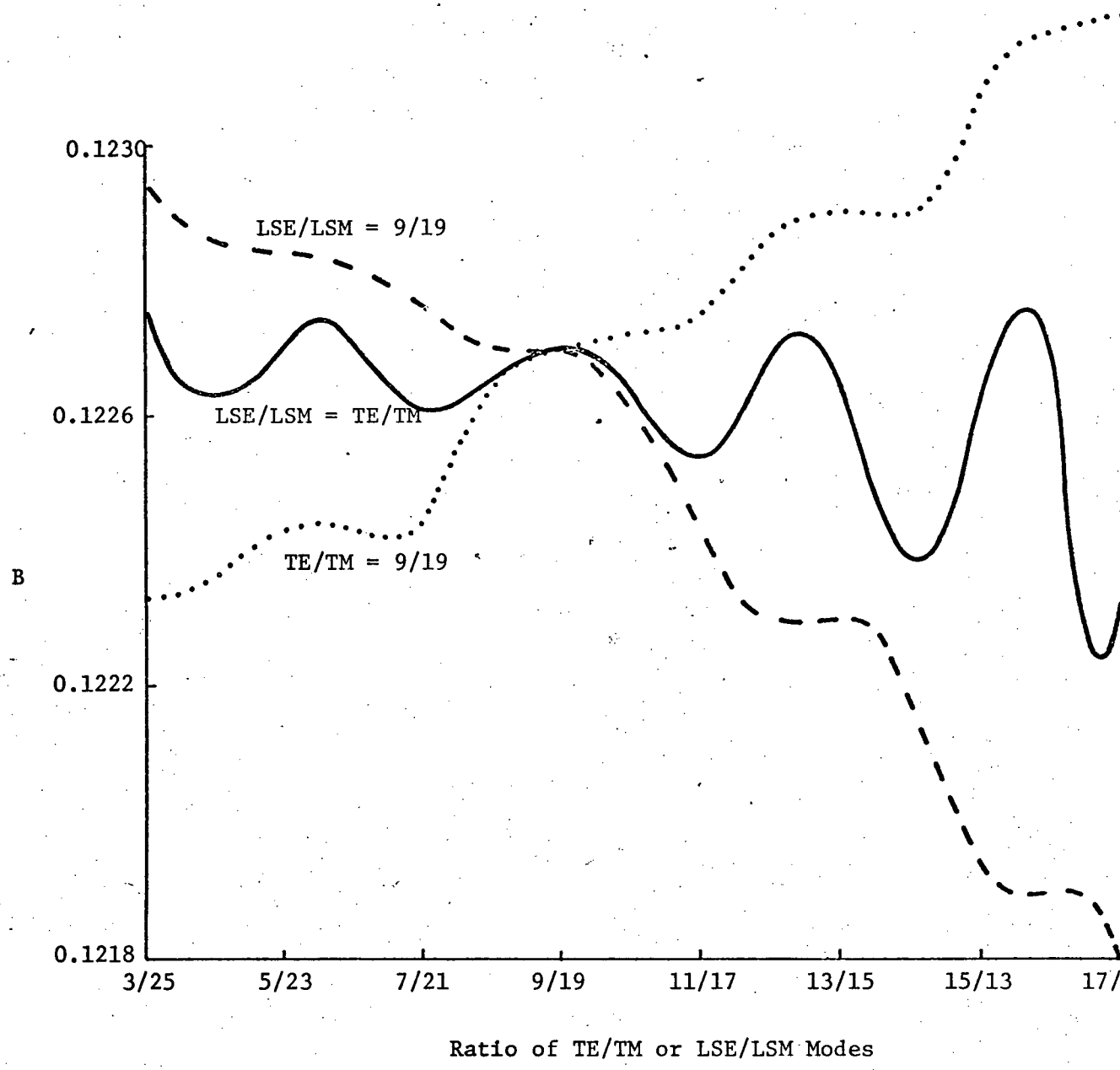

Fig. 11. Effect on the solution for B of varying the ratios of TE:TM and LSE:LSM modes separately and together; $b/\lambda_0 = 0.3$, $2t/b = 0.7$, $\varepsilon_r = 8.0$, $\mu_r = 0.75$, total no. of modes = 28.

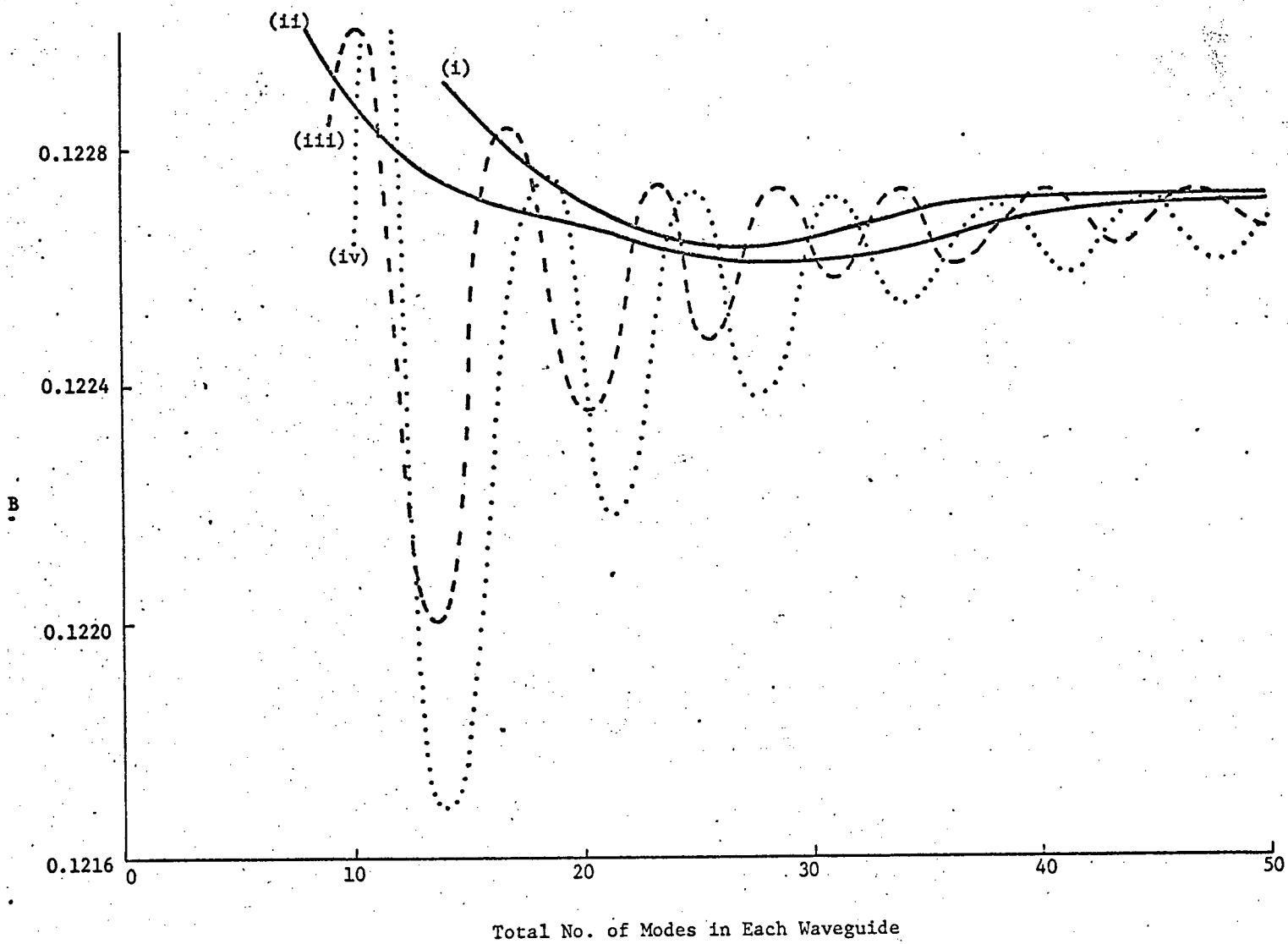

Fig. 12. Convergence of the solution for B with various ratios of TE:TM (= LSE:LSM) modes; $b/\lambda_0 = 0.3$, $2t/b = 0.7$, $\varepsilon_r = 8.0$, $\mu_r = 0.75$.

(i) ratio = 1:6
(ii) ratio = 1:3
(iii) ratio = 1:2
(iv) ratio = 1:1

in this section, the value of B is within 0.1% of its "true" value with a total of 27 or more modes in each waveguide.

The general behaviour of the characteristic admittance as a function of the dielectric thickness is shown in Fig. 10 where it is compared with the Y variations for the two types of E-plane loading considered. Because of the nature of the modes excited in H-plane loading, the next lowest order mode is the LSE_{12} or LSM_{13} mode. Thus, it is possible to use dielectrics with larger values of permittivity than can be used for E-plane loading and still have only one propagating mode. With E-plane loading, $\varepsilon_r \cdot \mu_r$ must be less than 4.712 but with H-plane loading, $\varepsilon_r \cdot \mu_r$ can be as big as 11.635. Two variations in ε_r and μ_r are considered here: (i) with the product $\varepsilon_r \cdot \mu_r$ equal to 6.0, μ_r is varied from 0.5 to 2.0, and (ii) with $\mu_r = 1.0$, ε_r is varied from 2.56 to 9.0. For the first variation, Y is plotted as a function of γ_B/γ_A in Fig. 13. The deviation of Y from γ_B/γ_A with $\mu = \mu_0$ is greater for the H-plane case than for the E-plane case (compare Figs. 8 and 13). The corresponding junction parameters, X and B, are plotted for both variations in Figs. 14 and 15. This time both elements are capacitive, which can be expected since the evanescent modes excited are primarily TM modes, for which the energy stored is predominantly electric. As shown in Fig. 14, with $\varepsilon_r \cdot \mu_r$ held constant, B increases rapidly with the ratio ε_r/μ_r while X remains virtually unchanged. With $\mu = \mu_0$, as ε_r is increased both X and B increase rapidly, although there is little variation in the maximum value of B when ε_r is greater than 6, as indicated in Fig. 15.

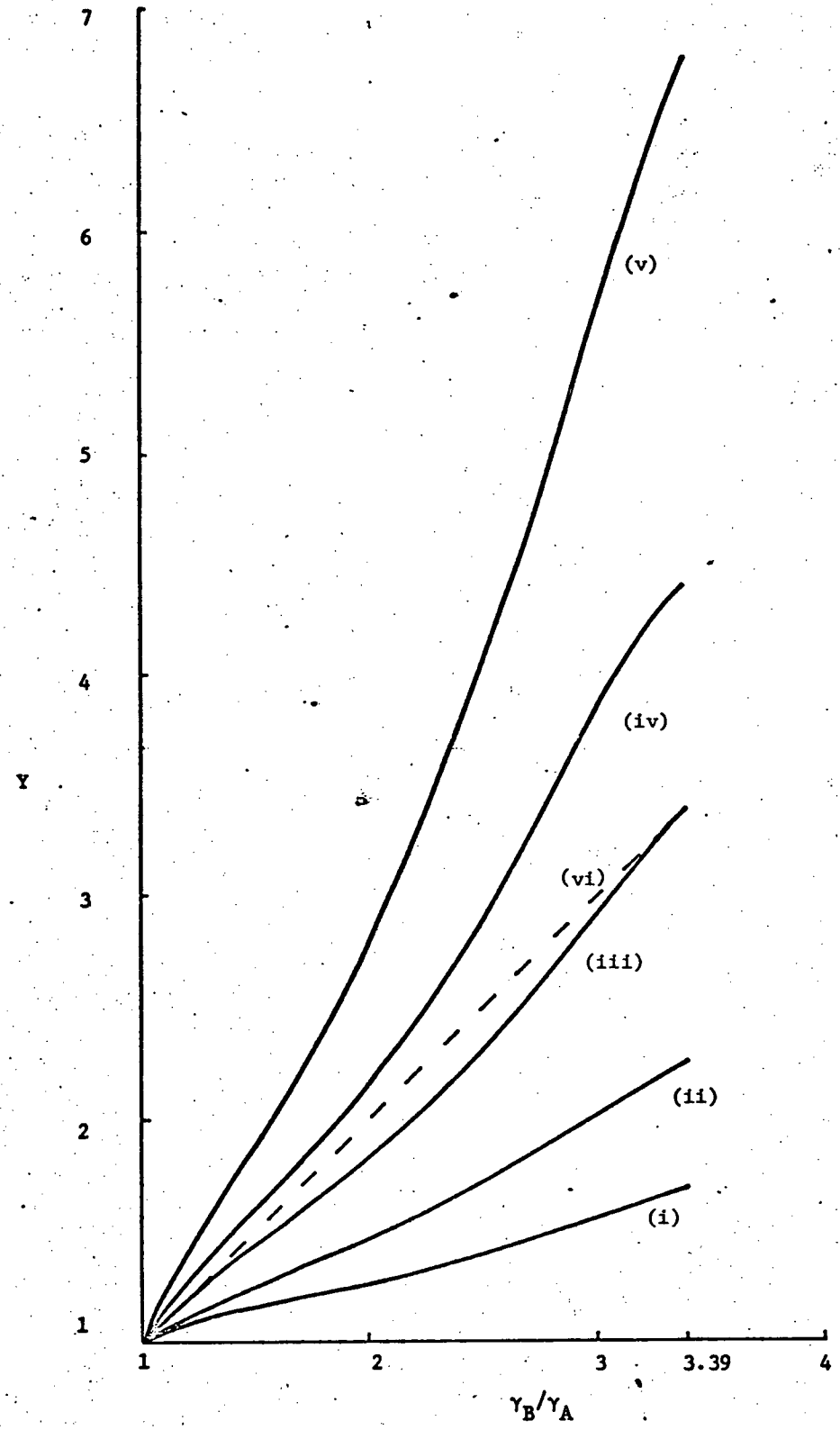

Fig. 13. Normalized characteristic admittance for H-plane loading; $\varepsilon_r \cdot \mu_r = 6.0$, $b/\lambda_0 = 0.3$.

(i) $\varepsilon_r = 3.0$, $\mu_r = 2.0$
(ii) $\varepsilon_r = 4.0$, $\mu_r = 1.5$
(iii) $\varepsilon_r = 6.0$, $\mu_r = 1.0$
(iv) $\varepsilon_r = 8.0$, $\mu_r = 0.75$
(v) $\varepsilon_r = 12.0$, $\mu_r = 0.5$
(vi) reference: $Y = \gamma_B/\gamma_A$

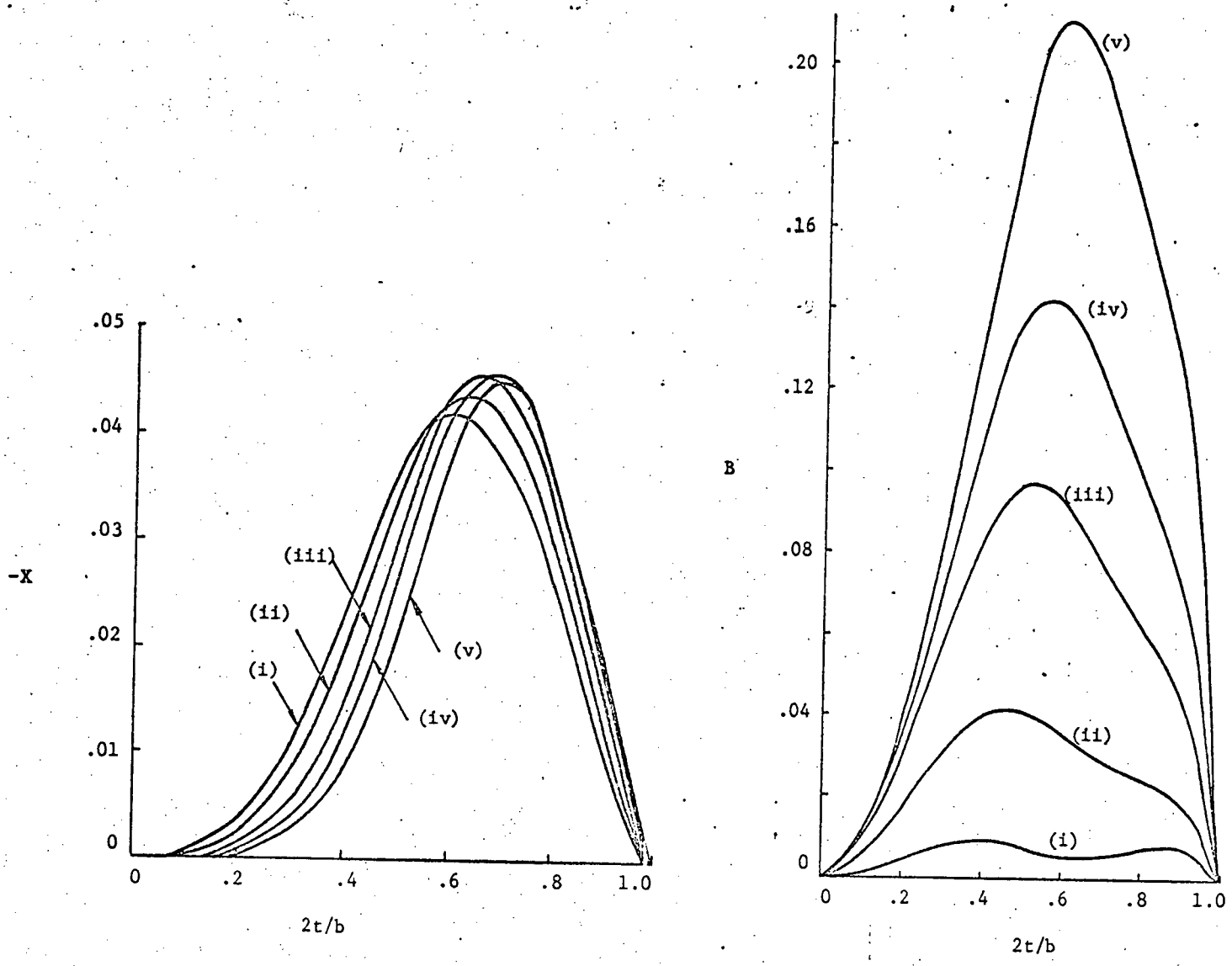

Fig. 14. X and B for H-plane loading; $\varepsilon_r \cdot \mu_r = 6.0$, $b/\lambda_0 = 0.3$.

(i) $\varepsilon_r = 3.0$, $\mu_r = 2.0$

(ii) $\varepsilon_r = 4.0$, $\mu_r = 1.5$

(iii) $\varepsilon_r = 6.0$, $\mu_r = 1.0$

(iv) $\varepsilon_r = 8.0$, $\mu_r = 0.75$

(v) $\varepsilon_r = 12.0$, $\mu_r = 0.5$

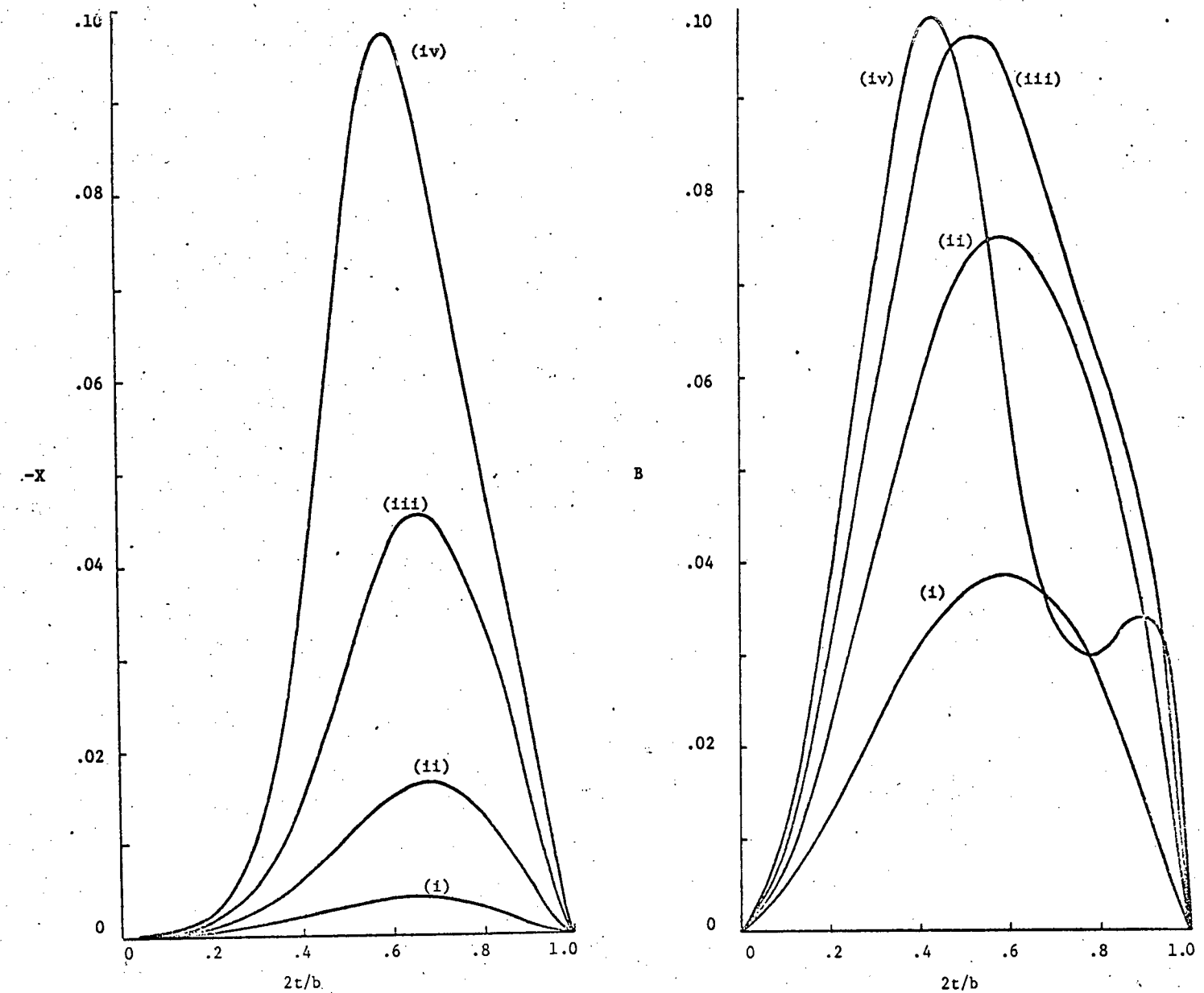

Fig. 15. X and B for H-plane loading; $\mu_r = 1.0$, $b/\lambda_0 = 0.3$.

(i) $\varepsilon_r = 2.56$ (iii) $\varepsilon_r = 6.0$

(ii) $\varepsilon_r = 4.0$ (iv) $\varepsilon_r = 9.0$

Chapter 3

NONRECIPROCAL INHOMOGENEOUS INTERFACE

3.1 Introduction

The analysis in this chapter is concerned with the properties of a nonreciprocal inhomogeneous waveguide interface, and it follows along the lines of that in Chapter 2. In nonreciprocal waveguides, however, the field distributions and the phase coefficients can be very different in the two directions of propagation[2]. Accordingly, one would expect the interface effect and the normalized characteristic admittance to be also different in these two directions. In some cases it is important to evaluate only the combined effect of these two factors. In others, however, it is necessary to isolate the two phenomena, e.g., in order to carry out the analysis and design of the device[10], or to measure a discontinuity within a nonreciprocal section of waveguide. The scattering parameters of a section of twin-slab ferrite-loaded waveguide between two reciprocal homogeneous waveguides have been recently determined[19]. The evaluation in ref. (19) did not require the explicit analysis of the nonreciprocal interface, and there has been as yet no attempt to analyse such an interface fully.

As in the reciprocal case, the nonreciprocal interface problem is solved numerically by means of the mode matching technique. The example chosen here is that of the twin-slab ferrite loaded waveguide, often used as a model for nonreciprocal ferrite phase shifters[2,19,20]. Using the solutions obtained for the reflection and transmission coefficients due to the nonreciprocal interface, it is shown that it is possible to derive simple equivalent transmission circuits which account for the effect of the interface and the equivalent characteristic

admittances of the nonreciprocal inhomogeneous waveguide, separately.

3.2 Mode matching

The configuration analysed is that shown in Fig. 16. The slabs are symmetrically placed about the centre of the waveguide and magnetized transverse to the direction of propagation. This limits the modes excited at the junction between the homogeneous and inhomogeneous waveguides to TE_{n0} modes, where n is odd. The width of the waveguides, a, is such that only the TE_{10} mode may propagate in either waveguide A or waveguide B. For clarity, the modes in the nonreciprocal waveguide, B, are referred to as TE^{+}_{n0} and TE^{-}_{n0} modes for propagation in the positive and negative directions of z, respectively. Only counterclockwise magnetization need be considered, as in Fig. 16(a), since reversal of the magnetization simply has the effect of interchanging junctions 1 and 2. It is necessary, however, to analyse both junctions because different sets of modes are excited at each. In fact, there are four separate situations to consider: the dominant mode from either waveguide A or waveguide B may be incident on either junction 1 or junction 2, as shown in Fig. 17.

The mode matching procedure in this case is basically the same as for reciprocal junctions[17,18]. The transverse electric and magnetic fields are made continuous over the cross-section of the waveguide at the interface and orthogonality relations for each set of modes are used to separate the continuity conditions on the fields into N equations involving the N unknown amplitude constants of the modes. The solution of these equations yields accurate values of the amplitudes of the dominant modes. The orthogonality relations and their implementation, however, are different in the present case; they are, in fact, biorthogonality relations[21]. The following simplified form of these relations is made applicable by

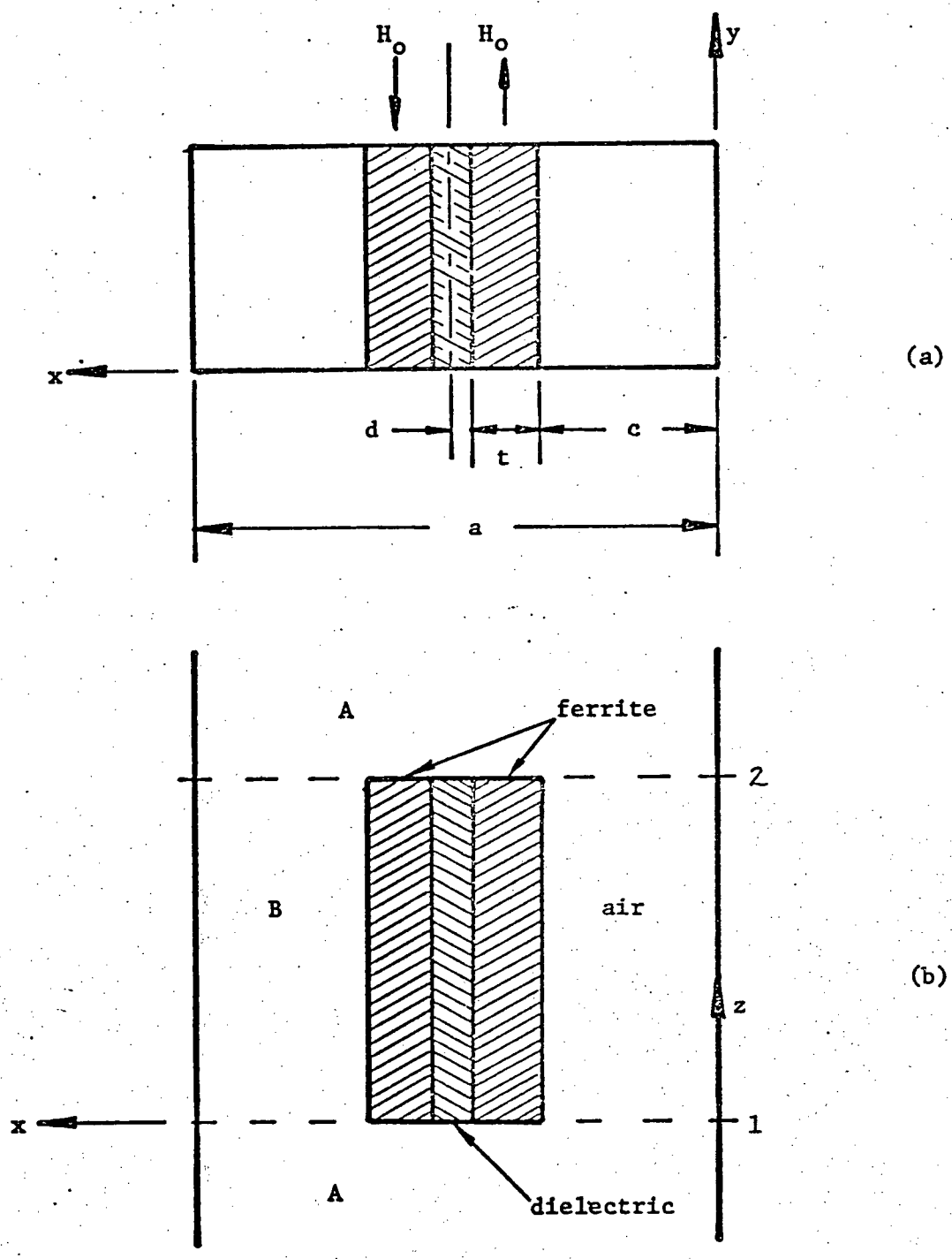

Fig. 16. Twin-slab ferrite phase shifter model.

(a) cross-section, identifying the loading parameters;
(b) longitudinal section, identifying interfaces 1 and 2.

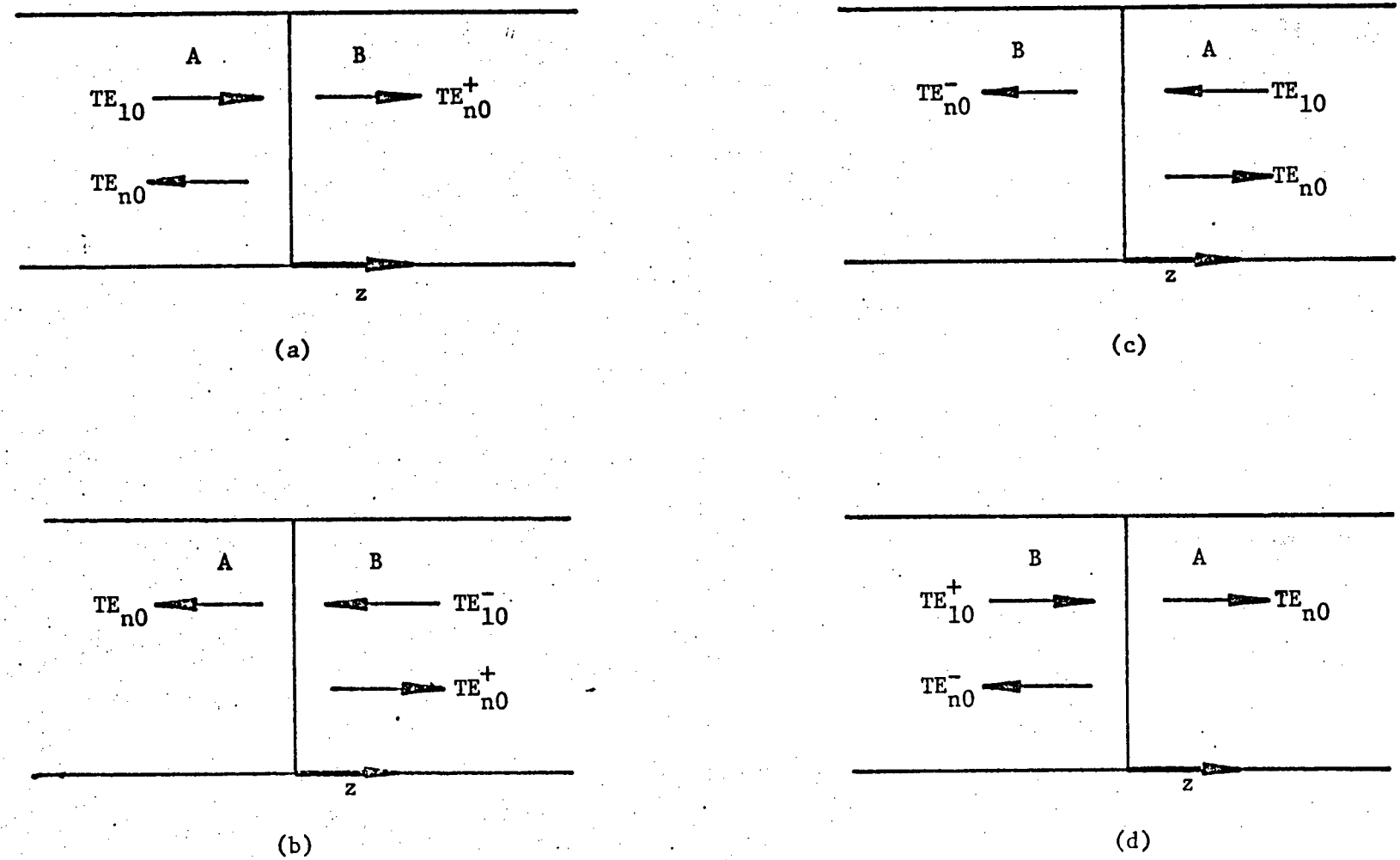

Fig. 17. The modes excited by a single mode incident from either A or B.

(a) interface 1, wave incident from A; (b) interface 1, wave incident from B; (c) interface 2, wave incident from A; (d) interface 2, wave incident from B.

the restriction to transverse magnetization[22]:

$$\int_S [\bar{h}_i \times \bar{e}_j + \bar{h}_j \times \bar{e}_i] \cdot \bar{a}_z ds = 0 \quad , \quad \gamma_i \neq \gamma_j \tag{3}$$

The integration is over the cross-sectional area, S, of the waveguide, $\{\bar{e}_i, \bar{h}_i\}$ is the transverse component of a waveguide mode with propagation coefficient γ_i and $\{\bar{e}_j, \bar{h}_j\}$ is the transverse component of a waveguide mode with propagation coefficient γ_j. The procedure used to separate the continuity conditions on the electric and magnetic fields into two sets of equations is similar to that which has been successfully employed to analyse an H-plane bifurcation in a plasma-filled waveguide[23].

Modal equations need be developed for only two of the four situations shown in Fig. 17: either (a) and (b) or (c) and (d). The other two can be treated similarly. Considering case (a), the total transverse fields are approximated by the following partial sums:

Waveguide A

$$\begin{aligned} \bar{E}_A &= \bar{e}_{A1} + \sum_{i=1}^{N} a_i \bar{e}_{Ai} \\ \bar{H}_A &= \bar{h}_{A1} - \sum_{i=1}^{N} a_i \bar{h}_{Ai} \end{aligned} \tag{4}$$

Waveguide B

$$\begin{aligned} \bar{E}_B &= \sum_{j=1}^{N} b_j^+ \bar{e}_{Bj}^+ \\ \bar{H}_B &= \sum_{j=1}^{N} b_j^+ \bar{h}_{Bj}^+ \end{aligned} \tag{5}$$

The continuity conditions on the transverse fields at the interface may be written either as:

$$\int_S [\bar{h}_{Bj}^- \times \bar{E}_A + \bar{H}_A \times \bar{e}_{Bj}^-] \cdot \bar{a}_z ds = \int_S [\bar{h}_{Bj}^- \times \bar{E}_B + \bar{H}_B \times \bar{e}_{Bj}^-] \cdot \bar{a}_z ds \tag{6}$$

or as,

$$\int_S [\bar{h}_{Bj}^+ \times \bar{E}_A + \bar{H}_A \times \bar{e}_{Bj}^+] \cdot \bar{a}_z ds = \int_S [\bar{h}_{Bj}^+ \times \bar{E}_B + \bar{H}_B \times \bar{e}_{Bj}^+] \cdot \bar{a}_z ds \tag{7}$$

Using eqn. (3), most terms on the right side of eqns. (6) and (7) may be eliminated since:

$$\int_s [\bar{h}^-_{Bn} \times \bar{e}^+_{Bj} + \bar{h}^+_{Bj} \times \bar{e}^-_{Bn}] \cdot \bar{a}_z ds = 0 \quad , \quad \text{for all } j \text{ and } n$$

$$\int_s [\bar{h}^+_{Bn} \times \bar{e}^+_{Bj} + \bar{h}^+_{Bj} \times \bar{e}^+_{Bn}] \cdot \bar{a}_z ds = 0 \quad , \quad j \neq n$$

Substituting eqns. (4) and (5) into (6) and (7) now yields the following two sets of eqns:

$$\int_s [\bar{h}^-_{Bj} \times (\bar{e}_{Al} + \sum_{i=1}^{N} a_i \bar{e}_{Ai}) + (\bar{h}_{Al} - \sum_{i=1}^{N} a_i \bar{h}_{Ai}) \times \bar{e}^-_{Bj}] \cdot \bar{a}_z ds = 0 \tag{8}$$

$$b^+_j = \frac{\int_s [\bar{h}^+_{Bj} \times \bar{e}_{Al} + \bar{h}_{Al} \times \bar{e}^+_{Bj}] \cdot \bar{a}_z ds + \sum_{i=1}^{N} a_i \int_s [\bar{h}^+_{Bj} \times \bar{e}_{Ai} - \bar{h}_{Ai} \times \bar{e}^+_{Bj}] \cdot \bar{a}_z ds}{2 \int_s \bar{h}^+_{Bj} \times \bar{e}^+_{Bj} \cdot \bar{a}_z ds} \tag{9}$$

The set of eqns. (8) consists of N equations in the N unknowns, a_i, $i = 1$ to N. Once determined, the coefficients a_i are then substituted into the set of eqns. (9) to determine the values of b^+_j.

In case (b), the total fields are again approximated by partial sums:

<u>Waveguide A</u>

$$\bar{E}_A = \sum_{i=1}^{N} a_i \bar{e}_{Ai}$$

$$\bar{H}_A = -\sum_{i=1}^{N} a_i \bar{h}_{Ai} \tag{10}$$

<u>Waveguide B</u>

$$\bar{E}_B = \bar{e}^-_{Bi} + \sum_{j=1}^{N} b^+_j \bar{e}^+_{Bj}$$

$$\bar{H}_B = \bar{h}^-_{Bl} + \sum_{j=1}^{N} b^+_j \bar{h}^+_{Bj} \tag{11}$$

The modal equations are:

$$\sum_{i=1}^{N} a_i \int_s [\bar{h}^-_{Bj} \times \bar{e}_{Ai} - \bar{h}_{Ai} \times \bar{e}^-_{Bj}] \cdot \bar{a}_z ds = 2\, \delta_{j,1} \int_s \bar{h}^-_{B1} \times \bar{e}^-_{B1} \cdot \bar{a}_z ds \tag{12}$$

$$b_j^+ = \frac{\sum_{i=1}^{N} a_i \int_s [\bar{h}^+_{Bj} \times \bar{e}_{Ai} - \bar{h}_{Ai} \times \bar{e}^+_{Bj}] \cdot \bar{a}_z ds}{2 \int_s \bar{h}^+_{Bj} \times \bar{e}^+_{Bj} \cdot \bar{a}_z ds} \tag{13}$$

where $\delta_{j,1}$ is the kronecker delta.

It is desirable that the expressions for $\{\bar{e}_{Ai}, \bar{h}_{Ai}\}$ and $\{\bar{e}^{\pm}_{Bi}, \bar{h}^{\pm}_{Bi}\}$ should have the same form in order to avoid difficulty when deriving the equivalent transmission line networks from a_1 and $b_1^{\pm}$. Suitable expressions are given in Appendix C, along with the transcendental equations for the $TE^{\pm}_{n0}$ modes.

3.3 Normalized reflection and transmission coefficients

Once solutions have been obtained for the amplitude coefficients, a_i and $b_j^{\pm}$, one can proceed to derive relations for the normalized reflection and transmission coefficients for the interface. Referring to Fig. 18 and using conservation of energy, we can write for case 17(a):

$$(1 - |a_1|^2)\, I_A = |b_1^+|^2\, I_B^+ \tag{14}$$

where $I_A = \int_s \bar{e}_{A1} \times \bar{h}^*_{A1} \cdot \bar{a}_z ds$,

$I_B^+ = \int_s \bar{e}^+_{B1} \times (\bar{h}^+_{B1})^* \cdot \bar{a}_z ds$

and a_1 and b_1^+ are determined from eqns. (8) and (9).

Rearranging, eqn. (14) has the form,

$$1 - |R_1|^2 = Y^+ |T_2|^2 = |\hat{T}_2|^2 \tag{15}$$

where $R_1 = a_1$ is the reflection coefficient in waveguide A

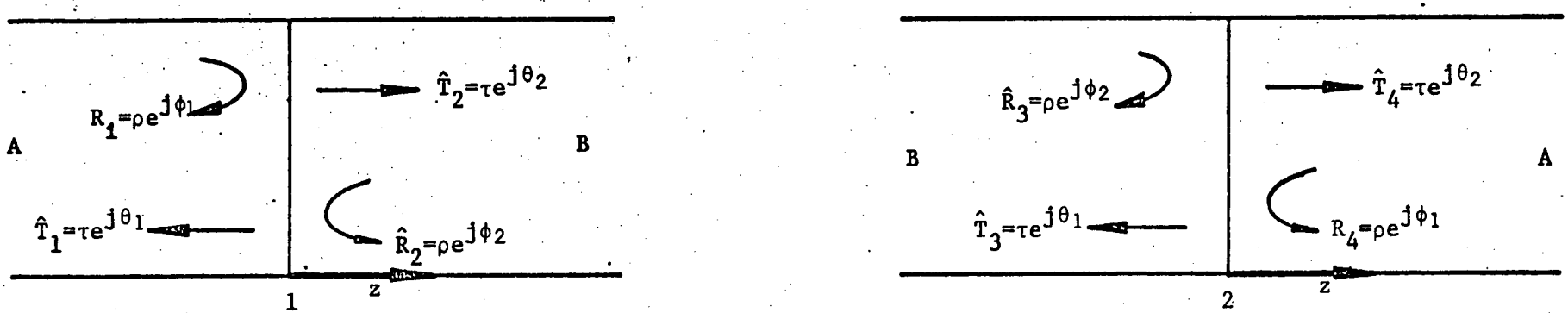

Fig. 18. Identification of the reflection and transmission coefficients. (a) interface 1; (b) interface 2.

and $\hat{T}_2 = b_1^+(I_B^+/I_A)^{\frac{1}{2}}$ is the normalized transmission coefficient in waveguide B. Similarly, for case 17(b):

$$I_B^- - |b_1^+|^2 I_B^+ = |a_1|^2 I_A \tag{16}$$

where $I_B^- = \int_s \bar{e}_{\bar{B}1} \times (\bar{h}_{\bar{B}1})^* \cdot \bar{a}_z ds$

and a_1 and b_1^+ are determined from eqns. (12) and (13).

Rearranging, eqn. (16) has the form,

$$1 - \frac{Y^+}{Y^-} |R_2|^2 = \frac{1}{Y^-} |T_1|^2 \tag{17a}$$

or, $$1 - |\hat{R}_2|^2 = |\hat{T}_1|^2 \tag{17b}$$

where $\hat{R}_2 = b_1^+(I_B^+/I_B^-)^{\frac{1}{2}}$ is the normalized reflection coefficient in waveguide B and $\hat{T}_1 = a_1(I_A/I_B^-)^{\frac{1}{2}}$ is the normalized transmission coefficient in waveguide A. In the above eqns., Y^+ and Y^- are the equivalent characteristic admittances of waveguide B normalized to that of waveguide A for propagation in the positive and negative directions of z, respectively.

The normalized scattering matrix for the interface is unitary. Thus, the following relations, as implied in Fig. 18, must be satisfied:

$$\begin{aligned} |R_1| &= |\hat{R}_2| = \rho \\ |\hat{T}_1| &= |\hat{T}_2| = \tau \end{aligned} \tag{18}$$

and in addition,

$$\begin{aligned} 1 - \rho^2 &= \tau^2 \\ \phi_1 + \phi_2 - \theta_1 - \theta_2 &= \pm\pi \end{aligned} \tag{19}$$

The numerical results are consistent with this condition provided a large number of modes (40 or more) are used for the mode matching. However, accurate results can be obtained with fewer modes, if the magnitudes and phase angles of the normalized reflection and transmission coefficients

are averaged. Referring to Fig. 18, the numerical results also show that $\hat{T}_3 = \hat{T}_1$, $\hat{T}_4 = \hat{T}_2$, $\hat{R}_3 = \hat{R}_2$ and $R_4 = R_1$.

3.4 Equivalent circuit representation

It is convenient to express the behaviour of the interface in terms of an equivalent transmission network, as shown in Fig. 19. With this representation, the nonreciprocal nature of the junction is accounted for by allowing the reactive elements to have different values corresponding to propagation in the positive or negative direction of z, and incidence from waveguide A or waveguide B. Hence, these parameters are identified by the superscripts + or - , and the subscripts A or B. The dashed boxes indicate that the series elements, $X_B^{\pm}$, appear at this alternative position for some values of ferrite loading parameters. This situation is signified by the overscript, ~. Waveguide B is represented by a nonreciprocal transmission line with normalized characteristic admittances, $Y^{\pm}$. The input impedance at port A is thus given by:

$$Z_{in}^{\pm} = j\, X_A^{\pm} + \frac{1}{Y^{\pm} + j\, B_A^{\pm}} = \frac{1 + \rho e^{j\phi_1}}{1 - \rho e^{j\phi_1}} \tag{20}$$

and at port B, the input admittance (or impedance) is given by:

$$Y_{in}^{\pm} = \frac{1}{Z_{in}^{\pm}} = j\, B_B^{\pm} + \frac{1}{1 + j\, X_B^{\pm}} \qquad (\tilde{X}_B^{\pm} = 0)$$

$$\text{or,} \qquad Z_{in}^{\pm} = j\, \tilde{X}_B^{\pm} + \frac{1}{1 + j\, B_B^{\pm}} \qquad (X_B^{\pm} = 0) \tag{21}$$

$$\text{where} \qquad Z_{in}^{\pm} = \frac{1 + \sqrt{Y^{\pm}/Y^{\mp}}\, \rho e^{j\phi_2}}{Y^{\pm} - \sqrt{Y^{+}Y^{-}}\, \rho e^{j\phi_2}} \tag{22}$$

The transmission coefficients, for modes incident from waveguide A, are:

$$\tau e^{j\theta_2} = \frac{(1 - \rho e^{j\phi_1})\sqrt{Y^{+}}}{Y^{+} + j\, B_A^{+}} \tag{23}$$

$$\text{and} \qquad \tau e^{j\theta_1} = \frac{(1 - \rho e^{j\phi_1})\sqrt{Y^{-}}}{Y^{-} + j\, B_A^{-}} \tag{24}$$

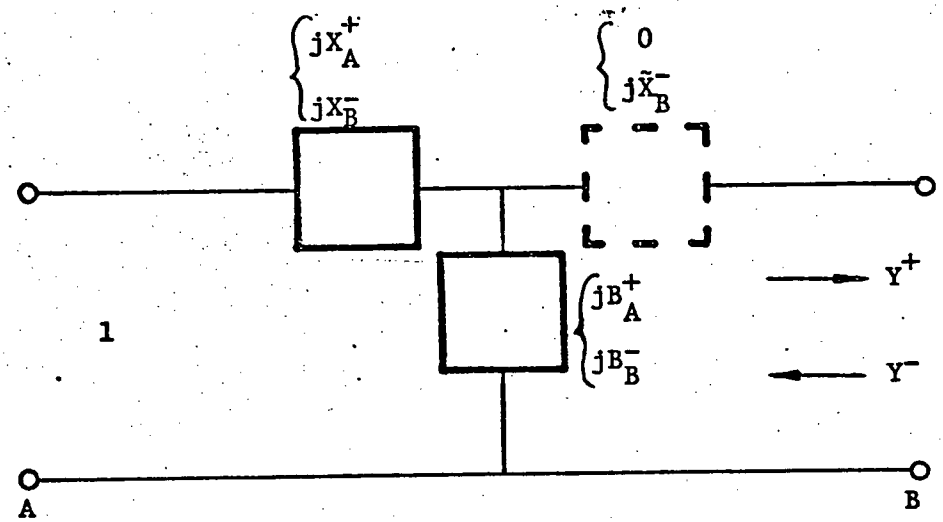

(a)

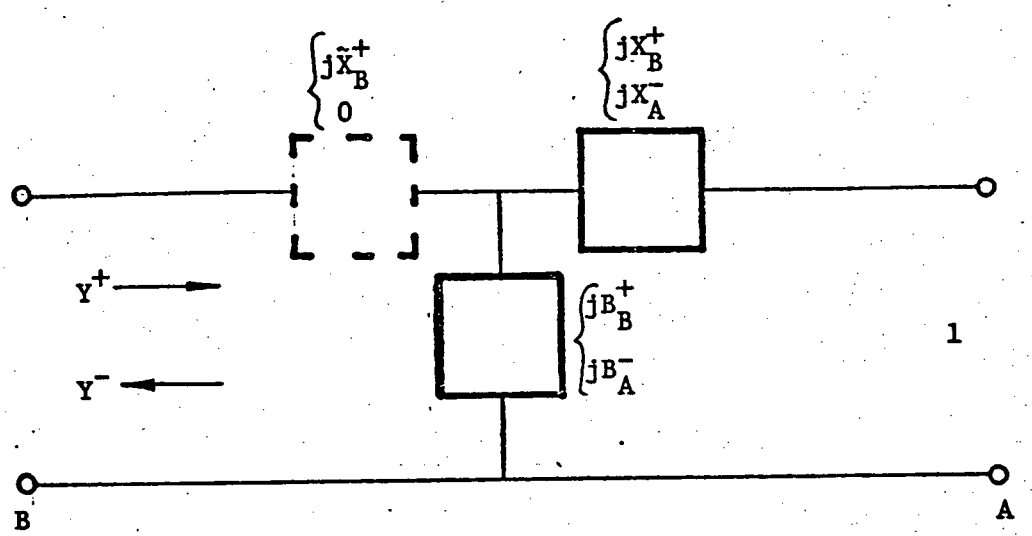

(b)

Fig. 19. Equivalent transmission line representation of the junction. (a) interface 1; (b) interface 2.

Equations (20) - (24) are used to calculate values for the equivalent circuit parameters from ρ, τ, ϕ_1, ϕ_2, θ_1 and θ_2. As compared with the reciprocal case where three circuit elements are derived from three independent measurable quantities, here five circuit elements are derived from four independent quantities. Consequently, the circuit elements are not independent in this case although they are unique. The reason for the extra circuit element is the fact that two reciprocal equivalent circuits, each valid in only one direction of propagation, are used to represent a nonreciprocal interface.

3.5 Numerical results and discussion

In order to obtain realistic results, the values chosen for the ferrite saturation magnetization and remanence ratio are typical of those of ferrites used at X-band in nonreciprocal phase shifters. The elements of the permeability tensor were derived from these values, based on empirical formulas recently published by Green and Sandy[24]. Table 2 lists the pertinent data. The twin-slab parameters, d, c and t, are identified in Fig. 16 and the loading dielectric is assumed to have a relative permittivity, ε_d, of either 1 or 16. The normalized waveguide width, a/λ_0, is 0.65 for all the results. The number of modes used for the mode matching solutions is 25 in all cases and the accuracy was checked by comparing the results of one case with the corresponding results obtained with 40 modes. This check indicated that the values calculated for the interface parameters are accurate to at least four decimal places.

Properties of the nonreciprocal waveguide, B, are shown in Fig. 20 where the normalized phase coefficients, β_B^+/β_A and β_B^-/β_A, the normalized equivalent characteristic admittance, Y^+, and the percentage

Table 2. Assumed characteristics of the ferrite

Saturation magnetization, $4\pi M_s$ (Gauss)	2000
Remanence ratio, M_r/M_s	0.8
$\gamma 4\pi M_s/\omega$ at 8.5 GHz	0.66
Permeability tensor:	
diagonal element, μ	0.96
off-diagonal element, κ	-0.528
Effective relative permeability, μ_e	0.67
Relative permittivity, ε_f	12.0

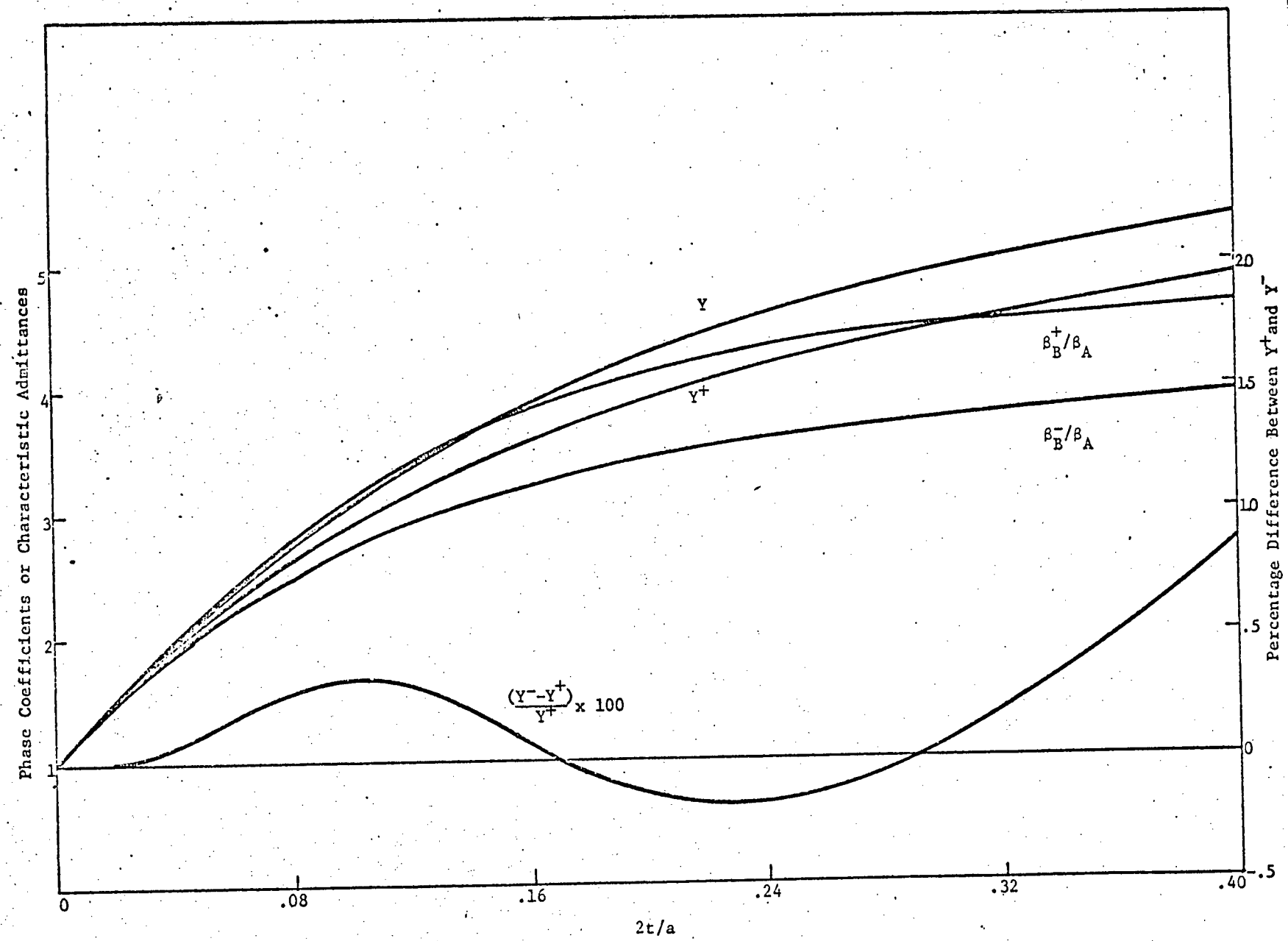

Fig. 20(a) Normalized phase coefficients and equivalent characteristic admittances of waveguide B versus 2t/a; 2d/a = 0.04, $\varepsilon_d = 1$.

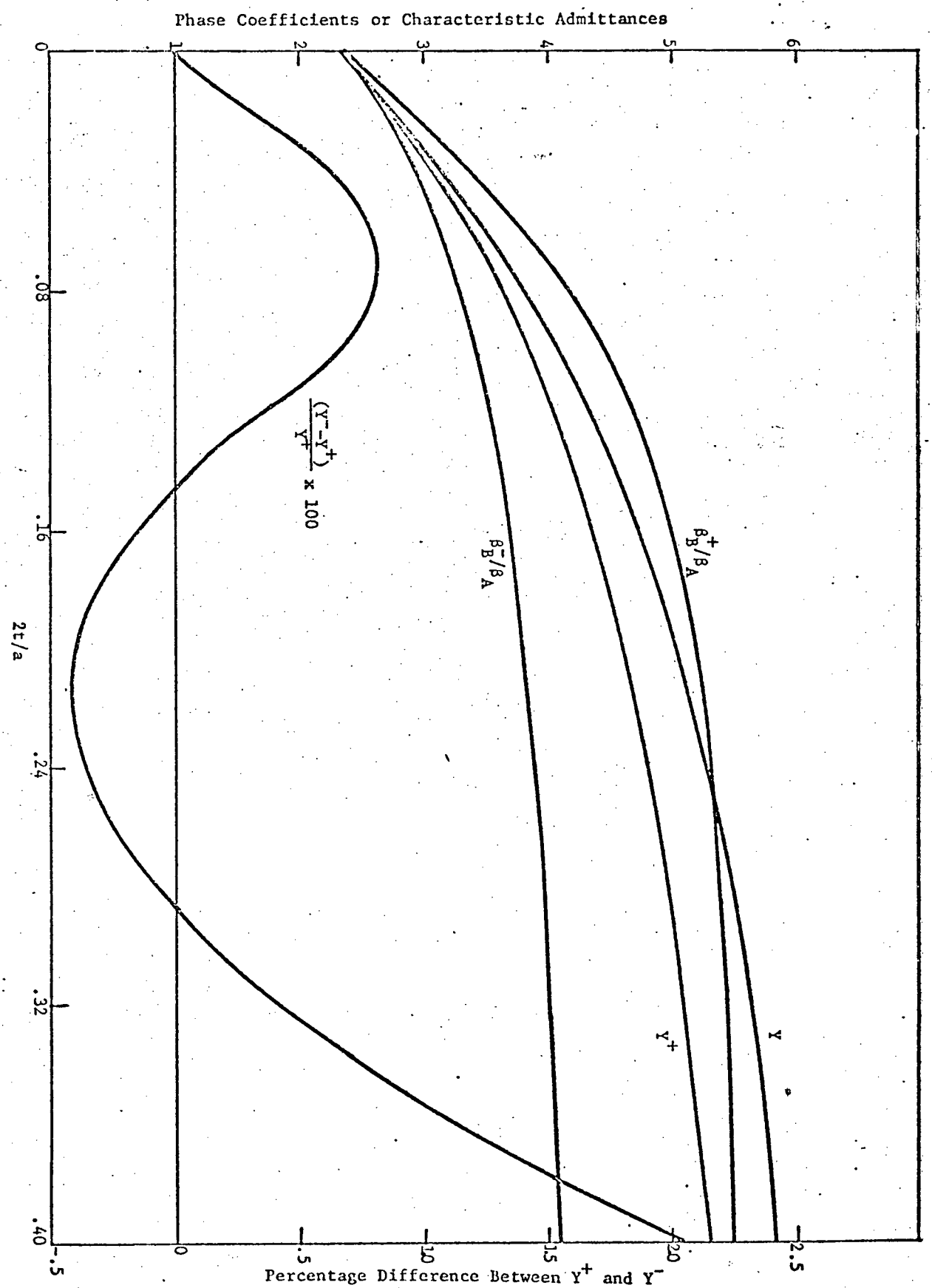

Fig. 20(b) Normalized phase coefficients and equivalent characteristic admittances of waveguide B versus 2t/a; 2d/a = 0.04, ε_d = 16.

difference between Y^+ and Y^- are plotted as a function of 2t/a. It is seen that although the normalized phase coefficients can be quite different, the difference between Y^+ and Y^- is very small indeed, contrary to initial (intuitive) expectations. With this result in mind ($Y^+ \doteq Y^-$), one might wonder whether these admittances could be determined from the simpler case of twin-slab dielectric loading. The relative admittance, Y, in Fig. 20 was obtained for a loading dielectric with relative permittivity, ε_f, and relative permeability, μ_e. The two curves, Y and Y^+ (or Y^-), are similar but for most values of the thickness, t, there is a significant difference between the two.

The properties of the interface between waveguides A and B are shown in Figs. 21 - 23. The magnitudes and phase angles of the normalized reflection and transmission coefficients, as defined in Fig. 18, are plotted in Fig. 21 for ε_d=1 (the curves for ε_d=16 are similar). The elements of the equivalent circuit of the interface, determined from these parameters, are plotted in Figs. 22 and 23 for the cases of ε_d=1 and 16, respectively. It is worth noting that there are two possible solutions for each of $X_B^{\pm}$ and $B_B^{\pm}$ as obtained from eqns. (21) and (22). However, only one solution is shown here.

It may be instructive to discuss the behaviour of the interface in terms of stored energy. An inspection of eqns. 20 - 22 shows that the reactive part of the interface impedance is positive when ϕ_1 (or ϕ_2) is between 0 and π radians, for incidence from waveguide A (or waveguide B). Referring to Fig. 21, the interface impedance from waveguide A has a positive reactance if 2t/a is less than 0.36; i.e., the stored energy is magnetic for small ferrite thicknesses, changing to electric for larger thicknesses. The junction behaviour is somewhat different when the wave is incident from waveguide B; the change from

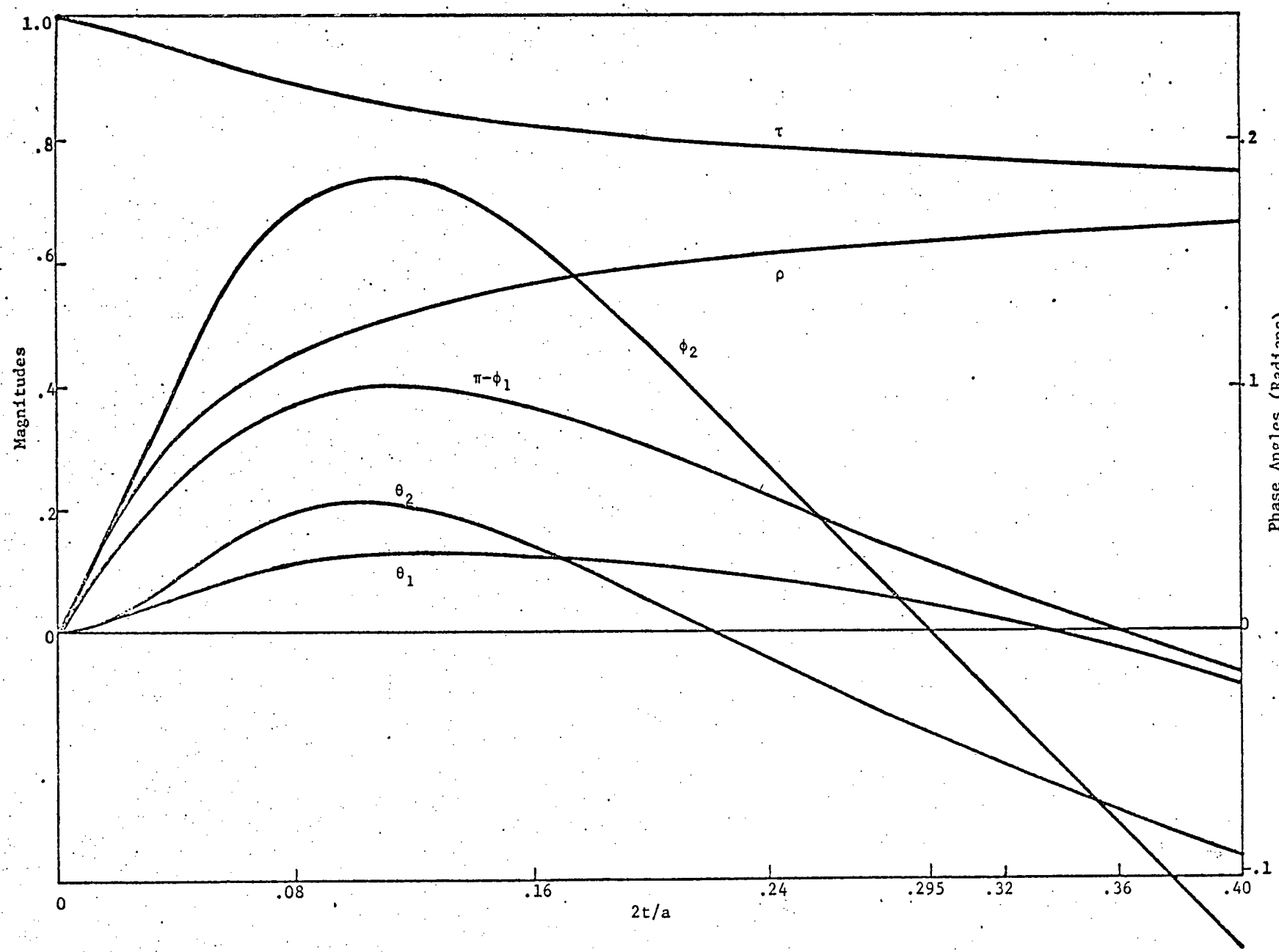

Fig. 21. Reflection and transmission coefficient parameters versus 2t/a; 2d/a = 0.04, $\varepsilon_d = 1$.

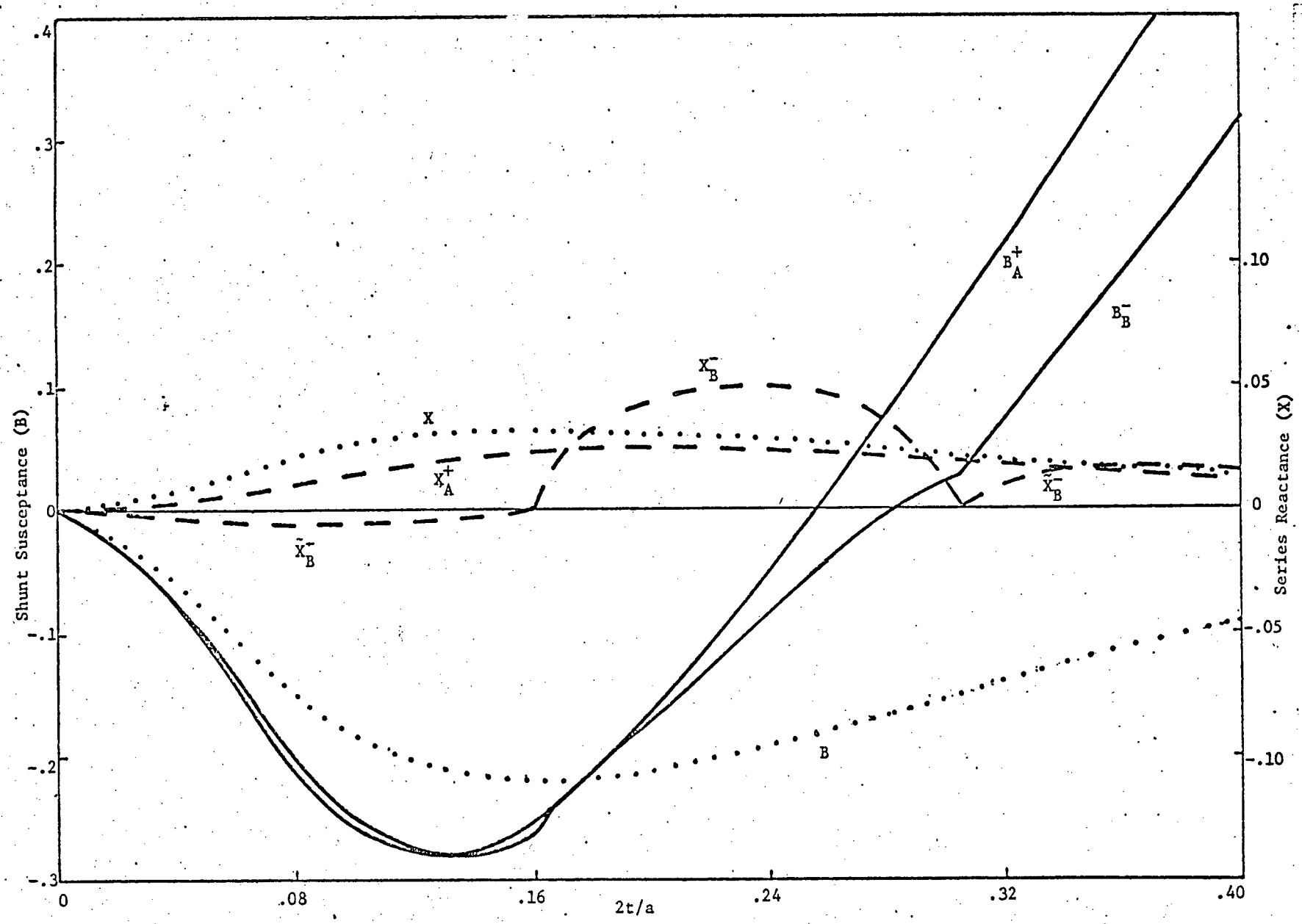

Fig. 22(a) Interface 1 equivalent circuit parameters versus 2t/a; 2d/a = 0.04, ε_d = 1.

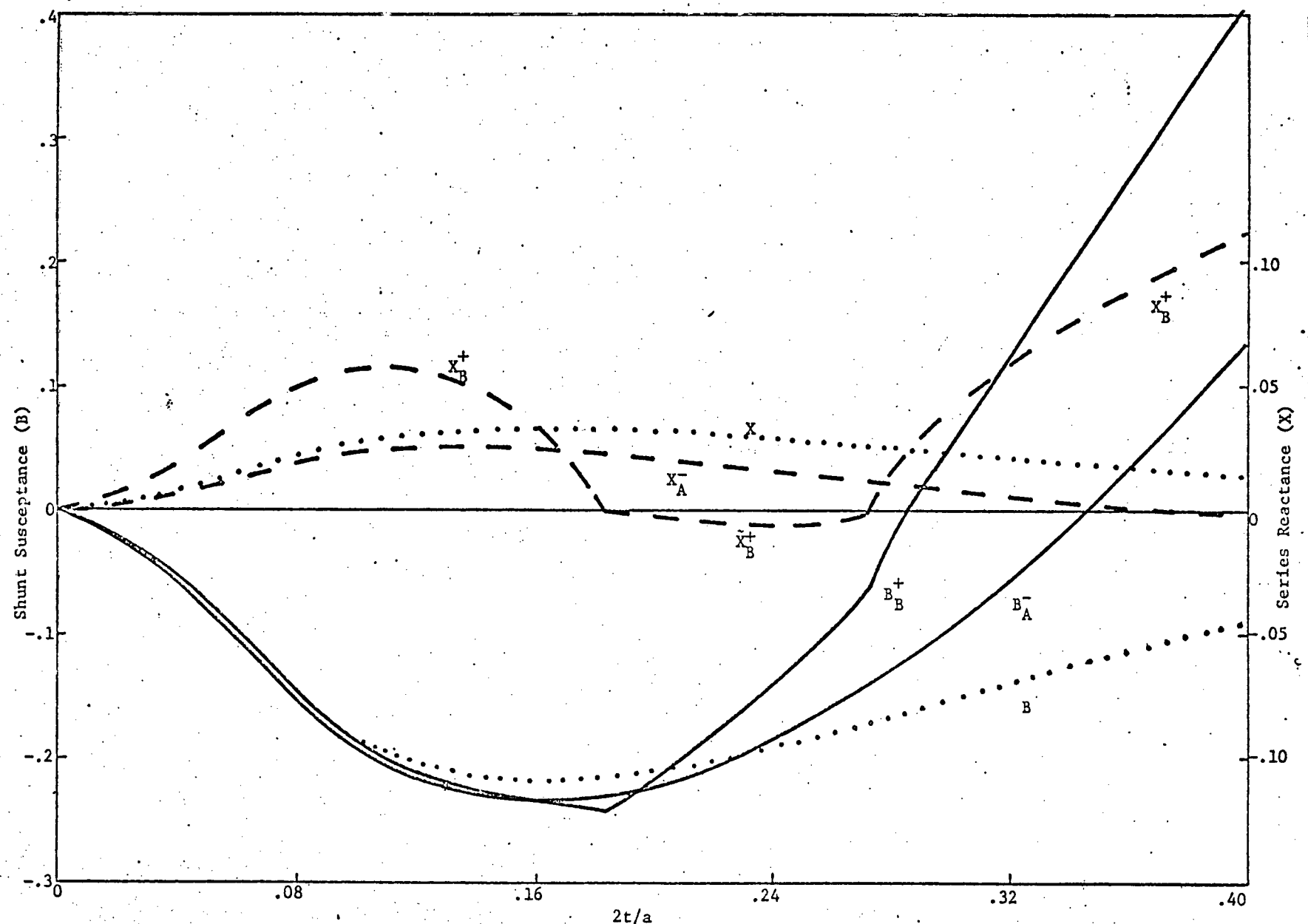

Fig. 22(b) Interface 2 equivalent circuit parameters versus 2t/a; 2d/a = 0.04, ε_d = 1.

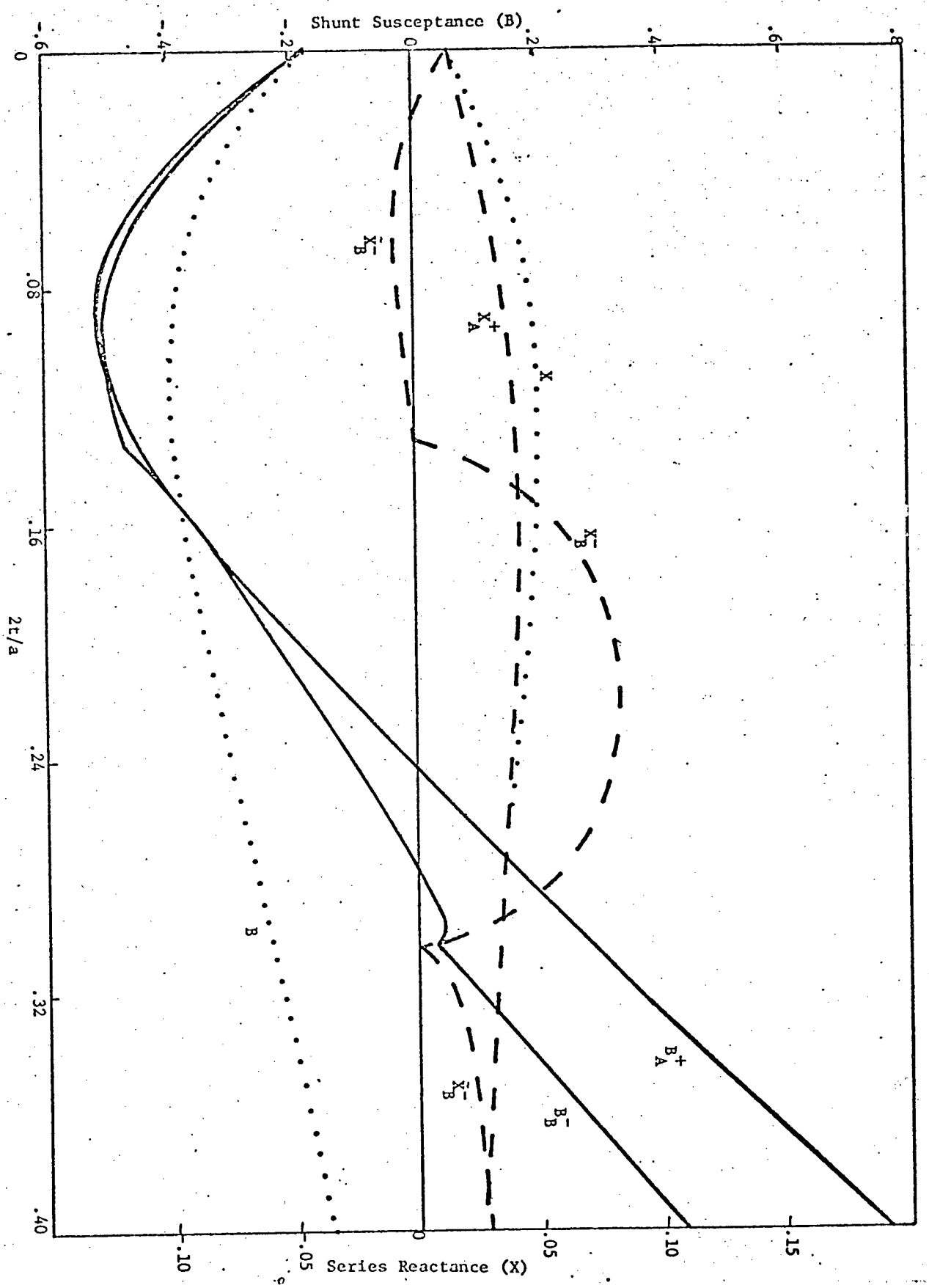

Fig. 23(a) Interface 1 equivalent circuit parameters versus 2t/a; 2d/a = 0.04, ε_d = 16.

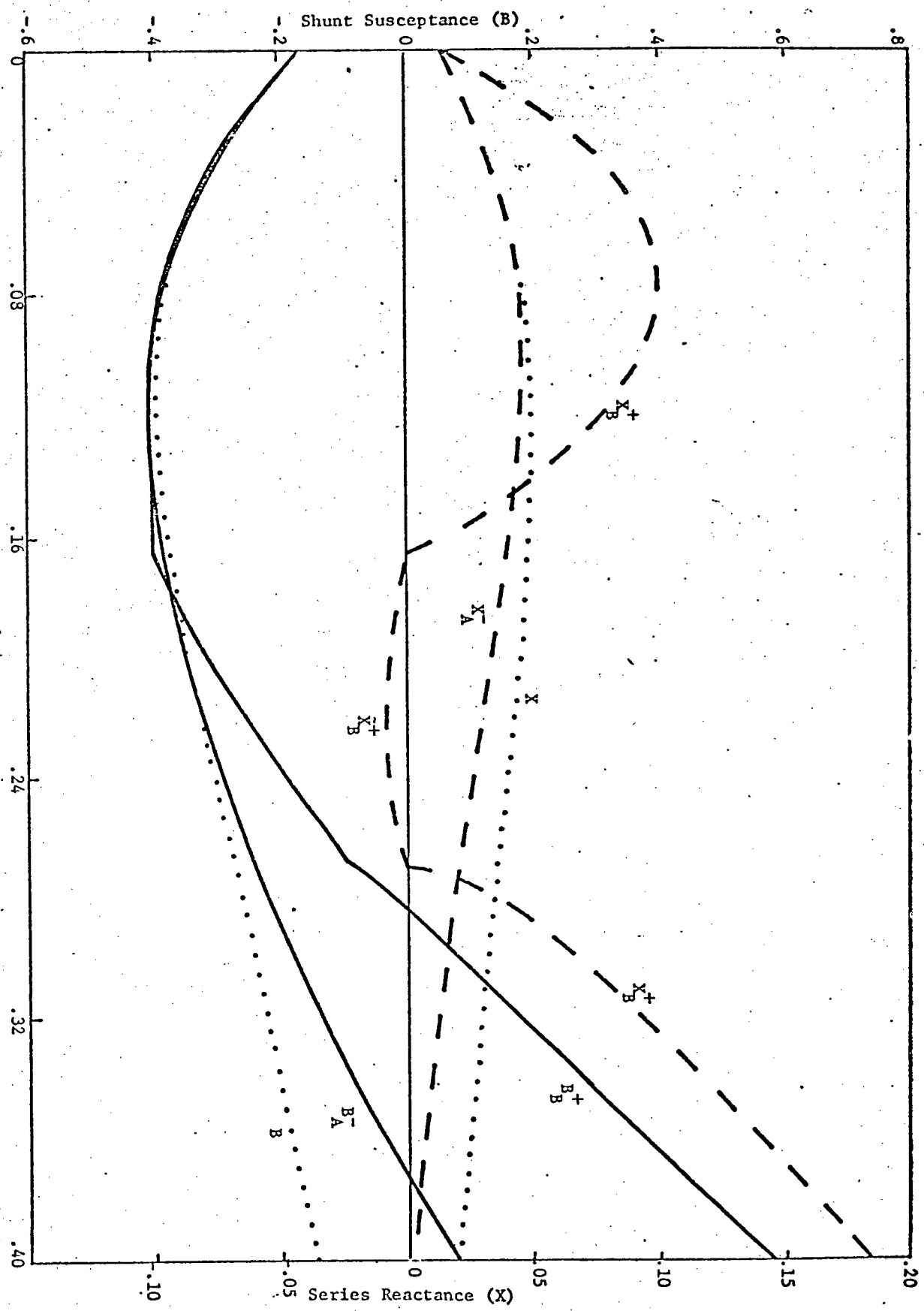

Fig. 23(b) Interface 2 equivalent circuit parameters versus 2t/a; 2d/a = 0.04, ε_d = 16.

magnetic to electric stored energy occurs at $2t/a = 0.295$. This behaviour is of course reflected in the values of the elements of the interface equivalent circuit.

The case of twin-slab dielectric loading again provides an interesting comparison. The equivalent circuit elements, X and B, obtained for this case are also shown in Figs. 22 and 23. It can be seen that the stored energy is magnetic for all values of the dielectric thickness, t, which is consistent with the results of Chapter 2. Thus, although the nonpropagating modes excited with either dielectric or ferrite loading are all TE, the effect of the interface can be markedly different in the two cases.

For the sake of completeness, the dependence of the various parameters on the slab separation, d, was also investigated. A typical case, where $2t/a = 0.24$ and $\varepsilon_d = 16$, is shown in Figs. 24 and 25. The difference between Y^+ and Y^- is again found to be very small and is virtually unaffected by changes in d, as shown in Fig. 24. The corresponding reactive elements of the equivalent circuit are plotted in Fig. 25.

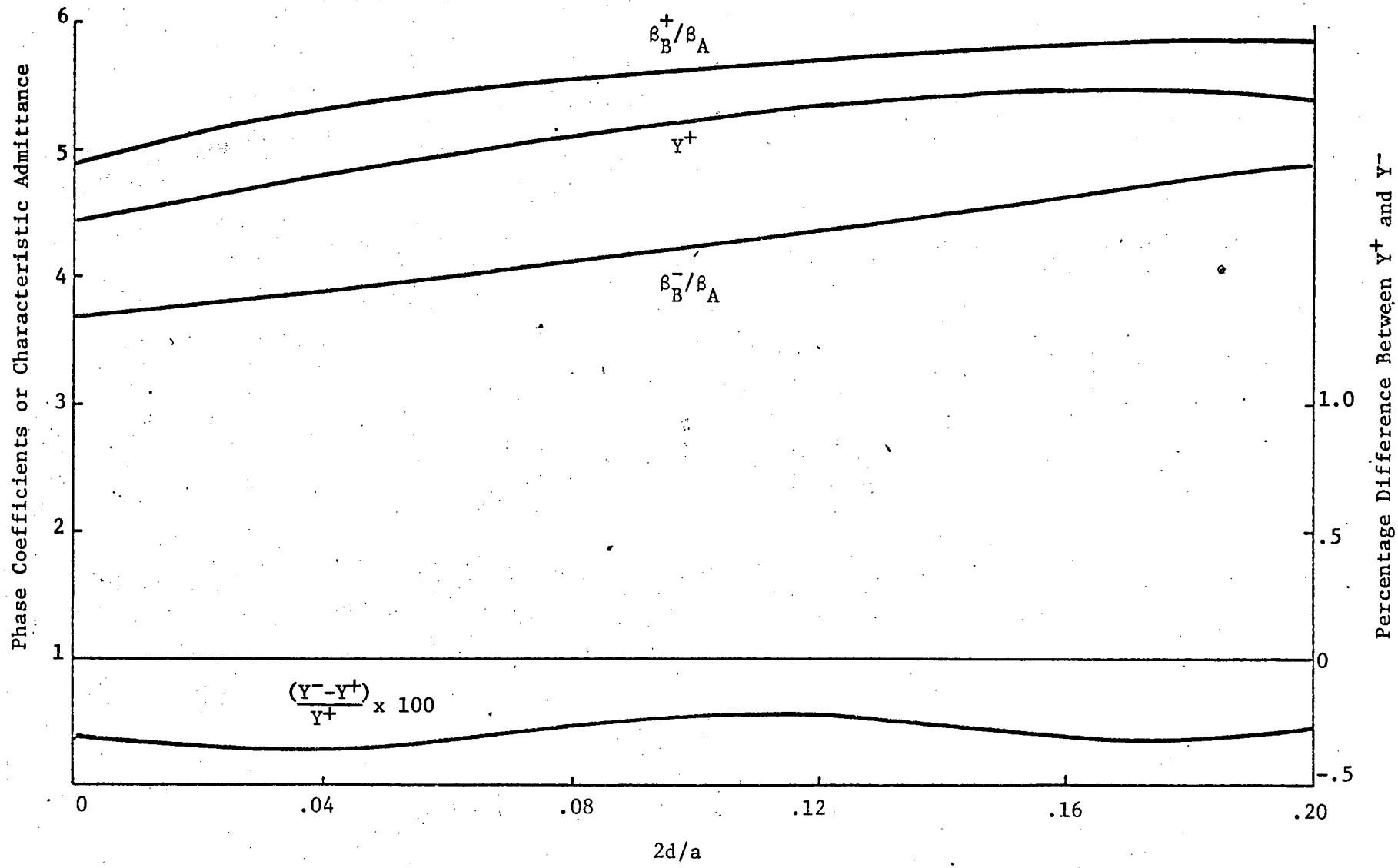

Fig. 24. Normalized phase coefficients and equivalent characteristic admittances of waveguide B versus 2d/a; 2t/a = 0.24, ε_d = 16.

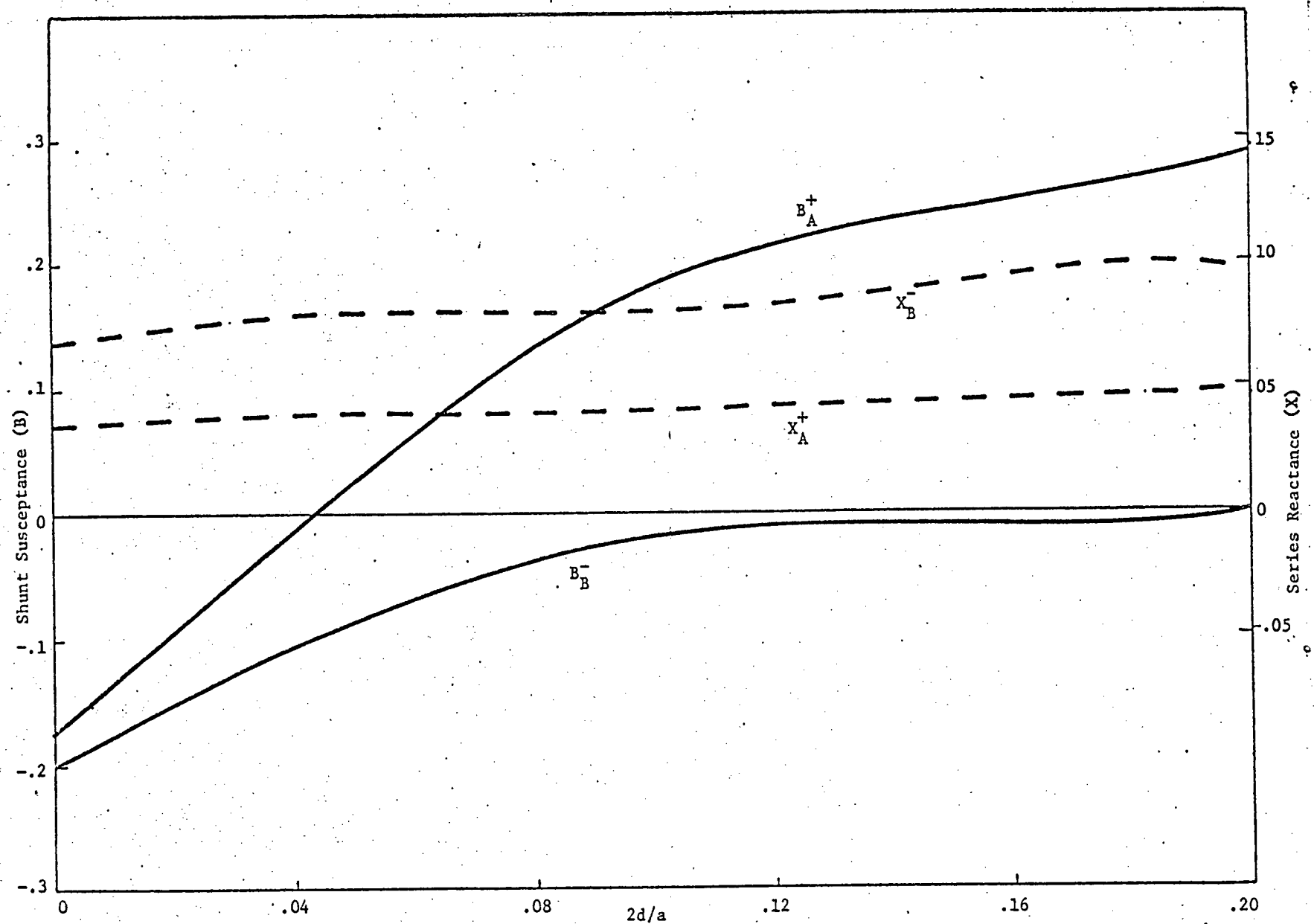

Fig. 25(a) Interface 1 equivalent circuit parameters versus 2d/a; $2t/a = 0.24$, $\varepsilon_d = 16$.

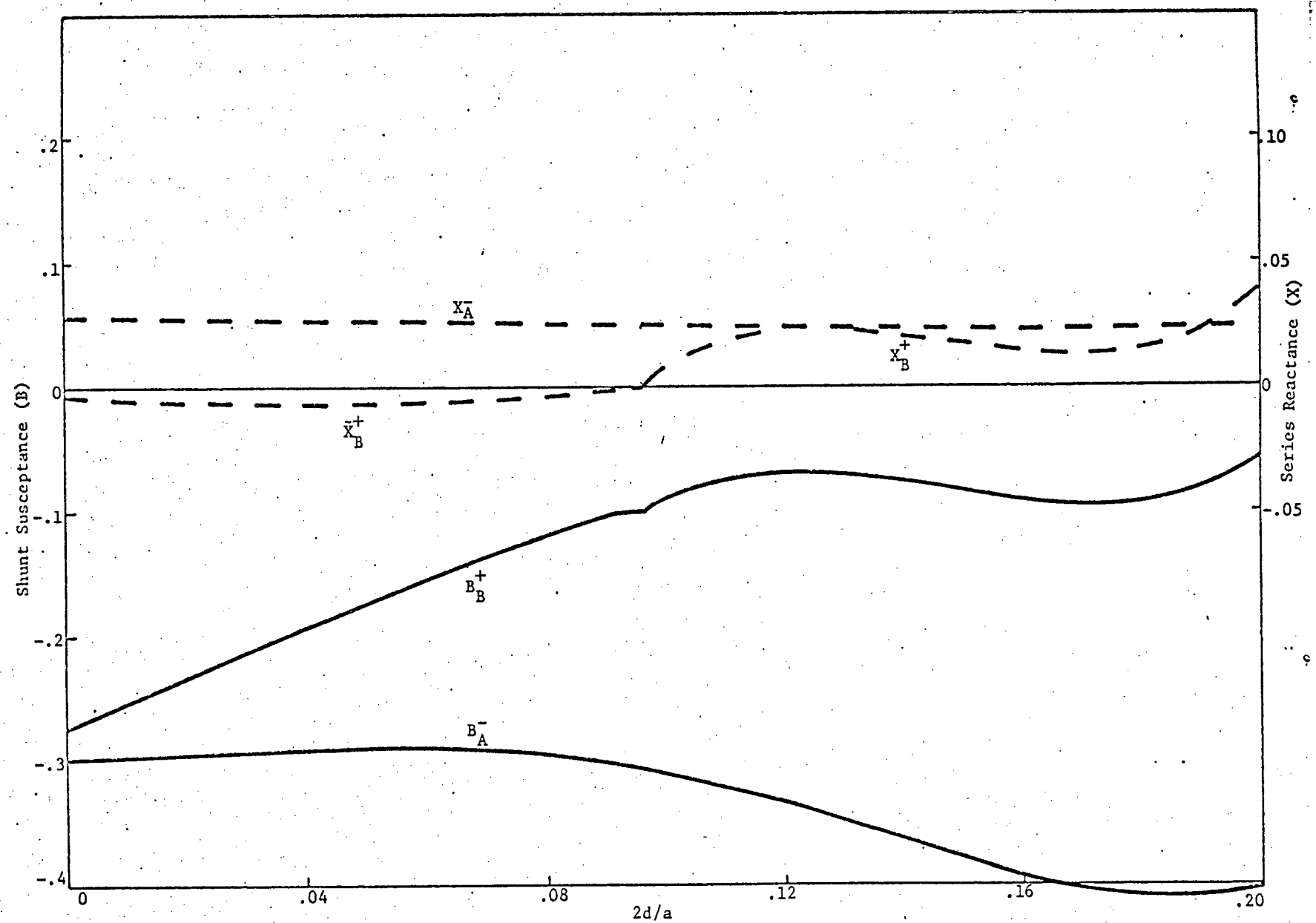

Fig. 25(b) Interface 2 equivalent circuit parameters versus 2d/a; $2t/a = 0.24$, $\varepsilon_d = 16$.

Chapter 4

EXPERIMENTAL INVESTIGATION

4.1 Introduction

The main objective of this thesis has been stated earlier as being the determination of the effect of a metal diaphragm in a nonreciprocal inhomogeneous waveguide. It may be possible to do this analytically for the theoretical twin-slab ferrite model but it was thought unlikely for the more complex ferrite toroid configurations used in practice. The modes in such structures are complicated hybrid modes, for which it would be very difficult to derive analytical expressions. Hence, it was decided that the effect of the diaphragm would have to be measured experimentally. Since a theoretical analysis did not appear feasible, the accuracy of the experimental results was difficult to assess. This was accomplished by an indirect method: the effect of a metal diaphragm in a reciprocal inhomogeneous waveguide was also determined experimentally, but the configuration was chosen so that theoretical results could be obtained for comparison. The accuracy of the results for the reciprocal case was then used as an indication of the accuracy of the results for the nonreciprocal case.

4.2 Method of measurement

Before the effect of a diaphragm in inhomogeneous waveguide could be measured, the problem of either measuring or matching the junction between empty waveguide and the inhomogeneous waveguide was encountered. Impedance matching was considered first, but this did not seem feasible for the nonreciprocal case. Thus, the effect of the inhomogeneous waveguide interface was measured so that the diaphragm measurements could be made on unmatched sections of the loaded waveguide. It was

then possible to eliminate the effects of the interfaces from the measurements as shown in section 4.3.

The quantities measured were complex reflection and transmission coefficients. The reflection coefficient, R, was measured by means of a calibrated attenuator and a slotted line, Fig. 26(a). A null bridge, Fig. 26(b), was used to measure the transmission coefficient, T. To determine the interface parameters, R and T were measured for two different lengths of the inhomogeneous section. Measurements of R and T of a section containing the metal diaphragm then yielded the information required to determine the equivalent circuit of the diaphragm as shown in section 4.3.2. In the nonreciprocal case, R and T were measured for both senses of the ferrite magnetization.

4.3 Derivation of the diaphragm effect from the measurements

4.3.1 Interface wave-transmission matrices

For the reciprocal case, the wave-transmission matrices of the interfaces are:

$$A_1 = \frac{1}{\tau e^{j\theta}} \begin{bmatrix} 1 & -\rho e^{j\phi_2} \\ \rho e^{j\phi_1} & e^{j2\theta} \end{bmatrix} \qquad \ldots(25a)$$

$$A_3 = \frac{1}{\tau e^{j\theta}} \begin{bmatrix} 1 & -\rho e^{j\phi_1} \\ \rho e^{j\phi_2} & e^{j2\theta} \end{bmatrix} \qquad \ldots(25b)$$

where $\rho e^{j\phi_1}$, $\rho e^{j\phi_2}$ and $\tau e^{j\theta}$ are the semi-infinite interface reflection and transmission coefficients shown in Fig. 27(a). Thus, ρ, τ, ϕ_1, ϕ_2 and θ are to be determined from measurements of R and T (only three of these parameters are independent). In addition, the wave-transmission matrix of a length, ℓ, of the inhomogeneous waveguide is:

$$A_2 = \begin{bmatrix} e^{(\alpha + j\beta)\ell} & 0 \\ 0 & e^{-(\alpha + j\beta)\ell} \end{bmatrix} \qquad \ldots(26)$$

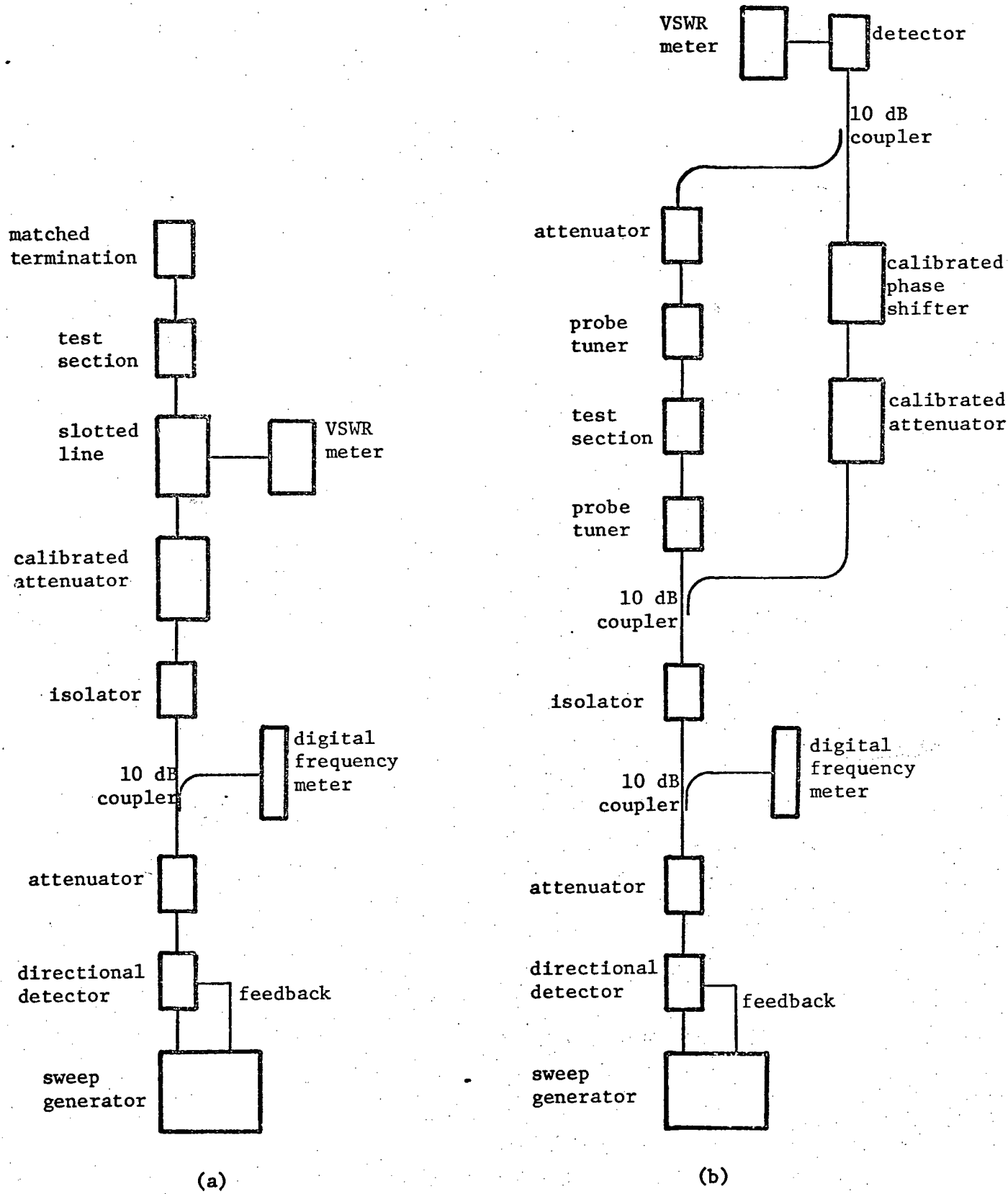

Fig. 26. Block diagrams of experimental systems. (a) reflection coefficient measurements; (b) transmission coefficient measurements.

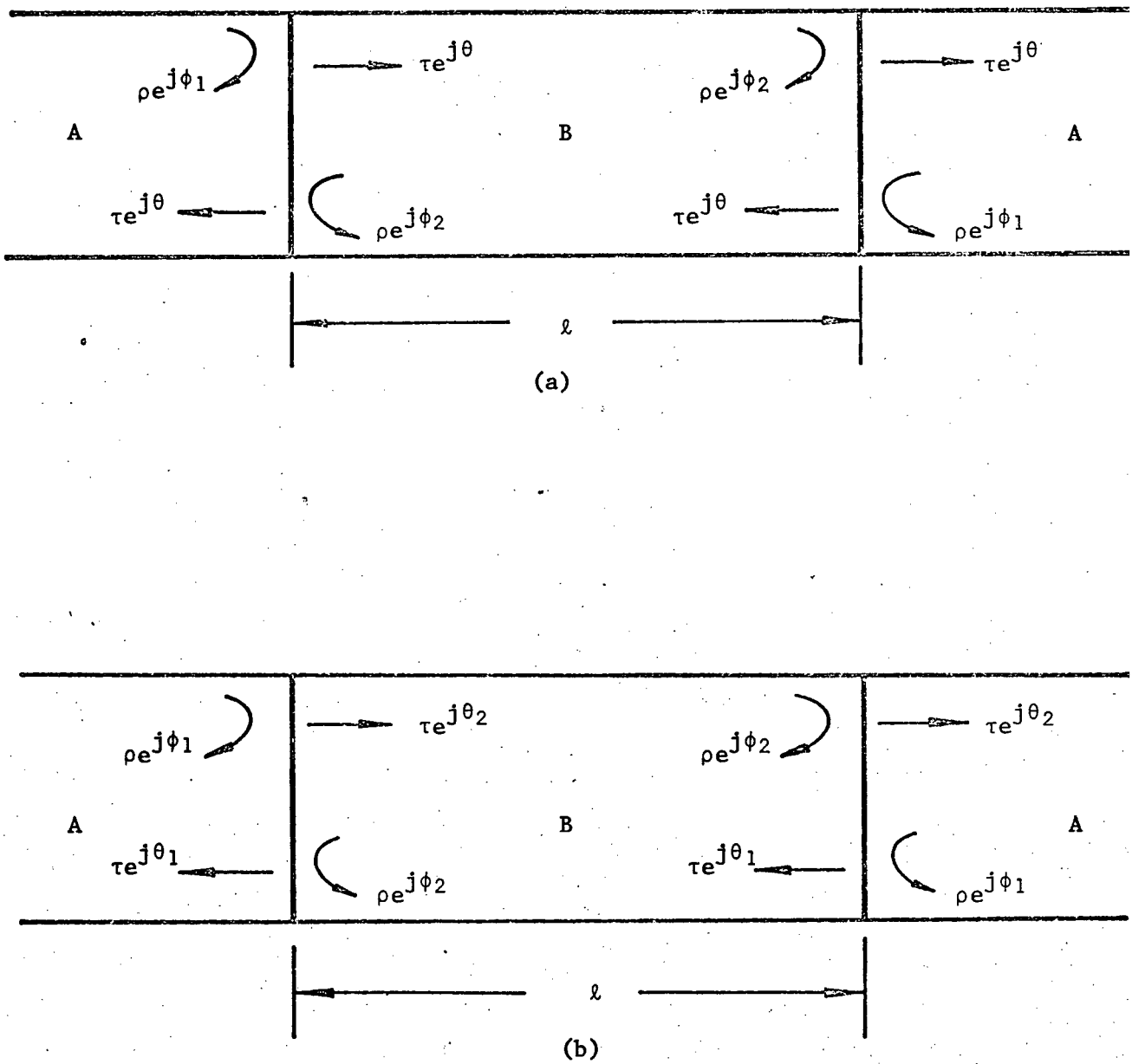

Fig. 27. Junctions of homogeneous and inhomogeneous waveguides identifying the semi-infinite interface parameters. (a) waveguide B is reciprocal; (b) waveguide B is nonreciprocal.

where $(\alpha + j\beta)$ is the complex propagation coefficient in the inhomogeneous waveguide. The overall wave-transmission matrix of the section is simply $A_1 \cdot A_2 \cdot A_3$, so R and T may be expressed as follows:

$$R = \rho e^{j\phi_1} \frac{[1 - e^{j2(\phi_2 - \beta\ell)}\ e^{-2\alpha\ell}]}{1 - \rho^2 e^{j2(\phi_2 - \beta\ell)}\ e^{-2\alpha\ell}} = \rho e^{j\phi_1} \frac{[1 - X^2 e^{j2\eta}]}{1 - \rho^2 X^2 e^{j2\eta}} \quad \ldots(27)$$

$$T = \frac{\tau^2 e^{j(2\theta - \beta\ell)}\ e^{-\alpha\ell}}{1 - \rho^2\ e^{j2(\phi_2 - \beta\ell)}\ e^{-2\alpha\ell}} = \frac{-(1-\rho^2)\ X\ e^{j(\phi_1 + \eta)}}{1 - \rho^2\ X^2\ e^{j2\eta}} \quad \ldots(28)$$

where $\eta = \phi_2 - \beta\ell$ and $X = e^{-\alpha\ell}$. Equations (27) and (28) may be separated into real and imaginary parts, so that they represent four equations in the four unknowns, ρ, ϕ_1, X and η. Linear iteration was used to solve for these unknowns for each length of inhomogeneous waveguide. This method proved to be reliable when all simultaneous solution methods failed: small experimental errors seemed to preclude convergence. Results for two lengths, then, were expected to yield the same values for ρ, ϕ_1 and α, while the two values for η, $\phi_2 - \beta\ell_1$ and $\phi_2 - \beta\ell_2$, determined ϕ_2 and β. Thus, the wave matrices for the interfaces and for the length of inhomogeneous waveguide were determined for the reciprocal case.

From the results of Chapter 3, the wave transmission matrices for the two nonreciprocal interfaces are:

$$A_1 = \frac{1}{\tau e^{j\theta_2}} \begin{bmatrix} 1 & -\rho e^{j\phi_2} \\ \rho e^{j\phi_1} & e^{j(\theta_1 + \theta_2)} \end{bmatrix} \quad \ldots(29a)$$

$$A_3 = \frac{1}{\tau e^{j\theta_2}} \begin{bmatrix} 1 & -\rho e^{j\phi_1} \\ \rho e^{j\phi_2} & e^{j(\theta_1 + \theta_2)} \end{bmatrix} \quad \ldots(29b)$$

where $\rho e^{j\phi_1}$, $\rho e^{j\phi_2}$, $\tau e^{j\theta_1}$ and $\tau e^{j\theta_2}$ are the semi-infinite interface

reflection and transmission coefficients, Fig. 27(b). For the opposite sense of magnetization, θ_1 and θ_2 are interchanged. The wave-transmission matrix of a length, ℓ, of the nonreciprocal waveguide is:

$$A_2 = \begin{bmatrix} e^{(\alpha^+ + j\beta^+)} & 0 \\ 0 & e^{-(\alpha^- + j\beta^-)} \end{bmatrix} \qquad \ldots(30)$$

where $(\alpha^+ + j\beta^+)$ and $(\alpha^- + j\beta^-)$ are the complex propagation coefficients in the forward and reverse directions, respectively. Here, reversing the sense of the magnetization has the effect of interchanging $(\alpha^+ + j\beta^+)$ and $(\alpha^- + j\beta^-)$. The overall wave-transmission matrix of the section is $A_1 \cdot A_2 \cdot A_3$, and is dependent on the sense of the magnetization. The reflection coefficient, however, is not. The coefficients, R, T^+ and T^-, may be expressed as follows:

$$R = \rho e^{j\phi_1} \frac{[1 - e^{j(2\phi_2 - (\beta^+ + \beta^-)\ell)} e^{-(\alpha^+ + \alpha^-)\ell}]}{1 - \rho^2 e^{j(2\phi_2 - (\beta^+ + \beta^-)\ell)} e^{-(\alpha^+ + \alpha^-)\ell}]}$$

$$= \rho e^{j\phi_1} \frac{[1 - X^2 e^{j2\eta}]}{1 - \rho^2 X^2 e^{j2\eta}} \qquad \ldots(31)$$

$$T^+ = \frac{\tau^2 e^{j(2\theta_2 - \beta^+\ell)} e^{-\alpha^+\ell}}{1 - \rho^2 e^{j(2\phi_2 - (\beta^+ + \beta^-)\ell)} e^{-(\alpha^+ + \alpha^-)\ell}}$$

$$= \frac{-(1 - \rho^2) X e^{j(\phi_1 + \eta)}}{1 - \rho^2 X^2 e^{j2\eta}} \cdot e^{j(x - y\ell/2)} \cdot e^{-z\ell/2} \qquad \ldots(32)$$

$$T^- = \frac{\tau^2 e^{j(2\theta_1 - \beta^-\ell)} e^{-\alpha^-\ell}}{1 - \rho^2 e^{j(2\phi_2 - (\beta^+ + \beta^-)\ell)} e^{-(\alpha^+ + \alpha^-)\ell}}$$

$$= \frac{-(1 - \rho^2) X e^{j(\phi_1 + \eta)}}{1 - \rho^2 X^2 e^{j2\eta}} \cdot e^{-j(x - y\ell/z)} \cdot e^{z\ell/z} \qquad \ldots(33)$$

where $X = e^{-\hat{\alpha}\ell}$, $\eta = \phi_2 - \hat{\beta}\ell$, $2\hat{\alpha} = \alpha^+ + \alpha^-$, $2\hat{\beta} = \beta^+ + \beta^-$, $x = \theta_2 - \theta_1$, $y = \beta^+ - \beta^-$ and $z = \alpha^+ - \alpha^-$. If a mean value of the transmission coefficients is defined such that $T = \sqrt{T^+ \cdot T^-}$, then

$$T = \frac{-(1 - \rho^2)\ X\ e^{j(\phi_1 + \eta)}}{1 - \rho^2\ X\ e^{j2\eta}} . \qquad \ldots(34)$$

Equations (31) and (34) have the same form as eqns. (27) and (28) so the procedure for determining the wave-transmission matrices of the interfaces is the same for the nonreciprocal case as it is for the reciprocal case. The terms x, y and z are readily determined since

$$\frac{T^+}{T^-} = e^{j(2x - y\ell)}\ e^{-z\ell} \qquad \ldots(35)$$

4.3.2 Diaphragm wave matrices and equivalent circuits

Once the interfaces had been measured, a thin metal diaphragm was placed at the center of an unmatched section of the inhomogeneous waveguide. The wave matrix then measured was A:

$$A = A_1 \cdot A_2' \cdot A_d \cdot A_2' \cdot A_3 \qquad \ldots(36)$$

where A_1 and A_3 are the interface wave matrices, defined in eqns. (25) and (29) for the reciprocal and nonreciprocal cases, respectively, A_2' is the matrix of half the length of transmission line between the interfaces and A_d is the wave-transmission matrix of the diaphragm. Since A_1, A_3 and A_2' are known from the interface measurements and are all easily inverted, it is now a simple matter to determine A_d. For a thin metal diaphragm of the type considered here, the matrix A_d has the forms:

$$A_d = \begin{bmatrix} \frac{1}{\tau} e^{-j\theta} & -\frac{\rho}{\tau} e^{j(\phi-\theta)} \\ \frac{\rho}{\tau} e^{j(\phi-\theta)} & \frac{1}{\tau} e^{j\theta} \end{bmatrix}, \text{ reciprocal case} \quad \ldots(37a)$$

$$= \begin{bmatrix} \frac{1}{\tau} e^{-j\theta^+} & -\frac{\rho}{\tau} e^{j(\phi-\theta^+)} \\ \frac{\rho}{\tau} e^{j(\phi-\theta^+)} & \frac{1}{\tau} e^{j\theta^-} \end{bmatrix}, \text{ nonreciprocal case} \quad \ldots(37b)$$

In the reciprocal case, the diaphragm may be represented by a single shunt element equivalent circuit, although there appear to be two independent measurable quantities, ρ and θ. In the nonreciprocal case, there are apparently three independent measurable quantities: ρ, θ^+ and θ^-. It was decided that in this case the diaphragm should be represented by a two-element equivalent circuit as shown in Fig. 28, with each element, X and B, assuming different values for a different sense of magnetization (or direction of propagation). These four quantities, $X^{\pm}$ and $B^{\pm}$, are not independent although they are unique.

4.4 Measurements

4.4.1 Preliminary work

Measurements were made to determine the effect of a metal diaphragm in three different configurations of inhomogeneously loaded waveguide. Cases (a) and (b), Figs. 29(a) and (b), were reciprocal, with symmetrical E-plane ceramic* loading. These cases served as a means of evaluating the accuracy of the measurements since theoretical results could be obtained for these cases. The third configuration was the nonreciprocal case, (c), shown in Fig. 29(c), and involved magnetized ferrite loading. The properties of the ferrite are listed in Table 3.

A fourth case, shown in Fig. 29(d), was also reciprocal, with

* dense Alumina, Al_2O_3

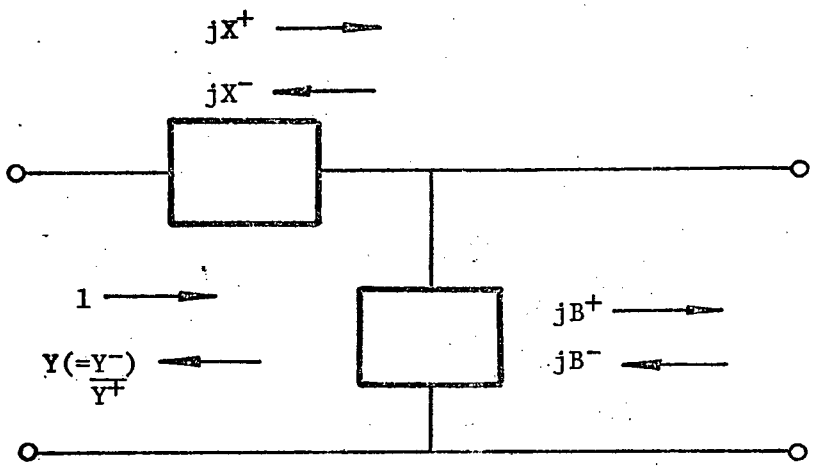

Fig. 28. Equivalent circuit of a thin metal diaphragm in a nonreciprocal waveguide.

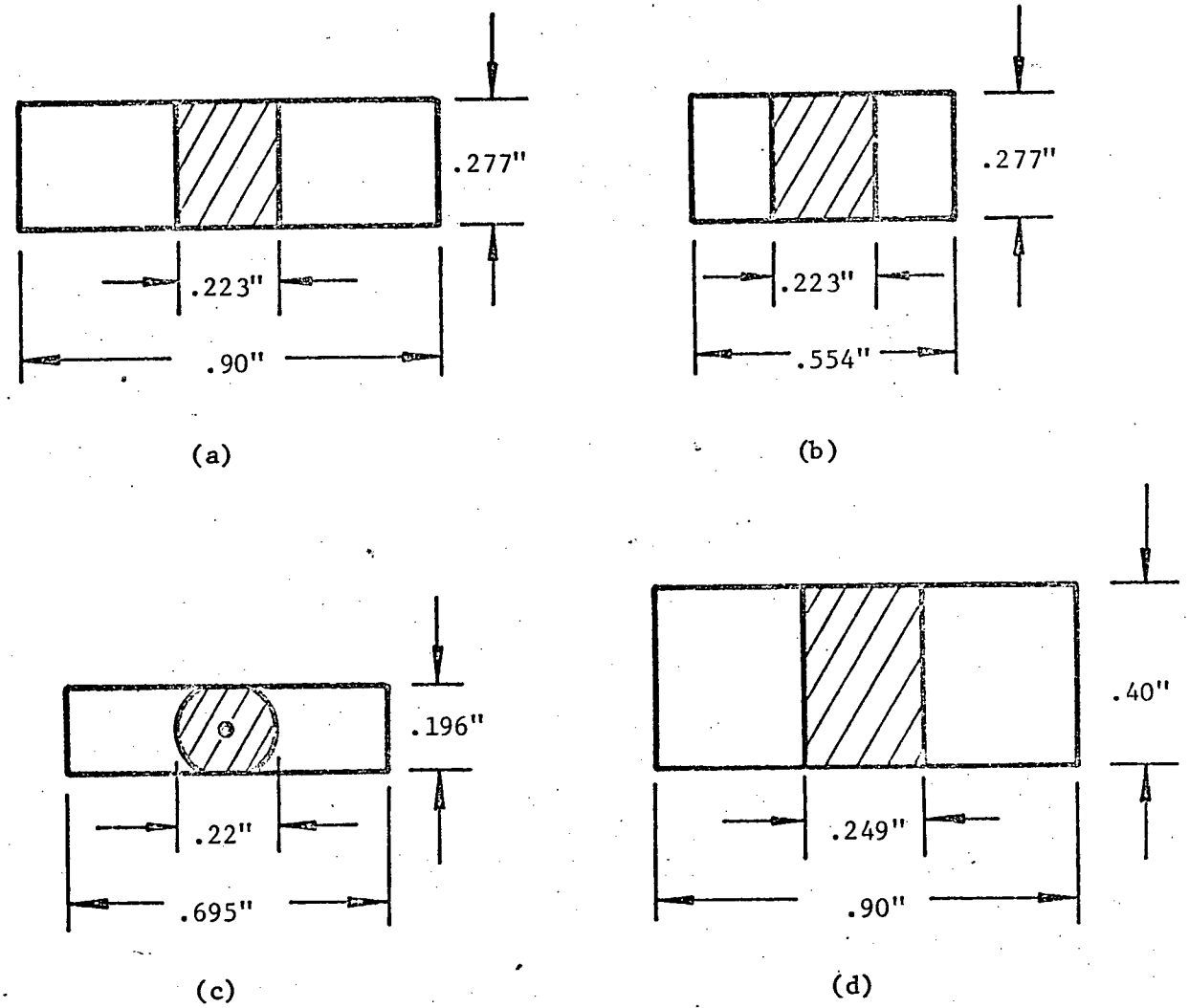

Fig. 29. Inhomogeneous loading configuration for the four experimental cases. (a) and (b) ceramic loading, $\varepsilon_r = 9.37$; (c) ferrite loading; (d) polystyrene loading, $\varepsilon_r = 2.53$.

Table 3. Characteristics of the ferrite.

Saturation magnetization, $4\pi M_s$ (Gauss)	1400
Remanence ratio, M_r/M_s	0.35
Dielectric loss tangent	<0.002
Relative permittivity, ε_f	12.0
Coercive force, H_c (Oersteds)	5.0
Type of ferrite	microwave spinel
Material composition	Nickel, Chromium, Iron
Supplier	Marconi, England

symmetrical E-plane polystyrene loading. This case was investigated earlier to provide confidence in the theoretical technique used to determine the effect of a diaphragm in inhomogeneous waveguide[25]. The measurement procedure was somewhat different but is worth noting: the inhomogeneous section was matched to the empty waveguide and the effect of the diaphragm measured directly. This procedure still required the determination of the effect of the homogeneous - inhomogeneous waveguide interface in order to design the quarter-wave transformers. However, the method could be applied to nonreciprocal cases, although the design of the quarter-wave transformers would be more complicated, and it might be preferable in some instances to the "unmatched technique" generally used in this type of work.

The inhomogeneous waveguides in cases (a)-(c), Fig. 29, are all smaller than standard X-band size. Two waveguide tapers were made to join each size of waveguide to the standard 0.9" x 0.4" waveguide at both ends of the inhomogeneous section. The tapers were made by electroforming copper onto polished stainless-steel forms, which gave the inner surfaces of the tapers a very smooth finish. The total length of each taper was approximately 5 in. In cases (b) and (c) the smallest waveguide cross-section, if air-filled, would have been beyond cut-off at the measurement frequency of 8.5 GHz, so this region was filled with polystyrene. The polystyrene loading was then tapered to a point in the center of the waveguide cross-section so as to match the polystyrene-filled, small size waveguide to the empty, standard size waveguide as shown in Fig. 30. Reflections from the polystyrene and waveguide tapers of cases (b) and (c) were measured and found to have a maximum value of about 0.07 over the frequency range from 8.25 - 9.5 GHz. The reflections

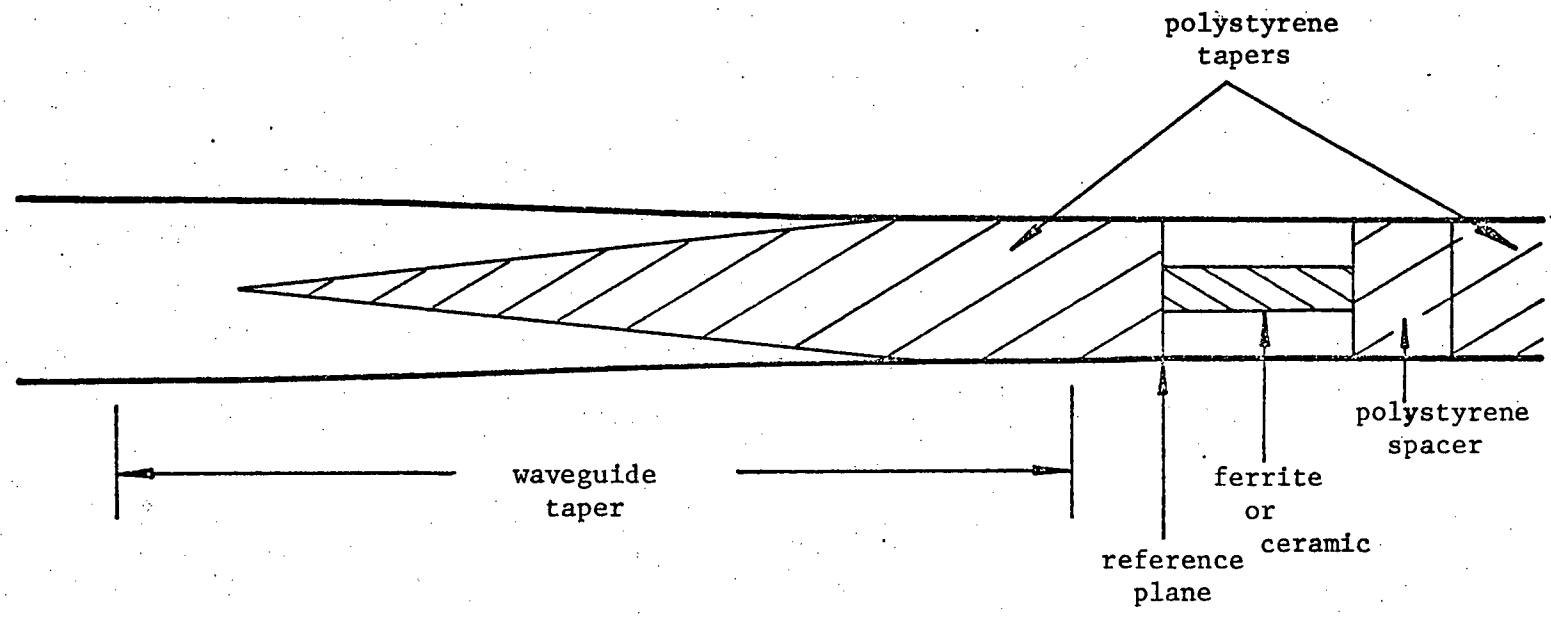

Fig. 30. Waveguide and polystyrene tapers relative to the inhomogeneous section for cases (b) and (c).

from the waveguide tapers used for case (a) were less than 0.02. The effect on the results of these reflections could not be predicted, but it was found by considering the accuracy of the results for cases (a) and (b), section 4.5.1, that this was not serious.

Several precautions were taken to ensure that the results would be repeatable. Aluminum spacers were made to locate the ceramic or ferrite in the center of the waveguide to ±0.001 cm. The polystyrene inserts for cases (b) and (c) were glued in place at the side walls of the waveguide so that they would exert pressure on the ceramic or ferrite and eliminate the possibility of air gaps at the interfaces. The waveguide sections which contained the inhomogeneous loading material were machined from brass blocks so that the tops could be removed. The dimensions for case (c) were such that pressure was exerted on the ferrite so there would be no gap between the ferrite and the broad walls of the waveguide.

4.4.2 Preliminary measurements on nonreciprocal waveguide sections

In order to magnetize the ferrite, wires were inserted into the waveguide through holes in the side walls, through slots in the polystyrene and through the center of the ferrite toroid. The wires and the slots in the polystyrene were found to have a very small effect on the measured quantities: less than 1° and 0.3 dB.

From the list of properties of the ferrite in Table 3, it is seen that the remanent magnetization was only a third of the saturation magnetization. By plotting curves of differential phase shift versus magnetizing current for various lengths of ferrite, it was apparent that a constant magnetizing current would have to be used for the measurements in order to ensure that the ferrite loaded waveguide was substantially nonreciprocal. A current of 15 amps was thus used, which meant that

the ends of the ferrite toroid, where the wire passed across to the waveguide wall, could be magnetized to a greater extent than the rest of the ferrite (normally, this would not be a problem since the device is used as a latching device). Initially, the arrangement of the magnetizing wires was as shown in Fig. 31(a): the wire passed through one side of the waveguide, through the ferrite and back out the same side, causing a nonsymmetric increase in the magnetization at the ends of the ferrite. It was thought that this nonsymmetry might excite a mode that is possible with only one ferrite slab positioned off-center in the waveguide. Thus, the magnetizing current was split so that half came from each side of the waveguide, Fig. 31(b). However, the results for the two arrangements were virtually the same.

From eqn. (35), the measured phase difference between T^+ and T^- of an unmatched section containing magnetized ferrite is:

$$\underline{/T^+} - \underline{/T^-} = 2(\theta_2 - \theta_1) + (\beta^- - \beta^+)\ell + K' \qquad \ldots(38)$$

where K' is the added differential phase shift due to the increased magnetization at the ends of the ferrite, $(\beta^- - \beta^+)$ is the true differential phase shift per unit length and $2(\theta_2 - \theta_1)$ is the theoretical effect of the interfaces. Equation (38) may be rewritten in the form:

$$\underline{/T^+} - \underline{/T^-} = \psi\ell + K \qquad \ldots(38a)$$

where ψ is the differential phase shift per unit length and K is the total interface effect. These two terms were determined from measurements on two lengths of ferrite, 1.0 in and 1.25 in, and are plotted in Fig. 32 versus magnetizing current. As the current is increased, the regions at the ends of the ferrite approach saturation so that the difference in magnetization between the ends of the toroid and the centre

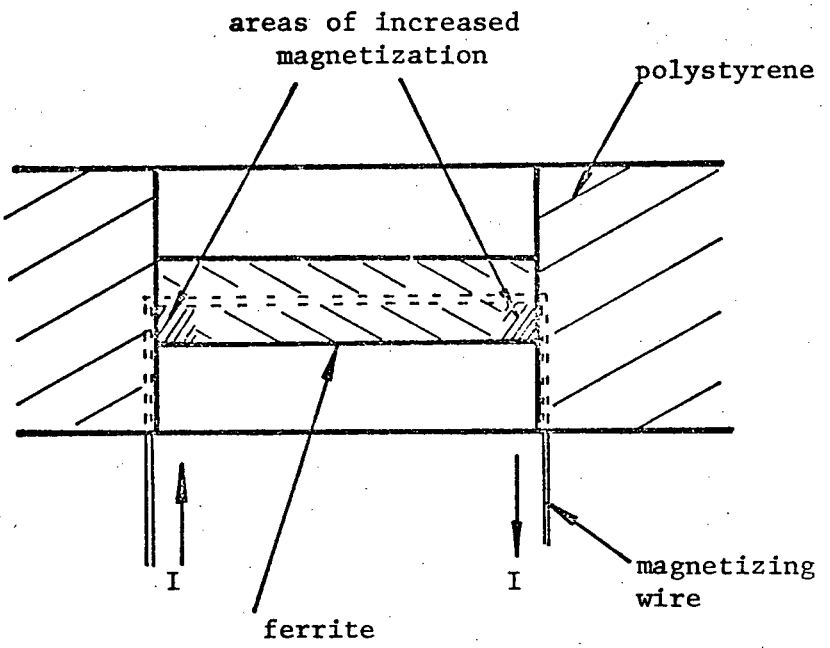

(a)

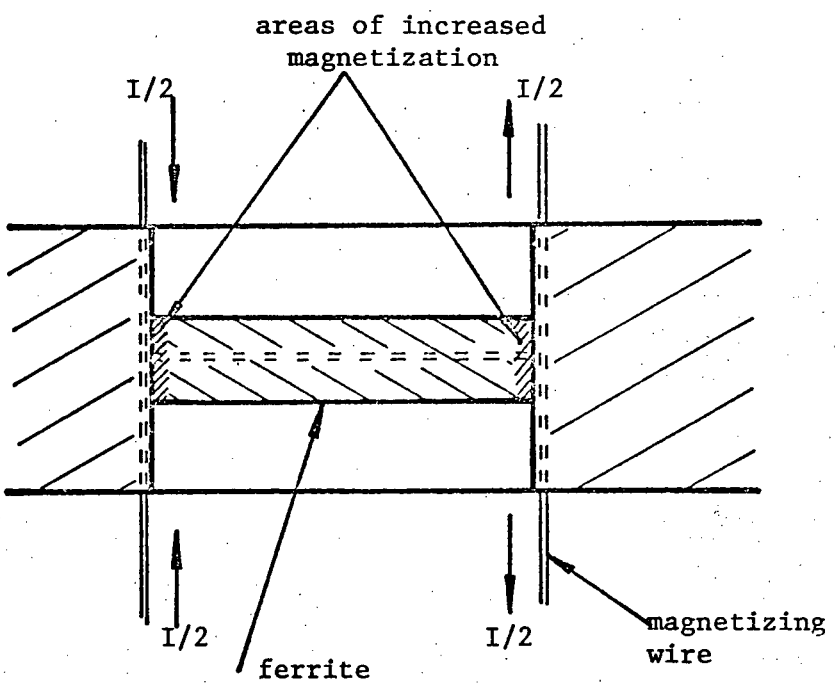

(b)

Fig. 31. Arrangement of the magnetizing wire. (a) initial arrangement; (b) final symmetric arrangement.

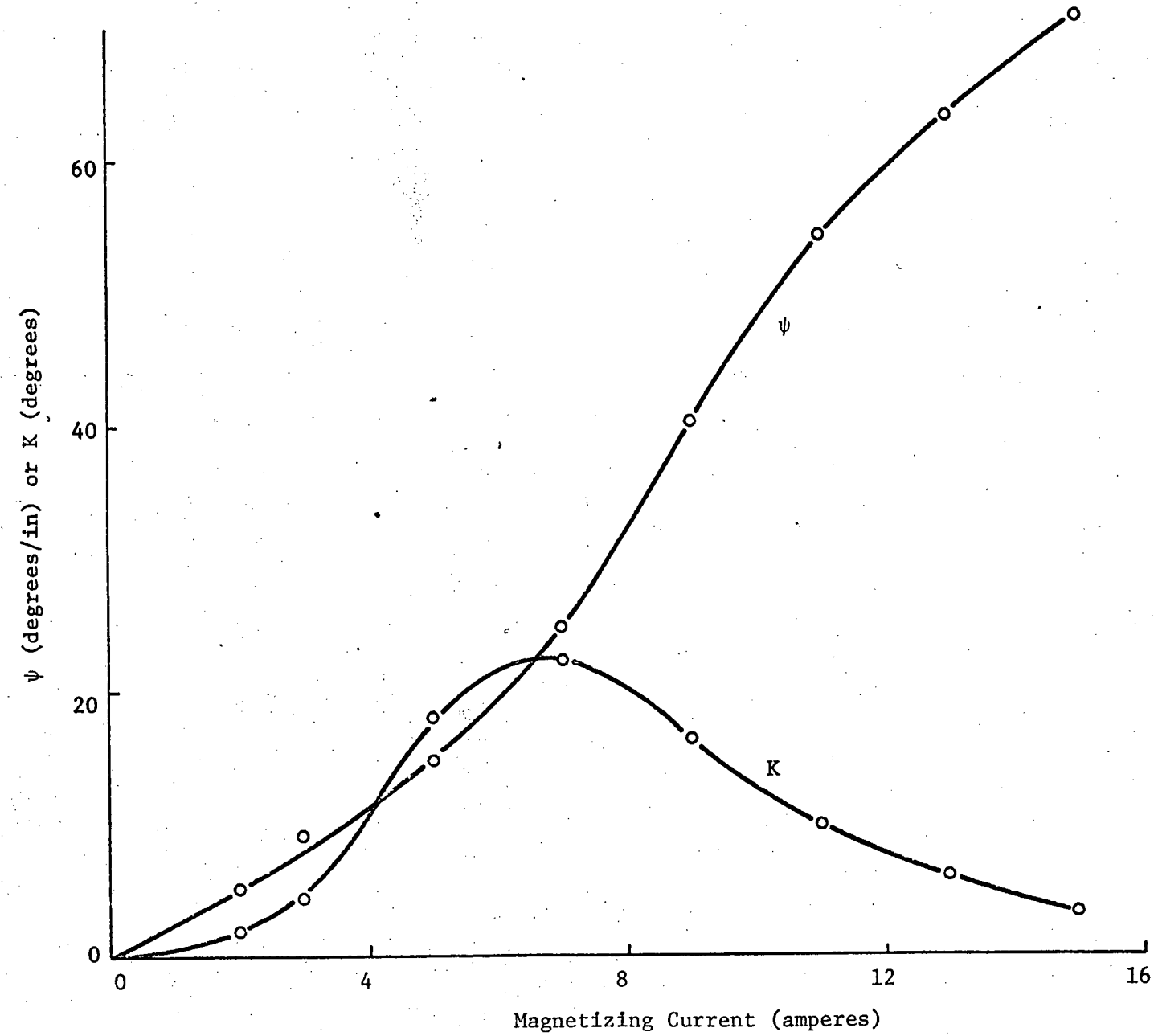

Fig. 32. Differential phase shift, ψ, and total interface effect, K, versus magnetizing current; lengths of ferrite, ℓ = 1.0 in. and 1.25 in.

becomes smaller. This is reflected in the behaviour of K in Fig. 32. Although K would apparently be smaller with a higher magnetizing current, a current of 15 amps was chosen to avoid overheating the ferrite.

Various sources of experimental error are listed in Table 4, along with indications of their effects on the accuracy of the results where possible. The maximum combined effect of these errors was estimated to be ±2° and ±1 dB in the measured values of reflection and transmission coefficients.

4.4.3 Interface measurements

In order to determine the properties of the homogeneous-inhomogeneous waveguide interfaces and the propagation coefficients in the inhomogeneous section, R and T were measured for two different lengths of the section. For each length, values were then calculated for ρ, ϕ_1, η and X as described in section 4.3.1. The effect on these parameters of small errors in the measured values of R and T was investigated. This was done by choosing a hypothetical case with typical values of ρ, ϕ_1, η and X and calculating the corresponding values of R and T. The magnitudes and phases of R and T were changed about their correct values and the effect on the derived values of ρ, ϕ_1, η and X was observed. Typical results are presented in Table 5 where it is seen that small errors in R and T can cause large errors in ρ, ϕ_1, η and X. Small errors in R and T were, however, inevitable. Thus, the measured angles were changed slightly (but within the estimated experimental error of 2°) in order to obtain approximately the same values of ρ, ϕ_1 and α $(= \frac{-\ln X}{\ell})$ for the two specimen lengths used. Typical changes required were 1° - 1.5°.

Table 4. Sources of experimental error.

Source of error	Maximum error	Effect on results
Centering of ferrite	±0.001 cm	——
Positioning of ferrite along the waveguide	±0.003 cm	±0.4°
Magnetization of ferrite		±1°, ±0.1 dB
Temperature variance of ferrite		±0.5°, ±0.02 dB
Positioning of metal diaphragm	±0.005 cm	
Frequency drift	±20 KHz	——
Oscillator amplitude drift		±0.03 dB
Reading accuracy		±0.05°, ±0.03 dB
Mismatch errors in bridge		±1°, ±0.1 dB
Reflections from tapers (magnitude)	0.02-0.07	

Table 5. Effect of errors in interface measurements.

Errors in measured quantities				Derived parameters			
$\|R\|$	$\angle R$ (deg.)	$\|T\|$	$\angle T$ (deg.)	ϕ_1(rad.)	$-\eta$(rad.)	X	ρ
	no error			3.002	5.703	0.900	0.301
.005				3.008	5.713	0.902	0.309
.010				3.015	5.724	0.904	0.318
.015				3.023	5.736	0.907	0.327
	1			3.052	5.761	0.902	0.325
	2			3.096	5.814	0.905	0.350
	3			3.135	5.862	0.908	0.377
		.005		3.025	5.730	0.906	0.311
		.010		3.049	5.759	0.911	0.322
		.015		3.074	5.789	0.917	0.335
			1	3.034	5.761	0.902	0.325
			2	3.061	5.814	0.905	0.350
			3	3.083	5.862	0.908	0.377
.005	1	.005	1	3.107	5.853	0.914	0.376
-.005	-1	-.005	-1	2.865	5.528	0.889	0.247

4.4.4 Diaphragm measurements

The diaphragm was made from two strips of 0.003 in. thick brass foil and held in place by pieces of polyfoam (ε_r = 10.3). Each metal strip was bent in the shape of a bracket, [, so that the flat ends would make proper contact with the broad walls of the waveguide and would at the same time fit over the polyfoam pieces for positioning. The diaphragm was placed half way between the two interfaces and in all cases, (a)-(c), measurements were made for several transverse positions, d, of the diaphragm in this plane, Fig. 33.

4.5 Results and discussion

4.5.1 Reciprocal inhomogeneous loading

The results of the interface measurements for cases (a) and (b), Fig. 29, are shown in Tables 6 and 7. The theoretical values for the interface parameters and propagation coefficients are listed for comparison in Table 7. The values of ρ, ϕ_1 and β are in good agreement with the theoretical values, but those of ϕ_2 and θ are not. The relatively large error in the last two parameters is due to the fact that ϕ_2 is small and is calculated from the small difference between two large values of η; the transmission angle, θ, is derived from ϕ_2 and ϕ_1 by eqn. (1). This error affects the values of the equivalent circuit parameters of the interface significantly as shown in Table 8, although the error in the characteristic admittance is less than 5%.

The wave-transmission matrix of the diaphragm is given by eqn. (37a). Experimentally determined values of the elements of this matrix are presented in Table 9 for a typical situation; i.e., for the inhomogeneous loading of case (a), a diaphragm width, d_{min} = 0.25 cm and position, d = 0.78 cm, where d_{min} and d are defined in Fig. 33. Because of

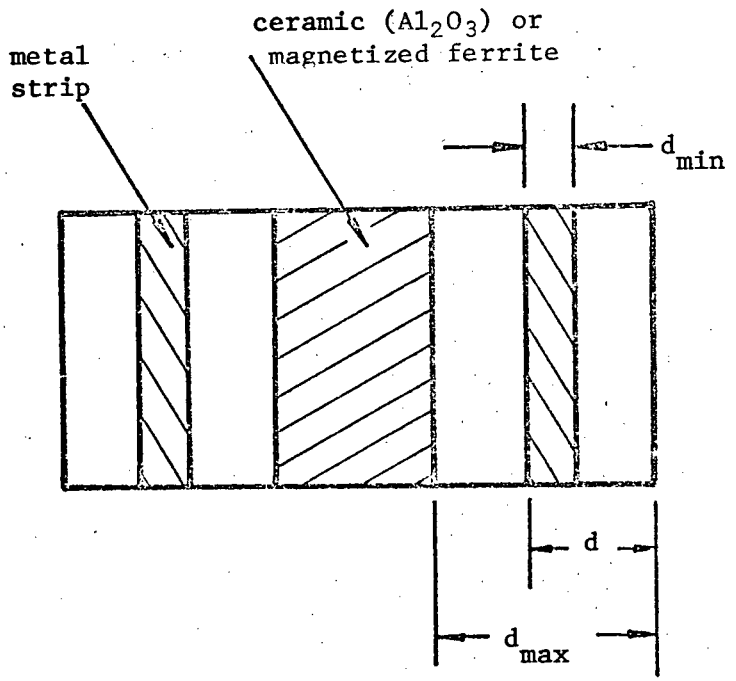

Fig. 33. Diaphragm configuration and transverse position.

Table 6. Interface measurements, ceramic (Al_2O_3) loading.

	Case (a)		Case (b)	
	ℓ = 2.0"	ℓ = 2.15"	ℓ = 2.0"	ℓ = 2.15"
ϕ_1(rad.)	3.030	3.032	3.161	3.129
$-\eta$(rad.)	22.572	24.245	22.434	24.098
$X(=e^{-\alpha\ell})$	0.977	0.960	0.981	0.964
ρ	0.583	0.583	0.423	0.424

Table 7. Semi-infinite interface parameters.

	Case (a)		Case (b)	
	Expt.	Theor.	Expt.	Theor.
ρ	0.583	0.591	0.424	0.426
ϕ_1 (rad.)	3.031	3.0216	3.145	3.1005
ϕ_2 (rad.)	-0.310	0.2015	-0.306	0.0724
θ (rad.)	-0.2103	0.0408	-0.1513	0.0157
β (rad./in)	11.124	11.223	11.064	11.106
α (nep./in)	0.019	—	0.011	—

Table 8. Interface equivalent circuit parameters.

	Case (a)		Case (b)	
	Expt.	Theor.	Expt.	Theor.
Y	3.672	3.848	2.412	2.478
B	0.629	-0.329	0.370	-0.069
X	0.097	0.034	0.061	0.006

Table 9. Typical diaphragm wave-transmission matrix, case (a): d_{min} = 0.25 cm, d = 0.78 cm.

Matrix element	Theoretical form	Experimental values
A_{d11}	$\frac{1}{\tau} e^{-j\theta}$	$1.0269/\underline{-10.418°}$
A_{d12}	$-\frac{\rho}{\tau} e^{j(\phi-\theta)}$	$0.1627/\underline{-80.945°}$
A_{d21}	$\frac{\rho}{\tau} e^{j(\phi-\theta)}$	$0.1627/\underline{99.055°}$
A_{d22}	$\frac{1}{\tau} e^{j\theta}$	$0.9983/\underline{10.876°}$

measurement errors, the various elements of the matrix are inconsistent; e.g., θ is not the same in A_{d11} and A_{d22}, $\phi - \theta$ is not $\pm 90°$ in A_{d12} and A_{d21}, and so on. For the various diaphragm positions, the magnitude, ρ/τ, and the two values of θ showed the most consistent behaviour. Thus, the values of ρ/τ and θ were taken as being the most correct and were used to determine ρ, τ, ϕ and θ from the unitary conditions. The values of these parameters were then used to calculate the values of the equivalent circuit elements of the diaphragm. The results for cases (a) and (b) are plotted in Fig. 34 along with the theoretical curves. The agreement of B with the theoretical values is within ±6%, and most values are within ±3%. Considering the overall accuracy obtained, it appears that the errors in ϕ_2 and θ (of the interface measurements) have little effect on the diaphragm measurements.

4.5.2 Nonreciprocal inhomogeneous loading

The results of the interface measurements for case (c), Fig. 29, are presented in Tables 10 and 11 and the equivalent circuit parameters are listed in Table 12. Values of the elements of the diaphragm wave-transmission matrix, eqn. (37b), are listed in Table 13 for a typical situation: the width of the diaphragm, d_{min} = 0.25 cm and the diaphragm position, d = 0.547 cm. As in the reciprocal cases, the magnitude, ρ/τ, and the angles, θ, were used to derive the values of ρ, τ, ϕ, θ^+ and θ^- from the unitary conditions. The equivalent circuit parameters, $B^{\pm}$ and $X^{\pm}$, are plotted in Fig. 35 as functions of d.

Comment on the values of X^+ and X^-

It is seen from Fig. 35 that relative to B^+, X^+ is of the order of 15-20% and relative to B^-, X^- is less than 9%. Thus, there is some

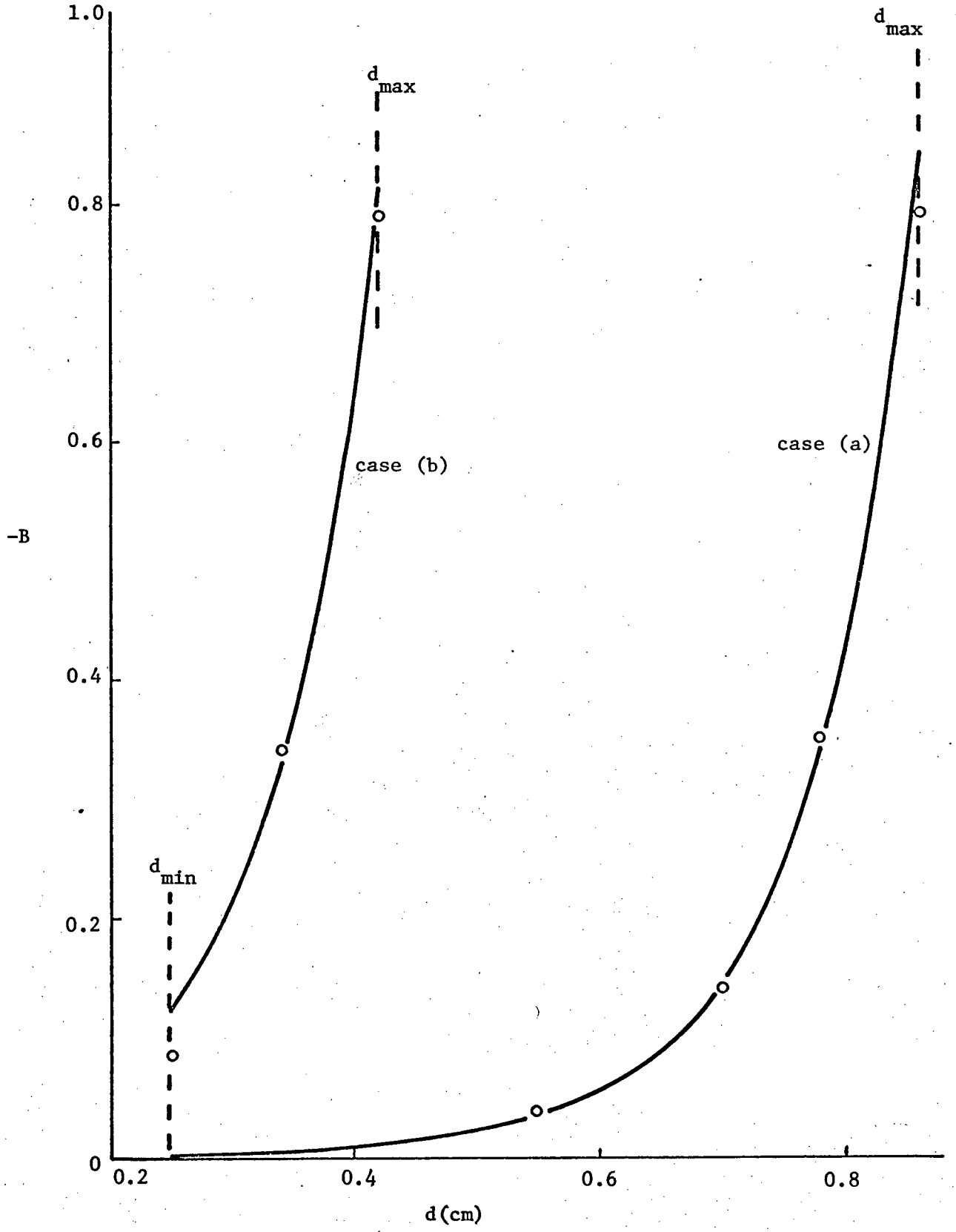

Fig. 34. Equivalent circuit parameters of a metal diaphragm in ceramic loaded waveguide. —— theory; ooo experiment.

Table 10. Interface measurements, magnetized ferrite loading.

	ℓ = 1.0"	ℓ = 1.25"
ϕ_1 (rad.)	3.087	3.089
$-\eta$ (rad.)	10.393	12.976
$X(=e^{-\hat{\alpha}\ell})$	0.903	0.874
ρ	0.321	0.359
T^+/T^- (dB/deg.)	.20/74.9°	.22/92.9°

Table 11. Semi-infinite interface parameters.

ρ	0.340
ϕ_1 (rad.)	3.088
ϕ_2 (rad.)	-0.062
θ_1 (rad.)	-0.0706
θ_2 (rad.)	-0.046
β^+ (rad./in)	9.70
β^- (rad./in)	10.96
α^+ (nep./in)	0.093
α^- (nep./in)	0.117

Table 12. Interface equivalent circuit parameters.

Y^+	1.942
Y^-	1.938
B_A^+	0.064
B_A^-	0.111
B_B^+	0.070
B_B^-	0.102
X_A^+	0.037
X_A^-	0.050
X_B^+	0.026
X_B^-	0.058

Table 13. Typical diaphragm wave-transmission matrix, case (c): d_{min} = 0.25 cm, d = 0.547 cm.

Matrix element	Theoretical form	Experimental values
A_{d11}	$\frac{1}{\tau} e^{-j\theta^+}$	1.0270/-16.144°
A_{d12}	$-\frac{\rho}{\tau} e^{j(\phi-\theta^+)}$	0.2033/-95.272°
A_{d21}	$\frac{\rho}{\tau} e^{j(\phi-\theta^+)}$	0.2033/84.728°
A_{d22}	$\frac{1}{\tau} e^{j\theta^-}$	1.0168/9.688°

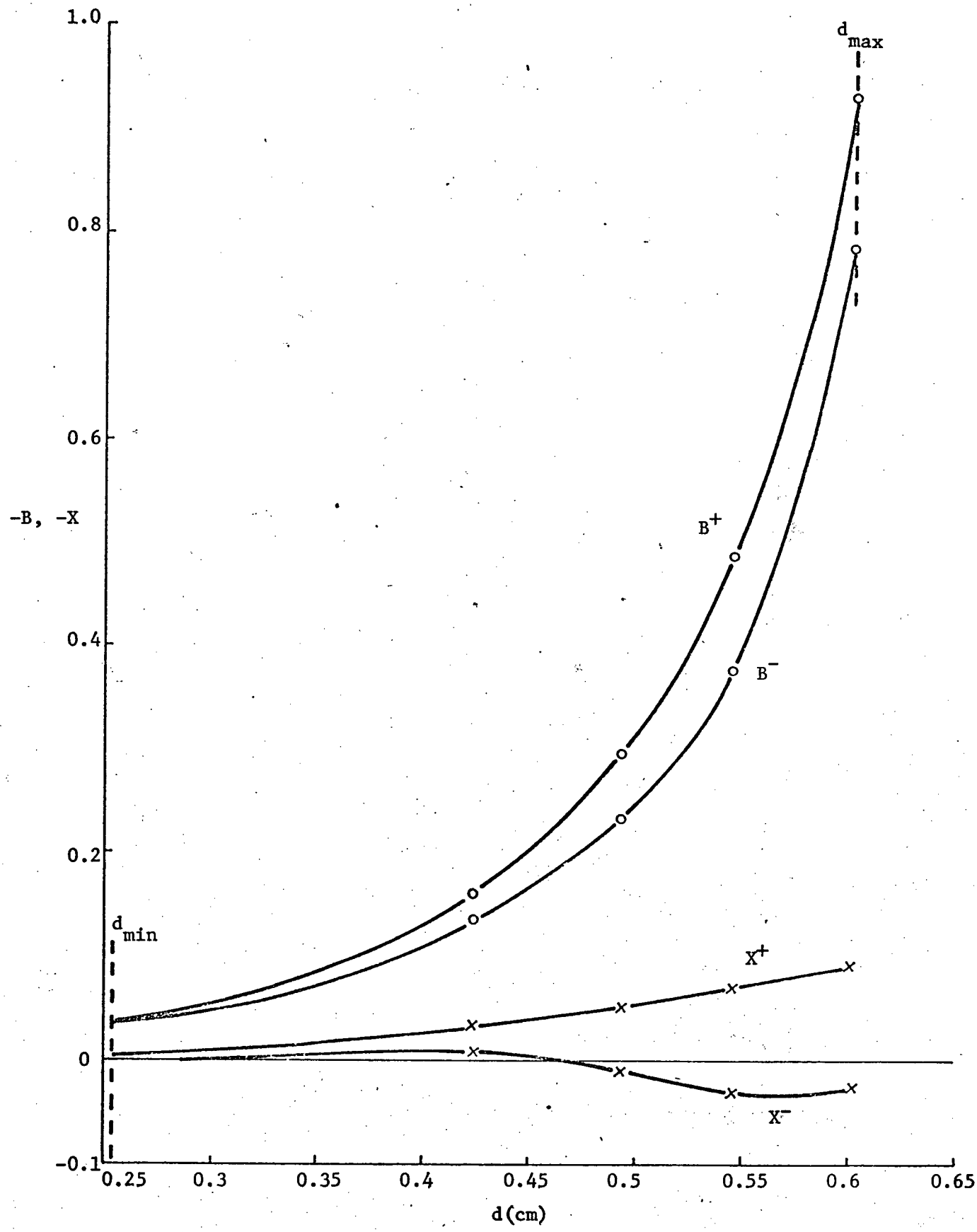

Fig. 35. Equivalent circuit parameters of a metal diaphragm in ferrite loaded waveguide; magnetizing current = 15 A.

question as to the significance of X^- (or X^+) , although the unitary conditions for the diaphragm wave matrix cannot be satisfied by B^+ and B^- alone. This was investigated by recalculating the diaphragm equivalent circuit elements for the reciprocal cases using the nonreciprocal circuit representation. Ideally, one would expect X^+ and X^- to be zero and B^+ and B^- to have the same values. The calculations showed that the values of B^+ and B^- were negligibly different from those of B and that the values of $X^\pm$ were of the order of 3-7% of B. This indicates that the values of X^+ and X^- determined for the nonreciprocal case may be greatly in error. However, they are small compared with the values of B^+ and B^- and may be ignored for some purposes.

Chapter 5

CONCLUSIONS

The main objective of this work was to determine an equivalent circuit representation for a thin metallic discontinuity in a nonreciprocal inhomogeneous waveguide. The configuration chosen for the nonreciprocal structure is typical of those found in latching nonreciprocal ferrite phase shifters. Because of the complexity of this configuration, a theoretical analysis did not seem possible. The effect of a metal diaphragm was determined experimentally but before the diaphragm could be represented by an equivalent circuit it was necessary to be able to derive values for the characteristic admittances of the nonreciprocal waveguide. The experimental technique involved the measurement of reflection and transmission coefficients of unmatched sections of the nonreciprocal waveguide, which introduced a further problem: it was necessary to determine the effect of a nonreciprocal inhomogeneous waveguide interface.

Before considering the diaphragm discontinuity, the related discontinuities of reciprocal and nonreciprocal inhomogeneous waveguide interfaces were analysed theoretically. In both cases, the numerical technique mode matching was used. A two-element equivalent circuit representation of a reciprocal interface led to a useful definition of the normalized equivalent characteristic admittance of an inhomogeneous waveguide. This was an important step towards the definition of the characteristic admittances in a nonreciprocal waveguide. Computed values of the normalized equivalent circuit elements and characteristic admittances were obtained for both E-plane and H-plane dielectric loading over a wide range of parameters.

A similar representation was used for a nonreciprocal inhomogeneous waveguide interface. In this case, the equivalent circuit elements and the characteristic admittance of the nonreciprocal section assumed different values depending on the direction of propagation. The nonreciprocal structure was a twin-slab ferrite loaded waveguide which is a theoretical model for ferrite toroid configurations. Contrary to expectation, the characteristic admittances for the two directions of propagation were found to be nearly the same over a wide range of parameters, although the difference between the two phase coefficients could be quite large.

The analysis of these two interface problems provided the understanding required to determine the effect of a diaphragm in a nonreciprocal waveguide from experimental measurements. The diaphragm was represented by a two-element equivalent circuit, each element having different values for the two directions of propagation. Measurements made at 8.5 GHz showed that the series elements are an order of magnitude smaller than the shunt elements.

The accuracy of these results could not be checked by comparison with theoretical results so an indirect method was used. The effect of a diaphragm in a reciprocal inhomogeneous waveguide was measured, with the inhomogeneous loading configuration chosen so that theoretical results could be obtained. The accuracy of the results for the reciprocal case then provided an indication of the accuracy of the results for the nonreciprocal case. The maximum error in the measured quantitites is estimated to be ±2° and ±1 dB, while the error in the derived values of the shunt elements is estimated to be less than ±6%. The percentage error in the values of the series elements may be much larger but for many purposes these elements are negligible.

Appendix A

REFLECTION AND TRANSMISSION COEFFICIENTS FOR A RECIPROCAL INTERFACE

Mode matching yields values for the normalized coefficients of the reflected and transmitted waves (dominant modes) at the interface. The reflection coefficient is obtained directly from these results; i.e., r_1/a_1. The transmission coefficient is obtained by equating the power flowing in the positive z-direction in the two waveguides, A and B:

$$(1 - |\frac{r_1}{a_1}|^2) \int_s \bar{e}_{A1} \times \bar{h}_{A1}^* \cdot \bar{a}_z ds = |\frac{b_1}{a_1}|^2 \int_s \bar{e}_{B1} \times \bar{h}_{B1}^* \cdot \bar{a}_z ds$$

i.e.,

$$1 - |\frac{r_1}{a_1}|^2 = |\frac{b_1}{a_1}|^2 \frac{\int_s \bar{e}_{B1} \times \bar{h}_{B1}^* \cdot \bar{a}_z ds}{\int_s \bar{e}_{A1} \times \bar{h}_{A1}^* \cdot \bar{a}_z ds} \triangleq |t_2|^2$$

$$\therefore \quad t_2^2 = (\frac{b_1}{a_1})^2 \frac{\int_s \bar{e}_{B1} \times \bar{h}_{B1}^* \cdot \bar{a}_z ds}{\int_s \bar{e}_{A1} \times \bar{h}_{A1}^* \cdot \bar{a}_z ds} \qquad \ldots (39)$$

where s is the waveguide cross-sectional area.

In the above expressions, $\bar{e}_{A1}$ and $\bar{h}_{A1}$ represent the dominant mode in A while $\bar{e}_{B1}$ and $\bar{h}_{B1}$ represent the dominant mode in B. The equivalent circuit parameters, Figs. 5(a) and 5(b), may then be defined in terms of r_1/a_1 and t_2.

Two-element circuit

$$Z_{in} = \frac{1 + r_1/a_1}{1 - r_1/a_1} = jX + \frac{1}{Y + jB}$$

$$t_2 = \frac{(1 - r_1/a_1)\sqrt{Y}}{Y + jB} \qquad \ldots (40)$$

Three-element circuit

$$Z_{in} = jX_1 + \frac{1 + jX_3Y'}{Y' (1 - X_3B_2) + jB_2} \qquad \ldots(41)$$

$$t_2 = \frac{(1 - r_1/a_1)\sqrt{Y'}}{Y' (1 - X_3B_2) + jB_2}$$

Appendix B

INTERFACE BETWEEN EMPTY AND H-PLANE DIELECTRIC SLAB LOADED WAVEGUIDES

The steps outlined here for the mode-matching solution follow the general procedure in refs. 17 and 18. Considering Fig. 36, waveguides A and B are matched so that the only reflections are those caused by the interface and the dimensions are such that only one mode may propagate in either A or B. If the TE_{10} mode is incident on the junction from waveguide A, the total transverse fields at z = 0 may be approximated by sums of mode fields:

Waveguide A

$$\bar{E}_A = (a_1 + r_1)\bar{e}_{A1} + \sum_{i=2}^{M} a_i \bar{e}_{Ai} \qquad \ldots (42)$$

$$\bar{H}_A = (a_1 - r_1)\bar{h}_{A1} - \sum_{i=2}^{M} a_i \bar{h}_{Ai} \qquad \ldots (43)$$

Waveguide B

$$\bar{E}_B = \sum_{j=1}^{N} b_j \bar{e}_{Bj} \qquad \ldots (44)$$

$$\bar{H}_B = \sum_{j=1}^{N} b_j \bar{h}_{Bj} \qquad \ldots (45)$$

In the above equations, $\bar{e}_{Ai}$ and $\bar{h}_{Ai}$ are the transverse electric and magnetic field components of the i-th mode excited in waveguide A and $\bar{e}_{Bj}$ and $\bar{h}_{Bj}$ are corresponding terms for waveguide B. Using the orthogonality relations for modes in each waveguide and satisfying the boundary conditions at the interface we have:

$$\frac{r_1}{a_1} \int_s \bar{e}_{Bn} \times \bar{h}_{A1} \cdot \bar{a}_z ds + \sum_{j=1}^{N} \frac{b_j}{a_1} \sum_{i=2}^{M} \frac{\int_s \bar{e}_{Bj} \times \bar{h}_{Ai} \cdot \bar{a}_z ds}{\int_s \bar{e}_{Ai} \times \bar{h}_{Ai} \cdot \bar{a}_z ds} \cdot \int_s \bar{e}_{Bn} \times \bar{h}_{Ai} \cdot \bar{a}_z ds$$

$$+ \frac{b_n}{a_1} \int_s \bar{e}_{Bn} \times \bar{h}_{Bn} \cdot \bar{a}_z ds = \int_s \bar{e}_{Bn} \times \bar{h}_{A1} \cdot \bar{a}_z ds \qquad \ldots (46)$$

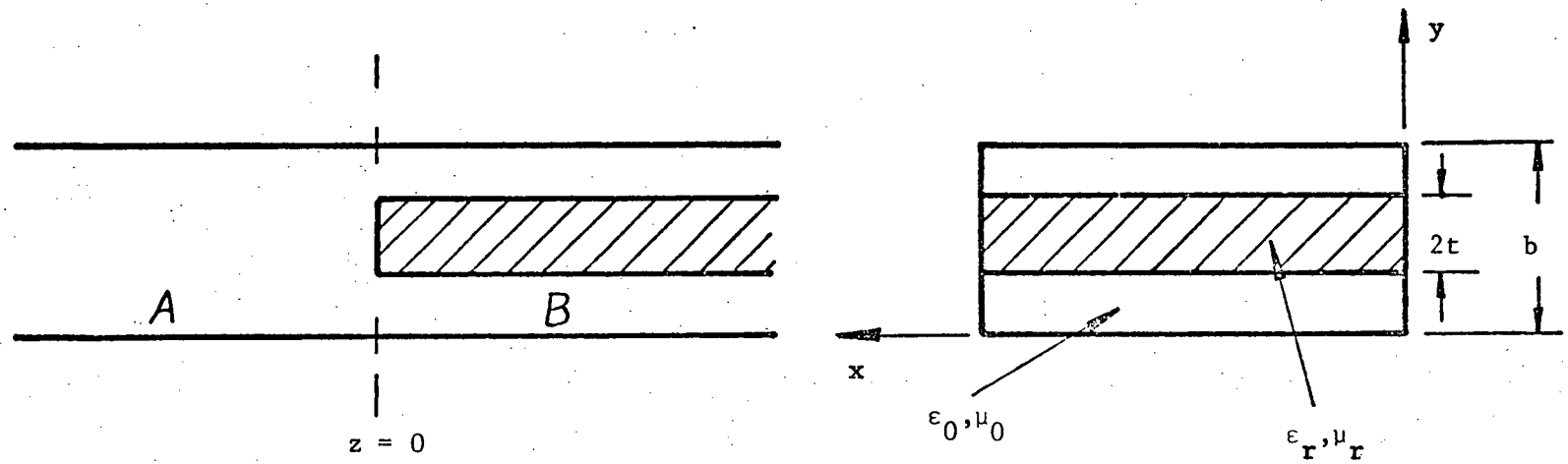

Fig. 36. Junction of empty and H-plane loaded waveguides.

and,

$$\frac{r_1}{a_1}\int_s \bar{e}_{A1} \times \bar{h}_{A1} \cdot \bar{a}_z ds - \sum_{j=1}^{N} \frac{b_j}{a_1}\int_s \bar{e}_{Bj} \times \bar{h}_{A1} \cdot \bar{a}_z ds = -\int_s \bar{e}_{A1} \times \bar{h}_{A1} \cdot \bar{a}_z ds \quad \ldots(47)$$

where s is the waveguide cross-sectional area.

Equations (46) and (47) represent a set of N + 1 equations in the N + 1 unknowns, $\frac{b_1}{a_1}, \frac{b_2}{a_1}, \ldots, \frac{b_n}{a_1}, \frac{r_1}{a_1}$. The amplitude coefficients of the modes reflected in waveguide A may be found from:

$$\frac{a_i}{a_1} = \sum_{j=1}^{N} \frac{b_j}{a_1} \frac{\int_s \bar{e}_{Bj} \times \bar{h}_{Ai} \cdot \bar{a}_z ds}{\int_s \bar{e}_{Ai} \times \bar{h}_{Ai} \cdot \bar{a}_z ds}, \quad i \neq 1 \quad \ldots(48)$$

To decide which modes to use to approximate the fields $\bar{E}_A$, $\bar{H}_A$, $\bar{E}_B$ and $\bar{H}_B$, consider the integrals, $\int_s \bar{e}_{Bj} \times \bar{h}_{Ai} \cdot \bar{a}_z ds$. We start with the TE_{10} mode, the (only) mode incident on the junction from waveguide A. This mode is of the type TE_{n0} (n odd) which we denote by the superscript I. The first step is to examine the integrals $\int_s \bar{e}_{Bj} \times \bar{h}_{Ai}^{I} \cdot \bar{a}_z ds$ for all the different types of modes that may exist in waveguide B. This reveals that the only modes excited directly by the TE_{10} mode are LSM_{1m} modes, m = 1,3,5,...; these are also denoted by the superscript I. Next, we determine which modes are excited in waveguide A by these LSM modes through an examination of the integrals $\int_s \bar{e}_{Bj}^{I} \times \bar{h}_{Ai} \cdot \bar{a}_z ds$. These integrals are zero for all but TE_{10}, TE_{1m} and TM_{1m} modes, m = 2,4,6,.... The TE_{1m} and TM_{1m} modes are denoted by the superscripts II and III, respectively. Now, for the corresponding modes excited in waveguide B, we find that $\int_s \bar{e}_{Bj} \times \bar{h}_{Ai}^{II,III} \cdot \bar{a}_z ds = 0$ for all but LSE_{1m} modes, m = 2,4,6,..., denoted by the superscript II. Finally, we find that $\int_s \bar{e}_{Bj}^{II} \times \bar{h}_{Ai} \cdot \bar{a}_z ds = 0$ for all but TE_{1m} and TM_{1m} modes, m = 2,4,6,..., which are

already excited by the LSM_{1m} modes as shown above. Thus, no other modes are exicted at the interface. These results may be summarized as follows:

Waveguide A

TE_{1m}, $m = 0,2,4,\ldots$

TM_{1m}, $m = 2,4,6,\ldots$

Waveguide B

LSE_{1m}, $m = 2,4,6,\ldots$

LSM_{1m}, $m = 1,3,5,\ldots$

Expressions for the fields in both waveguides are derived from similar equations. For TE_{nm} or LSE_{nm} modes:

$$\bar{E} = -j\,\omega\mu'\bar{\nabla} \times \bar{\Pi}_h$$

$$\bar{H} = k^2\,\bar{\Pi}_h + \overline{\nabla\nabla} \cdot \bar{\Pi}_h$$

where

$$\bar{\Pi}_h = \bar{a}_z\,\psi_h(x,y)e^{-\gamma z} \qquad \text{for TE modes}$$

$$= \bar{a}_y\,\psi_h(x,y)e^{-\gamma z} \qquad \text{for LSE modes}$$

and ψ_h satisfies the relation

$$\nabla_t^2\,\psi_h + (\gamma^2 + k^2)\psi_h = 0$$

For TM_{nm} or LSM_{nm} modes:

$$\bar{E} = k^2\bar{\Pi}_e + \overline{\nabla\nabla} \cdot \bar{\Pi}_e$$

$$\bar{H} = j\omega\,\varepsilon'\,\bar{\nabla} \times \bar{\Pi}_e$$

where $\bar{\Pi}_e = \bar{a}_z\,\psi_e(x,y)e^{-\gamma z}$ for TM modes

$$= \bar{a}_y\,\psi_e(x,y)e^{-\gamma z} \qquad \text{for LSM modes}$$

and ψ_e satisfies the relation

$$\nabla_t^2 \psi_e + (\gamma^2 + k^2)\psi_e = 0$$

In the above relations,

$$k^2 = \omega^2 \varepsilon'\mu'$$

$$\varepsilon', \mu' = \varepsilon_0, \mu_0 \qquad \text{in waveguide A}$$

$$= \varepsilon_r(y)\varepsilon_0, \mu_r(y)\mu_0 \qquad \text{in waveguide B}$$

The resulting equations for the fields are summarized below.

Waveguide A

TE_{nm} modes:

$$\bar{e}_A^{\,I} = -j\omega\mu_0 \frac{n\pi}{a} \sin \frac{n\pi}{a} x \, \bar{a}_y$$

$$\bar{h}_A^{\,I} = \gamma_{nm} \frac{n\pi}{a} \sin \frac{n\pi}{a} x \, \bar{a}_x \qquad \ldots(49)$$

$$\bar{e}_A^{\,II} = j\omega\mu_0 \frac{m\pi}{b} \left[\cos \frac{n\pi}{a} x \sin \frac{m\pi}{b} y\right] \bar{a}_x - j\omega\mu_0 \frac{n\pi}{a} \left[\sin \frac{n\pi}{a} x \cos \frac{m\pi}{b} y\right] \bar{a}_y$$

$$\bar{h}_A^{\,II} = \gamma_{nm} \frac{n\pi}{a} \left[\sin \frac{n\pi}{a} x \cos \frac{m\pi}{b} y\right] \bar{a}_x + \gamma_{nm} \frac{m\pi}{b} \left[\cos \frac{n\pi}{a} x \sin \frac{m\pi}{b} y\right] \bar{a}_y \qquad \ldots(50)$$

TM_{nm} modes:

$$\bar{e}_A^{\,III} = -\gamma_{nm} \frac{n\pi}{a} \left[\cos \frac{n\pi}{a} x \sin \frac{m\pi}{b} y\right] \bar{a}_x - \gamma_{nm} \frac{m\pi}{b} \left[\sin \frac{n\pi}{a} x \cos \frac{m\pi}{b} y\right] \bar{a}_y$$

$$\bar{h}_A^{\,III} = j\omega\varepsilon_0 \frac{m\pi}{b} \left[\sin \frac{n\pi}{a} x \cos \frac{m\pi}{b} y\right] \bar{a}_x - j\omega\varepsilon_0 \frac{n\pi}{a} \left[\cos \frac{n\pi}{a} x \sin \frac{m\pi}{b} y\right] \bar{a}_y \qquad \ldots(51)$$

Waveguide B

LSM_{nm} modes (m odd):

$$\bar{e}_B^{\,I} = -\frac{n\pi}{a} h_m [\sin h_m y \cos \frac{n\pi}{a} x]\, \bar{a}_x - \gamma_{0m}^2 [\cos h_m y \sin \frac{n\pi}{a} x]\, \bar{a}_y \qquad 0 \le y \le b/2-t$$

$$= \frac{n\pi}{a} A_m \ell_m [\sin \ell_m (b/2-y) \cos \frac{n\pi}{a} x]\, \bar{a}_x - \gamma_{0m}^2 A_m [\cos \ell_m (b/2-y) \sin \frac{n\pi}{a} x]\, \bar{a}_y \qquad b/2-t \le y \le b/2 \quad \ldots (52)$$

$$\bar{h}_B^{\,I} = j\omega\varepsilon_0 \gamma_{nm} [\cos h_m y \sin \frac{n\pi}{a} x]\, \bar{a}_x \qquad 0 \le y \le b/2-t$$

$$= j\omega\varepsilon\, \gamma_{nm} A_m [\cos \ell_m (b/2-y) \sin \frac{n\pi}{a} x]\, \bar{a}_x \qquad b/2-t \le y \le b/2$$

$$A_m = -\frac{h_m}{\ell_m} \frac{\sin h_m (b/2-t)}{\sin \ell_m t} = \frac{1}{\varepsilon_r} \frac{\cos h_m (b/2-t)}{\cos \ell_m t}$$

$$\gamma_{nm}^2 = h_m^2 + (\frac{n\pi}{a})^2 - k_0^2$$

$$= \ell_m^2 + (\frac{n\pi}{a})^2 - \varepsilon_r \mu_r k_0^2$$

LSE_{nm} modes (m even):

$$\bar{e}_B^{\,II} = -j\omega\mu_0 \gamma_{nm} [\sin h_m y \cos \frac{n\pi}{a} x]\, \bar{a}_x \qquad 0 \le y \le b/2-t$$

$$= -j\omega\mu\, \gamma_{nm} A_m [\sin \ell_m (b/2-y) \cos \frac{n\pi}{a} x]\, \bar{a}_x \qquad b/2-t \le y \le b/2$$

$$\bar{h}_B^{\,II} = -\frac{n\pi}{a} h_m [\cos h_m y \sin \frac{n\pi}{a} x]\, \bar{a}_x - \gamma_{0m}^2 [\sin h_m y \cos \frac{n\pi}{a} x]\, \bar{a}_y \qquad 0 \le y \le b/2-t \quad \ldots (53)$$

$$= \frac{n\pi}{a} A_m \ell_m [\cos \ell_m (b/2-y) \sin \frac{n\pi}{a} x]\, \bar{a}_x - \gamma_{0m}^2 A_m [\sin \ell_m (b/2-y) \cos \frac{n\pi}{a} x]\, \bar{a}_y \qquad b/2-t \le y \le b/2$$

$$A_m = \frac{1}{\mu_r} \frac{\sin h_m(b/2-t)}{\sin \ell_m t} = -\frac{h_m}{\ell_m} \frac{\cos h_m(b/2-t)}{\cos \ell_m t}$$

$$\gamma_{nm}^2 = h_m^2 + \left(\frac{n\pi}{a}\right)^2 - k_0^2$$

$$= \ell_m^2 + \left(\frac{n\pi}{a}\right)^2 - \varepsilon_r \mu_r k_0^2$$

Appendix C

$TE^{\pm}_{n0}$ (n odd) MODES IN THE TWIN-SLAB FERRITE LOADED WAVEGUIDE

For the twin ferrite slab configuration of Fig. 16, and magnetization in the y-direction, the permeability tensor has the form:

$$\hat{\mu} = \mu_0 \begin{bmatrix} \mu & 0 & \mp j\kappa \\ 0 & 1 & 0 \\ \pm j\kappa & 0 & \mu \end{bmatrix} \qquad \ldots(54)$$

where the upper signs correspond to magnetization in the positive direction of y. The $TE^{\pm}_{n0}$ modes have only E_y, H_x and H_z field components:

$$E_y = \psi_{Bn} e^{\mp \gamma_n Z} \qquad \ldots(55)$$

$$H_x = \frac{\pm j\mu\gamma_n \psi_{Bn} + \kappa \psi'_{Bn}}{\omega\mu_0(\mu^2 - \kappa^2)} e^{\mp \gamma_n Z} \qquad \ldots(56)$$

$$H_z = \frac{\pm\kappa \gamma_n \psi_{Bn} + j\mu \psi'_{Bn}}{\omega\mu_0(\mu^2 - \kappa^2)} e^{\mp \gamma_n Z} \qquad \ldots(57)$$

where $\psi'_{Bn} = \frac{\partial \psi_{Bn}}{\partial x}$ and the upper signs correspond to TE^{+}_{n0} modes. Superscripts, $\pm$, have been omitted from ψ_{Bn} and γ_n for simplicity. In eqns. (56) and (57) $\kappa = 0$ and $\mu = 1$ in the air and dielectric regions of the waveguide. For odd modes, ψ_{Bn} has the form:

$$\psi_{Bn} = \begin{cases} A_n \sin h_n x & 0 \le x \le c \\ B_n \sin \ell_n(x-c) + C_n \sin \ell_n(c+t-x) & c \le x \le c+t \\ D_n \cos q_n(a/2 - x) & c+t \le x \le a/2 \end{cases} \qquad \ldots(58)$$

and satisfies the wave equation:

$$\psi''_{Bn} + (\gamma_n^2 + k^2)\ \psi_{Bn} = 0 \qquad \ldots(59)$$

where $$k^2 = \begin{cases} k_0^2 & 0 \le x \le c \\ k_0^2 \varepsilon_f \mu_e & c \le x \le c + t \\ k_0^2 \varepsilon_d & c + t \le x \le a/2 \end{cases}$$

$$\mu_e = \frac{\mu^2 - \kappa^2}{\mu}$$

The modal expressions may be summarized as follows:

Waveguide B

$$\bar{h}^{\pm}_{Bn} = \pm j \frac{\gamma_n}{\omega\mu_0} A_n \sin h_n x \, \bar{a}_x$$

$$\bar{e}^{\pm}_{Bn} = A_n \sin h_n x \, \bar{a}_y$$

$0 \le x \le c$ . . .(60)

$$\bar{h}^{\pm}_{Bn} = \pm j \frac{\gamma_n}{\omega\mu_0\mu_e}[B_n \sin \ell_n(x-c) + C_n \sin \ell_n(c+t-x)]\bar{a}_x + \frac{\kappa/\mu}{\omega\mu_0\mu_e}[B_n \ell_n \cos \ell_n(x-c) - C_n \ell_n \cos \ell_n(c+t-x)]\bar{a}_x$$

$$\bar{e}^{\pm}_{Bn} = [B_n \sin \ell_n(x-c) + C_n \sin \ell_n(c+t-x)]\bar{a}_y$$

$c \le x \le c+t$ . . .(61)

$$\bar{h}^{\pm}_{Bn} = \pm j \frac{\gamma_n}{\omega\mu_0} D_n \cos q_n(a/2 - x)\bar{a}_x$$

$$\bar{e}^{\pm}_{Bn} = D_n \cos q_n(a/2 - x)\bar{a}_y$$

$c+t \le x \le a/2$ . . .(62)

Waveguide A

$$\bar{h}_{Ai} = j \frac{\gamma_i}{\omega\mu_0} \sin(\frac{i\pi}{a} x)\bar{a}_x$$

$$\bar{e}_{Ai} = \sin(\frac{i\pi}{a} x)\bar{a}_y$$

. . .(63)

In the empty waveguide, $\psi_{Ai} = \sin(\frac{i\pi}{a} x)$. Thus, the constants A_n, B_n, C_n and D_n should be chosen so that ψ_{Bn} is real in all three regions of the waveguide B cross-section, regardless of whether h_n, ℓ_n and q_n are real

or complex. This is done by normalizing the constants to D_n. Satisfying the boundary conditions at x = c and x = (c+t) yields the following:

$$\left.\begin{aligned} D_n &= 1 \\ B_n &= \cos q_n d / \sin \ell_n t \\ C_n &= [-\mu_e q_n \sin q_n d \sin \ell_n t + \ell_n \cos \ell_n t \cos q_n d \\ &\quad \mp j \frac{\kappa}{\mu} \gamma_n \sin \ell_n t \cos q_n d]/[\ell_n \sin \ell_n t] \\ A_n &= C_n \sin \ell_n t / \sin h_n c \end{aligned}\right| \quad \ldots(64)$$

The eigenvalue equation is obtained from these boundary conditions. If the subscript n is omitted, this has the form:

$$-q \mu_e \sin qd \cos hc \frac{\sin \ell t}{\ell} + (T_1 - T_2) \cos \ell t \pm j \frac{\kappa}{\mu} \gamma (T_1 + T_2) \frac{\sin \ell t}{\ell}$$

$$+ \frac{1}{\mu_e} [(\frac{\kappa}{\mu} \gamma)^2 - \ell^2] \frac{\sin hc}{h} \cos qd \frac{\sin \ell t}{\ell} = 0 \quad \ldots(65)$$

where $T_1 = \cos hc \cos qd$

$$T_2 = \frac{q}{h} \sin hc \sin qd$$

and the upper sign corresponds to TE^{+}_{n0} modes. Equation (59) may be written more explicitly for the three regions in the forms:

$$\gamma^2 = h^2 - k_0^2 \quad \ldots(66)$$

$$\ell^2 = h^2 + (\varepsilon_f \mu_e - 1) k_0^2 \quad \ldots(67)$$

$$q^2 = h^2 + (\varepsilon_d - 1) k_0^2 \quad \ldots(68)$$

With eqns. (66)-(68), solutions may be found for h from eqn. (65). For propagating modes, γ is imaginary and a solution exists for h which is either pure real or pure imaginary. For nonpropagating modes, however, γ is not pure imaginary and the solutions for h are complex. Thus, γ, ℓ and q are also complex. One simplification arises, however, since the TE^{+}_{i0} and TE^{-}_{i0} modes form a conjugate pair[26]; i.e., if $\gamma_i^{+} = \alpha_i + j \beta_i$,

then $\gamma_i^- = \alpha_i - j\,\beta_i$.

The eigenvalue equation was solved by Newton's method. If $h = \alpha + j\beta$ is a solution, then eqn. (65) may be written as:

$$F(h) = R(h) + jI(h) = 0 \qquad \ldots(69)$$

and,
$$\frac{d\,F(h)}{dh} = R_\alpha + j\,I_\alpha = I_\beta - j\,R_\beta \qquad \ldots(70)$$

Newton's iterative method:

$$\alpha_{i+1} = \alpha_i + \left[\frac{I\,R_\beta - R\,I_\beta}{R_\alpha I_\beta - I_\alpha R_\beta}\right]_i \qquad \ldots(71)$$

$$\beta_{i+1} = \beta_i + \left[\frac{R\,I_\alpha - I\,R_\alpha}{R_\alpha I_\beta - I_\alpha R_\beta}\right]_i \qquad \ldots(72)$$

Equations (71) and (72) converge provided the starting values, $\alpha_0 + j\beta_0$, are sufficiently close. It was found that for all solutions, $\beta \ll \alpha$ and suitable starting values were obtained by setting $\beta_0 = 0$ and finding α_0 by bisection such that $R(\alpha_0) = 0$.

REFERENCES

1. Van Trier, A.A.Th.M.: "Guided electromagnetic waves in anisotropic media", Appl. Sci. Res., 1953, 3B, pp. 305-371.

2. Lax, B., and Button, K.J.: "Microwave ferrites and ferrimagnetics", (McGraw-Hill, 1962).

3. Gurevich, A.G. (A. Tybulewicz, trans.): "Ferrites at microwave frequencies", (Boston Technical Publishers, Inc., 1965).

4. Treuhaft, M.A. and Silber, L.M.: "Use of microwave ferrite toroids to eliminate external magnets and reduce switching power", Proc. IRE, 1958, 46, (8), p. 1538.

5. Siekanowicz, W.W., Schilling, W.A., Walsh, T.E., Bardash, I. and Gordon, I.: "Design and performance of a 20-kilowatt latching non-reciprocal X-band ferrite phase shifter", R.C.A. Review, 1965, 26, (12), pp. 574-586.

6. Frank, J., Kuck, J.H. and Shipley, C.A.: "Latching ferrite phase shifter for phased arrays", Microwave Journal, 1967, 10, (3), pp. 97-102.

7. Querido, H., Frank, J. and Cheston, T.C.: "Wide band phase shifters", I.E.E.E. Trans., 1967, AP-15, (3), p. 300.

8. Spaulding, W.G.: "A periodically loaded, latching, non-reciprocal ferrite phase shifter", presented at the I.E.E.E. G-MTT international microwave symposium, Dallas, U.S.A., 1969.

9. Spaulding, W.G.: "The application of periodic loading to a ferrite phase shifter design", I.E.E.E. Trans., 1971, MTT-19, (12), pp. 922-928.

10. Kharadly, M.M.Z.: "Periodically loaded non-reciprocal transmission lines for phase shifter applications", I.E.E.E. Trans., 1974, MTT-22, (6), pp. 635-640.

11. Collin, R.E.: "Field theory of guided waves", (McGraw-Hill, 1960).

12. Chang, C.T.M.: "Equivalent circuit for partially dielectric-filled rectangular-waveguide junctions", I.E.E.E. Trans., 1973, MTT-21, (6), pp. 403-411.

13. Waldron, R.A.: "Characteristic impedances of waveguides", Marconi Rev., 1967, 30, (3rd Qtr.), pp. 125-136.

14. Chatterjee, S.K., and Chatterjee, R.: "Dielectric loaded waveguides - a review of theoretical solutions, Pt. III", The Radio and Electronic Engineer, 1965, 30, (6), pp. 353-364.

15. Clarricoats, P.J.B., and McBride, J.M.W.: "Properties of dielectric-rod junctions in circular waveguide", Proc. I.E.E., 1964, 111, (1), pp. 43-50.

16. Lengyel, B.A.: "A note on reflection and transmission", J. Appl. Phys., 1951, 22, (3), pp. 263-264.

17. Clarricoats, P.J.B., and Slinn, K.R.: "Numerical solution of waveguide-discontinuity problems", Proc. I.E.E., 1967, 114, (7), pp. 878-886.

18. Wexler, A.: "Solution of waveguide discontinuities by modal analysis", I.E.E.E. Trans., 1967, MTT-15, (9), pp. 508-517.

19. Bernues, F.J. and Bolle, D.M.: "The ferrite-loaded waveguide discontinuity problem", I.E.E.E. Trans., 1974, MTT-22, (12), pp. 1187-1193.

20. Ince, W.J., and Stern, E.: "Nonreciprocal remanence phase shifters in rectangular waveguide", I.E.E.E. Trans., 1967, MTT-15, (2), pp. 87-95.

21. Walker, L.R.: "Orthogonality relation for gyrotropic wave guides", J. Appl. Phys., 1957, 28, (3), p. 377.

22. Villeneuve, A.T.: "Orthogonality relationships for waveguides and cavities with inhomogeneous anisotropic media", I.R.E. Trans., 1959, MTT-7, (10), pp. 441-446.

23. Mittra, R. and Lee, S.W.: "Mode matching method for anisotropic guides", Radio Sci., 1967, 2, (8), pp. 937-942.

24. Green, J.J. and Sandy, F.: "Microwave characterization of partially magnetized ferrites", I.E.E.E. Trans., 1974, MTT-22, (6), pp. 641-645.

25. McRitchie, W.K., Kharadly, M.M.Z. and Corr, D.G.: "Field-matching solution of transverse discontinuities in inhomogeneous waveguides", Electron. Lett., 1973, 9, (13), pp. 291-293.

26. Bresler, A.D., Joshi, G.H. and Marcuvitz, N.: "Orthogonality properties for modes in passive and active uniform wave guides", J. Appl. Phys., 1958, 29, (5), pp. 794-799.

ADDITIONAL REFERENCE

McRitchie, W.K. and Kharadly, M.M.Z.: "Properties of interface between homogeneous and inhomogeneous waveguides", Proc. I.E.E., 1974, 121, (11), pp. 1367-1374.